Florida International University
FIU Digital Commons

FIU Electronic Theses and Dissertations | University Graduate School

3-22-2011

U-Th-Ba Elemental Fractionation during Partial Melting of Crustal Xenoliths and its Implications for U-series Disequilibria in Continental Arc Rocks

Raul Brens Jr.
Florida International University, RaulJr00@hotmail.com

Follow this and additional works at: http://digitalcommons.fiu.edu/etd

Recommended Citation
Brens, Raul Jr., "U-Th-Ba Elemental Fractionation during Partial Melting of Crustal Xenoliths and its Implications for U-series Disequilibria in Continental Arc Rocks" (2011). *FIU Electronic Theses and Dissertations.* Paper 406.
http://digitalcommons.fiu.edu/etd/406

This work is brought to you for free and open access by the University Graduate School at FIU Digital Commons. It has been accepted for inclusion in FIU Electronic Theses and Dissertations by an authorized administrator of FIU Digital Commons. For more information, please contact dcc@fiu.edu.

FLORIDA INTERNATIONAL UNIVERSITY

Miami, Florida

U-Th-Ba ELEMENTAL FRACTIONATION DURING PARTIAL MELTING OF CRUSTAL XENOLITHS AND ITS IMPLICATIONS FOR U-SERIES DISEQUILIBRIA IN CONTINENTAL ARC ROCKS

A thesis submitted in partial fulfillment of the

requirements for the degree of

MASTER OF SCIENCE

in

GEOSCIENCES

by

Raul Brens Jr.

2011

To: Dean Kenneth Furton
College of Arts and Sciences

This thesis, written by Raul Brens Jr., and entitled U-Th-Ba Elemental Fractionation during Partial Melting of Crustal Xenoliths and its Implications for U-series Disequilibria in Continental Arc Rocks, having been approved in respect to style and intellectual content, is referred to you for judgment.

We have read this thesis and recommend that it be approved.

_____
Grenville Draper

_____
Andrew Macfarlane

_____
Rosemary Hickey-Vargas, Major Professor

Date of Defense: March 22, 2011

The thesis of Raul Brens Jr. is approved.

_____
Dean Kenneth Furton
College of Arts and Sciences

_____
Interim Dean Kevin O'Shea
University Graduate School

Florida International University, 2011

ACKNOWLEDGMENTS

I would like to, first and foremost, thank my advisor, Dr. Rosemary Hickey-Vargas, for encouraging me to independently think, as well as, all the support and intellectual guidance she has provided throughout my entire time at F.I.U. Furthermore, I am very appreciative for the insightful input and feedback from my committee members Dr. Grenville Draper and Dr. Andrew Macfarlane. I wish to acknowledge the facility managers for FCAEM (Tom Beasly) and TEAF (Tatiana Trejos) for their substantial efforts in educating and helping me operate the instruments in their respective laboratories. Finally, I am very grateful to my family and friends for their loving support and motivation to excel in my educational endeavors.

ABSTRACT OF THE THESIS

U-Th-Ba ELEMENTAL FRACTIONATION DURING PARTIAL MELTING OF CRUSTAL XENOLITHS AND ITS IMPLICATIONS FOR U-SERIES DISEQUILIBRIA IN CONTINENTAL ARC ROCKS

by

Raul Brens Jr.

Florida International University, 2011

Miami, Florida

Professor Rosemary Hickey-Vargas, Major Professor

Understanding U-series isotopic disequilibria of partially melted crust is integral for determining the effect that crustal assimilation has on the U-series signature of magmas. In this work, U, Th and Ba (as a proxy for Ra) elemental abundances were gathered on the quenched glass in partially melted crustal xenoliths of granitic composition using microbeam techniques. The crustal xenoliths, which are found in basaltic lava, from Mirador Volcano in Chile, are old, and can be assumed to be at secular equilibrium, whereas melting occurred during eruption of Mirador in 1979. A comparison of the ratios Ba/Th and U/Th in the partial melts with those of the whole rock reveal how much fractionation has occurred during partial melting. Different ratios of U, Th and Ba compared to the whole rock substantiate fractionation via partial melting. Thus, assimilation of partial melts of crust can play a role in U-series isotopic disequilibria.

TABLE OF CONTENTS

CHAPTER PAGE

I. INTRODUCTION....1

II. BACKGROUND INFORMATION....3
2a. Geologic Setting....3
2a.I. Subduction Zone Volcanism....3
2a.II. The Andes and its Volcanic Zones....3
2a.III. The Southern Volcanic Zone....5
2a.IV. Mirador Volcano – basalt and xenoliths....6
2b. U-series disequilibria....7
2b.I. U-series disequilibrium in subduction-related magma....7
2b.II. U-series disequilibrium in crustal processes....8
2c. Objective of work....10

III. PREVIOUS STUDIES OF U-SERIES DISEQUILIBRIUM DURING CRUSTAL MELTING....12
3a. Theoretical Studies....12
3b. Distinction between this work and previous studies....13

IV. DESCRIPTION OF XENOLITH SAMPLES....14
4a. Thin sections and pictures of whole xenoliths....14
4b. Interpretation of xenoliths....18

V. SAMPLE PREPARATION AND ANALYTICAL TECHNIQUES....19
5a. Sample Preparation....19
5b. Electron Microprobe Analysis (EPMA)....20
5b.I Elemental Mapping....20
5b.II. In-Situ Chemical Analysis....20
5c. Laser Ablation Inductively Coupled Mass Spectrometer (LA-ICP-MS)....21
5d. Solution Introduction Inductively Coupled Mass Spectrometer (SI-ICP-MS)....23

VI. RESULTS – GEOCHEMISTRY OF XENOLITH AND GLASSES....24
6a. Bulk xenolith and basalt analyses....24
6b. Xenolith EPMA elemental map....27
6c. Xenolith EPMA chemical compositions....30
6d. LA-ICP-MS results....35

VII. DISCUSSION....43
7a. LA-ICP-MS Results....43

7b. Interpretation of trace element ratios relative to the bulk xenolith.....43
7c. Potential impact of fractionation during crustal assimilation.....49

VIII. CONCLUSIONS AND FUTURE DIRECTIONS……...…….……...51

REFERENCES…….....52

APPENDICES.....55

LIST OF TABLES

TABLE PAGE

1. A compiled list (acquired from literature) of experimental studies done testing each mineral's partition coefficients for U, Th, Ra and Ba (adapted from Berlo et al., 2004)……9

2. A compiled list of accessory phase mineral and their partition coefficients for U and Th at certain P and T…...……..……..13

3. Description of labeling for Hand Sample and the multiple thick sections within each hand sample.……...……...…14

4. Parameters for LA-ICP-MS……...……...…21

5. Published mineral partition coefficients for Andesitic and Rhyolitic liquids……...…36

6. Ba/Th and Th/U Ratios for the xenolith (bulk rock), basalt, and all the lasered spots on the thick sections.....46

LIST OF FIGURES

FIGURE PAGE

FIGURE 1. Map of the 4 active volcanic regions in the Andes Mountains……....4

FIGURE 2. (1. a-d) As the convergent boundary is compressing the fault becomes transpressional (2) Along the coast it is mostly east-west extension…….…..5

FIGURE 3. Part of the chart of nuclides illustrating the ^{238}U decay chain including half-lives……..7

FIGURE 4. Fractionation of fluid mobile vs. non-mobile elements within a subduction zone and inputs and outputs of the magma chamber…..……..…….…8

FIGURE 5. Evolution of ^{238}U and ^{230}Th through the continental crust…….…...….10

FIGURE 6. Schematic Illustration of subduction zone beneath Mirador Volcano in the SVZ…….11

FIGURE 7. Photographs of partially melted granitic xenoliths (71-73% SiO2) encased by basalt, typically found in the form of bombs, erupted in 1978…..……17

FIGURE 8. Total Alkali (Na_2O+K_2O) versus Silica (TAS) Diagrams for both the xenolith and the basalt in order to classify the type of igneous rock…….…25

FIGURE 9. Multi-element plots normalized to primitive mantle (McDonough & Sun, 1995) for the crustal xenolith and basalt……..……...…….26

FIGURE 10. EPMA elemental maps of one of the samples (J-1-spot6b) from the Mirador Volcano (Chile).....……...29

FIGURE 11. Harker diagrams for major elements for the bulk xenolith, basalt and microprobed spots……...…….……..35

FIGURE 12. Multi-element diagram (Ba, Sr , REE, U, Th and HFSE) for the glass (partial melt), major mineral (feldspar) and accessory minerals…….……..42

FIGURE 13. Ba/Th v Th/U ratios for partial melts (sample) compared with the whole rock (WR)……..…..47

FIGURE 14. Ba/Th v Th/U ratios for identified accessory minerals and the major mineral (feldspar) compared with the whole rock…….…48

I. INTRODUCTION

Convergent plate boundaries have a major role in the production of continental crust. The U-series isotopic analysis approach has been a crucial tool to help elucidate many igneous processes at convergent plate margins including but not limited to crustal assimilation, and residence time for magma in magma chambers, that in the past have been very difficult to ascertain. Modeling of U-series isotopes has been used by scientists to infer: 1) fractionation of U, Th, Ra by subduction processes in the mantle wedge 2) the extent of crustal assimilation affecting mantle wedge derived magmas and 3) the length of time a particular batch of magma has sat in the crust. In the case of (2) most work has been theoretical, and not constrained by samples or experiments.

Most U-series isotope studies have been done on rocks from ocean island arcs because the underlying crust is inferred to be thin and young, and therefore have a lesser impact on the composition of ascending magma (Turner et al., 2003; Snyder et al., 2007; Huang et al., 2008). According to Turner et al. (2003), the most juvenile lavas have a ^{238}U excess although there are juvenile lavas, which exhibit a ^{238}U-depleted signature or are in equilibrium. In addition, ^{226}Ra excesses are observed and these decrease with increasing SiO_2 content (Turner et al. 2001). The downgoing slab releases fluids containing both uranium and radium, the addition lowers the melting temperature of the surrounding peridotite mantle and constitutes the initial production of the magma. Once the initial melt reaches the main magma chamber it undergoes a series of assimilation, crystallization and recharge all of which may alter the U-series isotopic makeup (Huang

et al., 2008). One interpretation of the ^{226}Ra trend is that it is time dependent, the longer it stays in a chamber the closer it will be to secular equilibrium.

The objective of this project is to determine whether crustal partial melting can cause U-series disequilibrium. I will use a suite of partially melted granitic xenoliths in young basalts from the Mirador volcano in the Southern Volcanic Zone of Chile. My research will aid further investigations of magma chamber processes, such as assimilation and residence time of crustal xenoliths.

II. BACKGROUND INFORMATION

2a. Geologic Setting

2a.I. Subduction Zone Volcanism

The worldwide phenomenon that creates the majority of crustal rocks through arc magmatism is known as subduction zone magmatism. Subduction zone magmatism is the by-product of two plates converging and the colder, denser plate (slab) sinking beneath the more buoyant upper plate. The convergence may be between two oceanic plates or an oceanic and continental plate. In either case, the denser material is subducted; oceanic crust, composed of mafic basalt, is denser than continental crust, which is composed on average of more felsic granite and hence much more buoyant.

The subduction process removes oceanic crust from earth's surface. It also inhibits the continental crust from horizontally expanding because of compressional forces. At a depth of approximately 100 kilometers, dehydration of the slab induces melting and mixing within the mantle wedge. Melts then rise, as a result of buoyancy, and are the magmatic source of the volcanoes that often form an arcuate shape (von Huene and Scholl, 1991). The input into the crust is the juvenile magma that replenishes what is consumed during subduction (Stern, 2002).

2a.II. The Andes and its Volcanic Zones

The Andes Mountains are one such example of crust and volcanoes formed by subduction. Stern et al. (2007) illustrates in figure 1 the four different volcanic regions along the Andes Mountains. This mountain range is the longest terrestrial mountain range in the world and starts in Southern Chile extending up the western side of the South American continent and into the northern part of South America. This volcanic chain

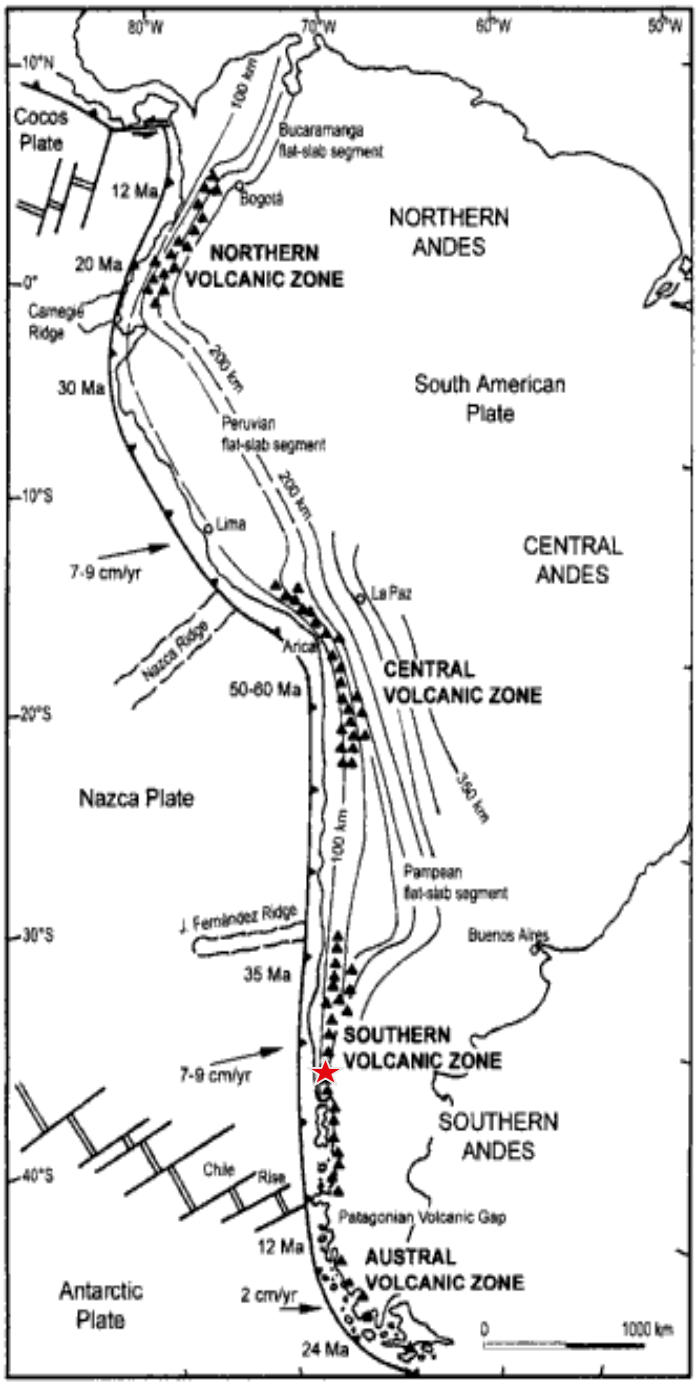

forms part of what is termed the 'ring of fire'—the areas of land along the Pacific Ocean that are rimmed with active volcanoes. The Andes volcanic system is divided into four main areas: 1) the Northern Volcanic Zone (NVZ) which extends from Colombia to Ecuador, 2) the Central Volcanic Zone (CVZ) which runs through southern Peru, Bolivia, Argentina and northern Chile, 3) the Southern Volcanic Zone (SVZ) and 4) the Austral Volcanic Zone (AVZ); the SVZ and AVZ extend along the border of Chile and Argentina. The Austral Volcanic Zone is the only

Figure 1: Map of the 4 active volcanic regions in the Andes Mountains. The illustration also shows the direction and convergence rate of the subducting oceanic plates. The depths of the benioff zones are expressed in km on the S. American plate. Mirador volcano is located in the Southern Volcanic Zone (marked by a red star). Diagram from Stern et al. (2007).

segment that is not being magmatically supplied by subduction of the Nazca plate, but rather the Antarctic Plate.

2a.III. The Southern Volcanic Zone

The Southern Volcanic Zone (SVZ) consists of numerous stratovolcanoes and several fields of small eruptive centers sited on crust of 55 km to 35 km thickness. The Liquiñe-Ofqui Fault Zone (LOFZ) is the main fault in the Southern Volcanic Zone. It is a NNE-SSW dextral strike slip fault. The LOFZ has aided in the lineament of the volcanoes in the Southern Volcanic Zone; small eruptive centers are located to the east of the LOFZ and the composite stratovolcanoes for the most part are located to the west of the LOFZ which may be attributed to the tensions placed in the area. To the west where the taller composite stratovolcanoes are located there are shortening tensional forces from the convergent zone, thus making the volcanoes taller. Moreover, the transpressional tectonism occurring is

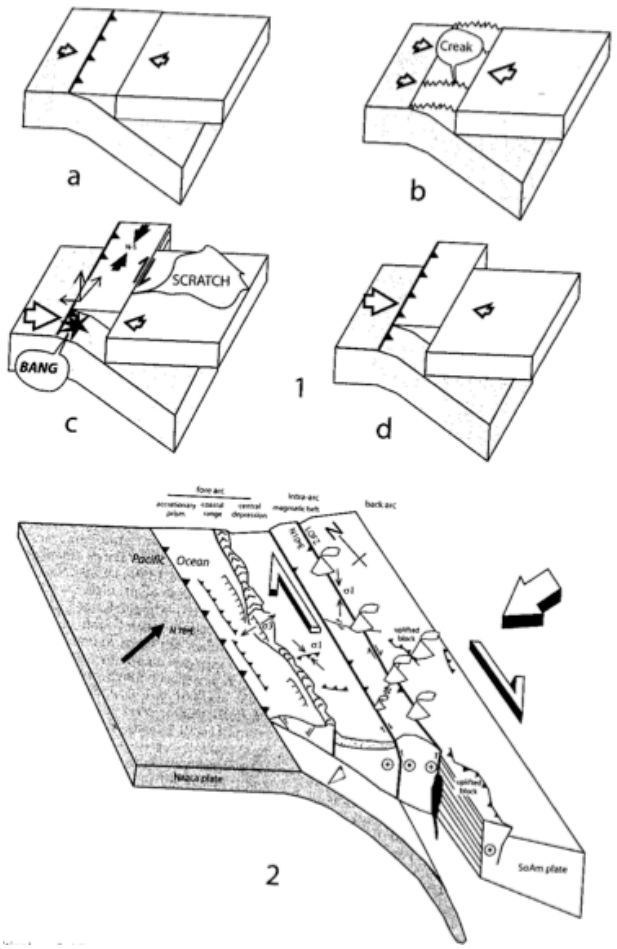

Figure 2: *(1.a-d)* As the convergent boundary is compressing the fault becomes transpressional (*2)* Along the coast it is mostly east-west extension. In the forearc zone, there is north-south compression. In the Liquiñe-Ofqui Fault Zone (LOFZ) there are transpressional forces and the volcanoes are located along the fault for easy magma transport. Figure from Charrier et al. (2007).

currently the driving force behind the movement of the LOFZ. As observed in Figure 2, as the convergent boundary is compressing, the tensional forces are building up and have to release in some manner. The tension on the plate is released along the transcurrent fault of the LOFZ, resulting in a pull-apart basin (Cembraño et al., 2007). The diagram in figure 2 displays the volcanoes situated along the fault where it is easier to transport the magma through the crust.

2a.IV. Mirador Volcano – basalt and xenoliths

The Mirador Volcano is a minor eruptive center within a larger volcanic group named Carran-Los Venados located in the Southern Volcanic Zone (Figure 1). It last erupted in 1979 producing 3 lava flows and pyroclastic material (Lopez-Escobar and Moreno, 1981). Moreover, the 1979 eruption emitted numerous partially melted granitic xenoliths, often found in the form of bombs completely encased by basalt. The lavas and pyroclastic material produced by this volcano are predominantly mafic in composition. The xenoliths are believed to originate as granitic country rocks surrounding the magma chamber, which were entrained by the magma upon ascent and expelled with the mafic type magma. Xenoliths occur at many other SVZ centers, but they were not erupted in historic times, as large, or partially melted. Therefore, while Mirador is representative of the larger network of active volcanoes that make up a portion of a series of volcanoes and mountains known as the Andes Mountains, these crustal xenoliths are unique.

2b. U-series disequilibria

2b.I. U-series disequilibrium in subduction-related magma

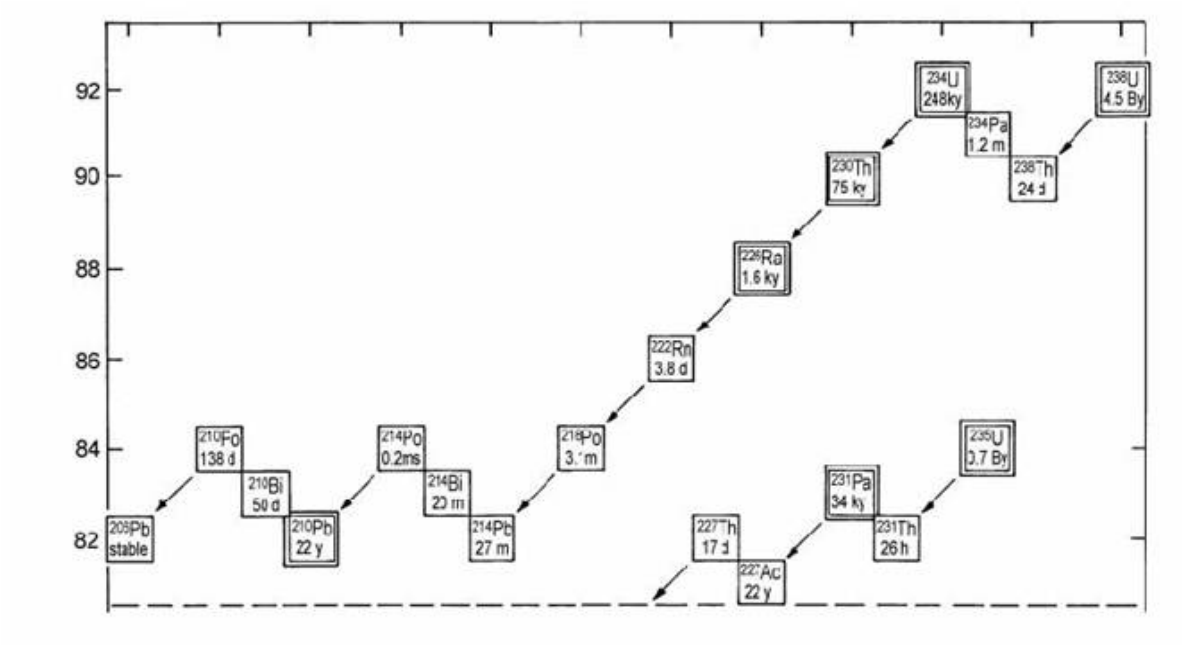

Figure 3: Part of the chart of nuclides illustrating the ^{238}U decay chain including half-lives. The y-axis is the number of protons in the element Figure after Dickin (1997).

Uranium-238 is a radioactive isotope of the trace element uranium that decays into short-lived nuclides, which ultimately decay into ^{206}Pb (Figure 3). Short-lived daughters include ^{230}Th with a half-life ($t_{1/2}$) of 7.54×10^4 years (Faure and Mensing, 2005). Thorium-230 then decays into ^{226}Ra, which has a half-life ($t_{1/2}$) of 1599 years (Faure and Mensing, 2005). Since U, Th and Ra behave differently, fractionation may occur during subduction zone processes. Uranium and radium are both fluid mobile while thorium is not fluid mobile and preferentially remains in the solid state (Figure 4). In subduction zones, it is observed that juvenile magma will most likely contain a ^{238}U excess, and more ^{226}Ra than ^{230}Th (Turner et al., 2003). However, it is possible to have a ^{230}Th excess, which must be attributed to either accessory minerals that preferentially

take up ^{238}U (i.e., zircon as seen in Table 2 (Berlo et al., 2004)) or a mantle-derived magma that originally had a larger amount of ^{232}Th (Garrison et al., 2006). The latter is attributed to garnet in the residue during partial melting. Garnet retains U more than Th.

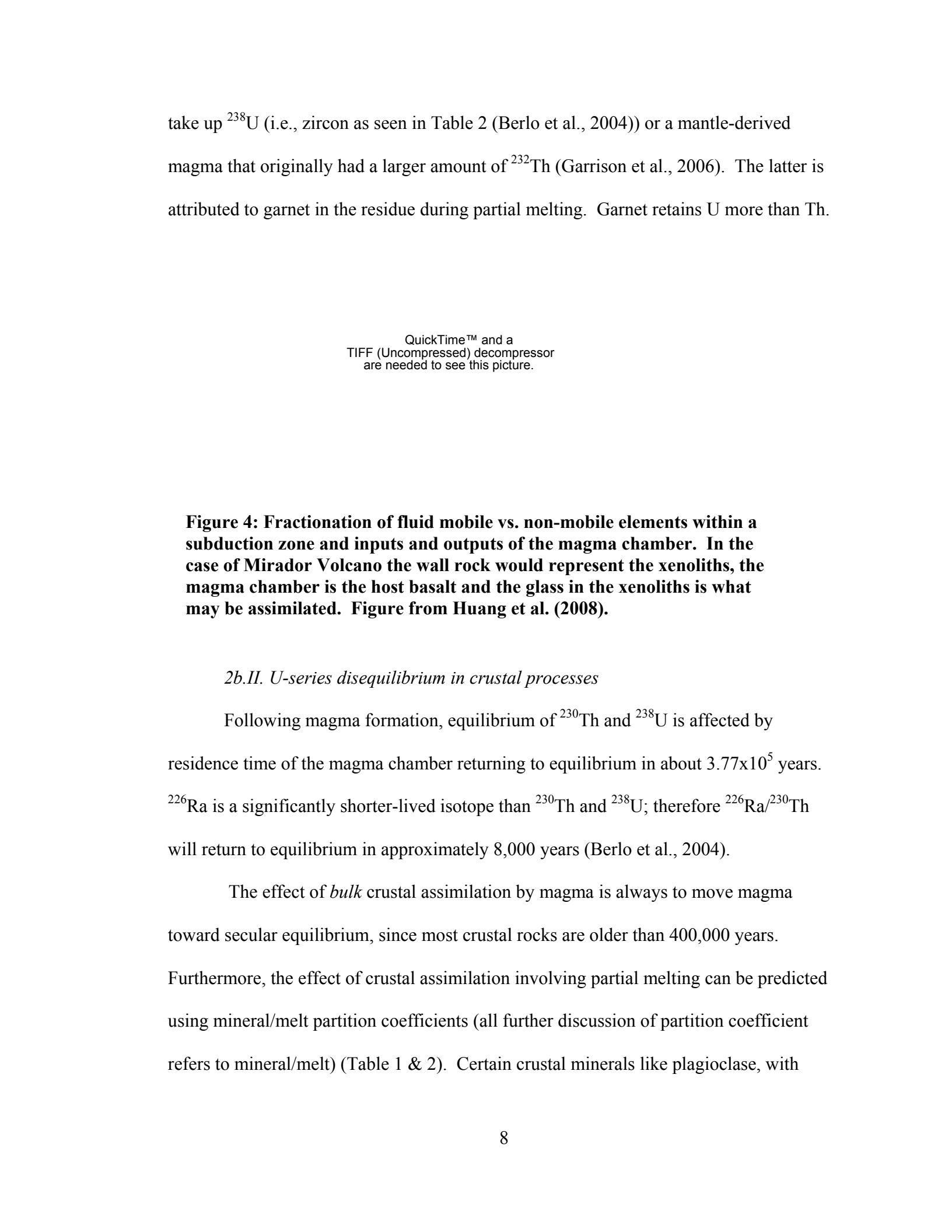

Figure 4: Fractionation of fluid mobile vs. non-mobile elements within a subduction zone and inputs and outputs of the magma chamber. In the case of Mirador Volcano the wall rock would represent the xenoliths, the magma chamber is the host basalt and the glass in the xenoliths is what may be assimilated. Figure from Huang et al. (2008).

2b.II. U-series disequilibrium in crustal processes

Following magma formation, equilibrium of ^{230}Th and ^{238}U is affected by residence time of the magma chamber returning to equilibrium in about $3.77x10^5$ years. ^{226}Ra is a significantly shorter-lived isotope than ^{230}Th and ^{238}U; therefore $^{226}Ra/^{230}Th$ will return to equilibrium in approximately 8,000 years (Berlo et al., 2004).

The effect of *bulk* crustal assimilation by magma is always to move magma toward secular equilibrium, since most crustal rocks are older than 400,000 years. Furthermore, the effect of crustal assimilation involving partial melting can be predicted using mineral/melt partition coefficients (all further discussion of partition coefficient refers to mineral/melt) (Table 1 & 2). Certain crustal minerals like plagioclase, with

significantly different mineral/melt partition coefficients for Ra and Th, can account for fractionation of $^{226}Ra/^{230}Th$ (Table 1). Melting of the lower crust and fractionation of accessory phase minerals can create a greater fractionation between ^{238}U and ^{232}Th in thicker crust. If the magma is in the crust for a longer period of time, as a result of thickness, it may have more time to undergo processes outlined in figure 5, either enriching the melt in ^{232}Th because of partial melting of the lower crust or, depending the accessory mineral, driving the melt to enrichment in ^{238}U.

	U	Th	Ba	Ra
Amphibole (1025°C; 0.8 GPa)	0.007	0.022	0.353	0.028
Clinopyroxene (1025°C; 0.8 GPa)	0.008	0.045	$6x10^{-5}$	$9x10^{-7}$
Garnet (975°C; 1.3 GPa)	0.023	0.01	5x10-4	$1x10^{-8}$
Orthopyroxene (950°C; 0.8 GPa)	0.0007	0.0015	$7x10^{-5}$	$1x10^{-7}$
Plagioclase (1025°C; 0.8 GPa)	$6x10^{-5}$	$3x10^{-4}$	0.397	0.081

Table 1: A compiled list (acquired from literature) of experimental studies done testing each mineral's partition coefficients for U, Th, Ra and Ba (adapted from Berlo et al., 2004). Ra was calculated using the lattice strain model. These minerals are believed to have varying effects on U-series signature at the lower mafic crust. The plagioclase and amphibole may be residual if granite melts partially. The cpx, opx and garnet are not present in granitic xenoliths.

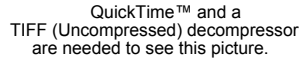

Figure 5: Evolution of ^{238}U and ^{230}Th through the continental crust. ^{230}Th excesses are generated with lower crustal melting (step 2). ^{238}U excesses are generated with fluid addition and crystallization of accessory minerals (steps 1 and 3). Step 2 is what will be analyzed in this thesis, however, it is a much shallower (mid crustal) position and there is no garnet influence. Each number in diagram A correlates to the same number in diagram B. Figure from Garrison et al. (2006).

2c. Objective of work

My purpose is to use natural partial melts in crustal xenoliths, which were erupted quickly enough that they have not mixed into their basalt host. The glasses represent partial melts of crustal rocks (the granitic xenoliths, see Figure 6) that could contaminate ascending mantle derived basaltic magma (the basalt lava). In this study, I use Ba as a proxy for Ra, because it has similar chemical behavior, but is much more abundant and

readily analyzed. This approach is commonly used in published research on U-series disequilibrium (Turner et al., 2003).

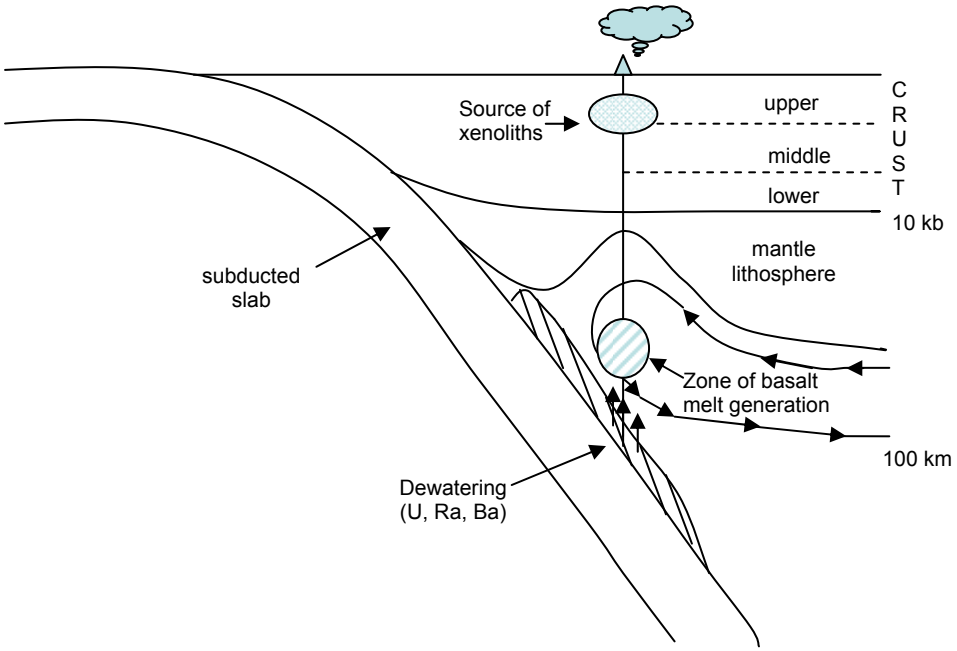

Figure 6: Original schematic of subduction zone beneath Mirador Volcano in the SVZ. The subducted slab is the Nazca plate and the upper plate is the South American plate. Dewatering occurs, leading to the generation of melt at a depth of approximately 100 km. It is believed that the mantle lithosphere is thinner where the melt rises. The source of the xenoliths is in the surrounding wallrock of the magma chamber, which is located at a shallow depth in the upper crust. This country rock is of granitic composition and Miocene to Paleozoic in age.

III. PREVIOUS STUDIES OF U-SERIES DISEQUILIBRIUM DURING CRUSTAL MELTING

3a. Theoretical Studies

Prior studies have added to our knowledge of U-series isotopic disequilibria (within volcanic settings). However, scientists have focused on modeling derived from partition coefficients (Table 1 and Table 2) because U-series analyses cannot be done with any microbeam technique. The U-series isotope analyses are normally done by TIMS, and require between 2-10 grams of sample. Similarly, natural partially melted and quenched crustal rocks, like those found at Mirador, are rarely encountered.

On the basis of results from modeling, one leading hypothesis provided by Berlo et al. (2004) is that U-series disequilibria are not affected very much by partial melting of the mafic lower crust, because only small disequilibria form. Garrison et al. (2006), however, believe that crustal assimilation plays a major role in forming U-series disequilibrium signatures because continental arc rocks have displayed both excesses in ^{238}U and ^{230}Th. Both do agree that assimilation occurs at the lower crust (Figure 4 and Figure 5), where it is of a mafic composition.

Using a different approach (K. Knesel, pers. comm.), through experimental melting and separation of phases, shows that low pressure (shallow) melting of granites containing accessory minerals associated with the intrusions from mafic magma can indeed alter the U and Th isotopic concentrations creating disequilibria. For the aforementioned study (K. Knesel, pers. comm.) the experimental results hinge on the fact that there are zircon and allanite phases present and thus causing the experimental glass to have either a U or Th-excess resulting in isotopic disequilibria associated with them.

There seems to be a general consensus on reasons for fractionation. These vary from accessory phase minerals to major minerals located in the lower crust. A number of different scientists have worked to determine the partition coefficients for these minerals, which Berlo et al. (2004) compiled in Tables 1 and 2. With these partition coefficients different scientists have been able to hypothesize reasons why U-series isotopic disequilibria is occurring within these igneous rocks.

	Allanite	**Apatite**	**Sphene**	**Zircon**
$\mathbf{D_U}$	20	0.001	0.18	100
$\mathbf{D_{Th}}$	61	0.12	0.22	17
P, T, comp	*2.0 Gpa; 900°C; hydrous granite*	*1,250°C; carbonatite*	*1.5 Gpa; 850°C; lamproitic*	*calculated estimate*
Reference	Hermann (2002)	Klemme and Dalpé (2003)	Tiepolo et al. (2002)	Blundy and Wood (2003)

Table 2: A compiled list of accessory phase mineral and their partition coefficients for U and Th at certain P and T. Each partition coefficient was obtained from the reference list provided in the table. These phases do not crystallize from basaltic magma, but can be residual if granite melts partially. Table adapted from Berlo et al. (2004).

3b. Distinction between this work and previous studies

In two of the previously mentioned studies (Berlo et al., 2007 and Garrison et al., 2006), U-series results on rock suites were interpreted using models derived from partition coefficients. In the other study (K. Knesel, pers. comm.) partial melting was done under controlled experimental settings, and only bulk separates of glass and minerals were analyzed. The present study is unique because fractionation of U, Th and Ba by partial melting is examined in situ, using natural samples.

IV. DESCRIPTION OF XENOLITH SAMPLES

4a. Thin sections and pictures of whole xenoliths

The rock suite was collected on January 25, 1982 and December 29, 1987, mostly in the form of volcanic bombs. Five xenoliths were examined: Mirador D, F, H, J and 29-4 using multiple thin sections of each sample (Table 3).

Hand Sample	Thick Sections
Mirador D	25182d
	d-1
Mirador F	25182f
	F-4
Mirador H	25182h
	h-5
	h-12
Mirador J	j-1
Mirador 29-4	29-4a
	29-4b

Table 3: Description of labeling for Hand Sample and the multiple thick sections within each hand sample.

Sample Mirador D

Sample Mirador D (25182d) is a basalt dominated rock with a small xenolith encased measuring ~3 cm in length. In hand sample, the xenolith is extremely vesicular and porphyritic with large grains of quartz. With the exception of several quartz minerals (5%) the grain boundaries are not extremely distinguishable amongst the minerals via hand sample. The basalt has migrated into the xenolith but there is still a distinct difference between the two.

In thin section, Mirador D (25182d) is continuously porphyritic consisting of a very fine-grained matrix surrounding several quartz grains. The matrix is composed mostly of glass with very small plagioclase feldspars. Basalt has begun to intrude the

xenolith and it is apparent at the boundary with the xenolith (in thin section) that there is the onset of mixing as a result of the migration of the small plagioclase feldspar located in the basalt also being located amongst the grains of quartz from the xenolith.

Sample Mirador F

Sample Mirador F (25182f) is also porphyritic with visible mineral grains, however minerals are undistinguishable in hand sample. The xenolith is ~6 cm in length, and is encased by basalt on all sides. The basalt is intermingled into portions of the granite with veins extending no longer than 5 cm long and <1 cm thick. In thin section, the granite is porphyritic with grains of plagioclase and quartz within an isotropic glass matrix. No major mixing is apparent in the boundary between the xenolith and basalt, however, there is encroaching of basalt in the xenolith where ~80-85% of the thin sections are xenolith and ~10-15% are basalt for both thin sections (25182f and F-4).

Sample Mirador H

Sample Mirador H (Figure 7a) is aphanitic in hand sample (where the basalt has started mixing along the edge of the xenolith). The xenolith is ~10 cm length and ~7 cm height, very vesicular with grain boundaries indistinguishable. In thin section, sample h-12 is porphyritic containing more grains of quartz and plagioclase than any other of the thin sections in sample Mirador H. Thin section h-12 is hosted in an isotropic glass matrix with no basalt present in the thin section. While another Mirador H thin section (25182h) had basalt, xenolith and an area of mixing between the two (as seen in Mirador D). The thin section 25182h is very vesicular, porphyritic with quartz and plagioclase grains within an isotropic glass matrix. However, the mixing is occurring along the boundary between the basalt and xenolith where mixing begins and seems to get larger.

Sample Mirador J

Sample Mirador J is aphanitic and the most partially melted sample in the rock suite. It is very vesicular (~25%) with no basalt intrusions in the xenolith.

Sample Mirador 29-4

Sample Mirador 29-4 is porphyritic with large quartz grains. It is a vesicular xenolith with ~7 cm diameter.

(a)

(b)

Figure 7: Photographs of partially melted granitic xenoliths (71-73% SiO2) encased by basalt, typically found in the form of bombs, erupted in 1978. The first xenolith (a) is sample Mirador H and the second xenolith (b) is sample 29-5, which was not partially melted and therefore was not studied.

4b. Interpretation of xenoliths

Geologists observing the eruption have interpreted the origin of the granitic xenoliths encased by basalt as fragments of country rock entrained in the basaltic magma during ascent (Lopez-Escobar et al., 1981). Previous studies on the geochronology of the basement rock in that area clarify the age and origin of the xenolith. Munizaga et al. (1988) dated the granitoids in the region of the South-Central Chile; their results showed that the area had a large constituency of granitoid plutons and batholiths. Through K-Ar and Rb-Sr dating they placed age constraints on different granitoids in the region with the youngest being Miocene in age and the oldest Paleozoic. In the Lago Ranco area, which is very close to Mirador Volcano (Carran-Los Venados), different granitic rock units had ages of 13.1 Ma and 309 +/- 8 Ma, all of which will be at secular equilibrium.

These crustal xenoliths are believed to have come from either the magma chamber or captured in the basaltic magma within the conduit during eruption. Maximum residence times before completely melting, calculated using a simple thermal conduction model are on the order of 30 minutes (White, 1988). This suggests a relatively shallow origin. The large amount of vesicles is indicative of volatiles (H_2O) present in the system. Partial melting may have occurred under hydrous conditions at a magma temperature of 1200^{o}C (K. White, 1988).

V. SAMPLE PREPARATION AND ANALYTICAL TECHNIQUES

I used ICP mass spectrometry along with electron microprobe analysis to study the xenoliths. The mass spectrometer was used to analyze U, Th and Ba both in whole rocks and in the quenched partial melts allowing for the comparison of the ratios of these elements (Ba/Th & U/Th) in the partial melts with the whole rock.

5a. Sample Preparation

The samples used for this analysis are of granitic composition. Their host liquid that is of basaltic composition envelops many of the xenoliths. For whole rock composition U-series data the granites were cut using an Isomet saw equipped with a 0.3 mm-thick diamond wafer blade and then polished to remove saw marks. Large blocks of rock were used in order to represent the whole sample. A ceramic ball mill was used to powder the sample in order to ensure homogeneity across the sample.

For the preparation of the same xenoliths in order to analyze the partial melts, which is in the form of quenched glass, rocks were also cut using the Isomet saw equipped with a 0.3 mm-thick diamond wafer blade. These were subsequently cut into billets to be made into thick sections. Since the samples tend to be relatively vesicular they were impregnated with epoxy prior to making the thick sections. The thick sections were polished to microprobe standards. Once the thick sections were made, they were then analyzed with a petrographic microscope to find the quenched glass (marking the areas of interest). For the Electron Microprobe Analysis (EPMA), the thick sections were carbon coated to 250 Å (blue) using the PAC-1 PELCO Advanced coater 9500. The same samples, once analyzed on the EPMA, were analyzed using a laser ablation ICP-MS.

5b. Electron Microprobe Analysis (EPMA)

5b.I. Elemental Mapping

A JEOL 8900R Superprobe (electron microprobe), at the Florida Center for Analytical Electron Microscopy (FCAEM) (Florida International University, Miami, FL), was used to locate and analyze glass pockets in the samples for major elements (SiO_2, Al_2O_3, FeO, MgO, CaO, Na_2O, K_2O, TiO_2 and PO_4). Elemental maps were set up to scan, for the given elements, to observe relative concentrations of each major element to identify glass (Appendix A). With these maps a basic understanding for the composition of the potential assimilates was attained. The pixel size for the initial maps was 2.0 µm x 2.0 µm, a dwell time of 15 and a probe diameter of 1.5 µm, in order to get the area of interest. Then for higher resolution secondary maps were run, within a smaller area of interest at a 1.0 µm x 1.0 µm pixel size, a dwell time of 15 and a probe diameter of 1.5 µm.

5b.II. In-Situ Chemical Analysis

Probing the glasses allowed us to contrast the elemental compositions across the varying samples. The conditions for spot quantitative analysis with the probe were: 2.00 e-08 volts, correction method: oxide, a defocused beam (to reduce Na migration) with a beam diameter of 20 µm and the following minerals acted as our calibrated standards [Apatite (P), Obsidian (Si, Al, Na, K), Rhodonite (Mn), BHVO (Ti and Ca)]. The samples were analyzed against a standard USGS glass (BHVO) or obsidian. The points chosen to analyze for chemical composition were guided by the maps previously run on these areas of interest within the thick section. The areas with a homogenous BSE image

and chemical criteria that on the maps appeared to meet that of glass. The same criteria were implemented for the accessory phase minerals and feldspar.

5c. Laser Ablation Inductively Coupled Mass Spectrometer (LA-ICP-MS)

An Element 2 (Thermo-Finnigan) high resolution (magnetic field ICP-MS) operated in low-resolution mode coupled to a laser ablation unit (New Wave Research), at the Trace Evidence Analysis Facility (TEAF) (Florida International University, Miami, FL), was used to measure the concentrations of U, Th and Ra in the glasses located using EPMA. Given that Ra is difficult to measure Ba served as a proxy because they have similar ionic radius, ionic charge and chemical behavior. The LA-ICP-MS gas flow is composed of a He and Ar mix. When ablating the spot on the sample the LA-ICP-MS ran in two-minute intervals, of which the first minute was just calculating background and the second minute was the sample being ablated and fed into the plasma to be atomized, ionized and finally calculated. This is the result of instability within the counts of the machine; a period of time to see how the background behaves is needed. Table 4 outlines the optimized parameters used as the method of ablating and analyzing via ICP-MS.

Parameters		
Laser	Laser λ	213 nm
	Spot Size	40 µm & 55 µm
	Ablation Time	60 s.
	Frequency	10 Hz
	Flash Lamp Energy	100%
	Ablation Mode	single spot
	Fluence	29 J/cm^2
ICP	Radio Frequency	1300 W
	Sample Gas	.8-.85 L/min (Ar)
	Carrier Gas	.77-.84 L/min (He)
	Acquisition Mode	low resolution (350)

Table 4: Parameters for LA-ICP-MS.

The standards were analyzed under the same spot size and power settings as the samples. The following were used as standards: USGS glass (BHVO-2G) as a quality control check for accuracy and precision, NIST 610 (synthetic glass) as a calibrator and/or control and NIST 612 (synthetic glass) as a calibrator. The ICP gave us parts per million counts (ppm) that then had to be condensed via normalization to ^{29}Si (or ^{42}Ca for apatite), the internal standard, and identification of the standard concentrations. The signal was acquired in transient mode with the final 30 seconds used for integration using the software 'GLITTER' (GEMOC, Sydney). The final concentrations of each laser-ablated spot were found through the following equation:

[((Normalized peak count * ^{29}Si conc.)- Calibration line intercept)/Calibration line slope]

Where the calibration slope and intercept are related to the standard and their concentrations.

The areas deemed to possibly be glass on the maps were areas of a homogenous backscatter image, as well as, having met the criteria via in-situ chemical analysis for Ca (<12%), Na (<10%), K (<7%) and Fe (<4%). Also, moderate amounts of Al (13%-27%) and large enough amounts of Si (54%-75%) are needed to meet the glass requirements; however not extremely high levels of Si where it would be considered quartz. Furthermore, no other notable concentrations of Mg, Ti, P or Mn (<1%) were to be in the spots being analyzed. Areas that were analyzed as feldspars, were areas that were high in K (>7%) and areas for the accessory minerals particularly sphene and apatite were areas that had a high concentration of Ca and either Ti or P on the elemental maps.

5d. Solution Introduction Inductively Coupled Mass Spectrometer (SI-ICP-MS)

A SI-ICP-MS was used to analyze the whole rock powders for major elements as well as U, Th and Ba. Samples were fused with Li-tetraborate, dissolved and analyzed at the Washington State University.

VI. RESULTS – GEOCHEMISTRY OF XENOLITH AND GLASSES

6a. Bulk xenolith and basalt analyses

There were 5 bulk xenolith analyses done both via XRF and LA-ICP-MS for samples Mirador B, C, H, 29-4 and 29-10. Results are summarized in Appendix B. Mirador samples b, c, h and 29-4 all are rhyolitic in composition containing a SiO_2 wt% of 71.08-72.4 and a total alkali wt% of 7.5-8.0 (Figure 8). However, xenolith 29-10 plots in the dacite range with 63.61 wt% SiO_2 and a total alkali content of 6.0 wt%. The trace elemental composition (Figure 9) of the xenoliths are similar to each other with a slightly higher amount of U and Th than Ba compared with primitive mantle; also, a slight HFSE and LREE enrichment. The order of the elements on the multi-element diagrams are in terms of grouping HFSE, REE and the higher atomic masses of U & Th. Note, when referring to the bulk composition of the xenoliths I will be referring to the average of the rhyolitic xenoliths (omitting the dacitic sample 29-10).

There were 4 analyses completed on magma erupted at Mirador volcano (Hickey-Vargas, unpublished. Appendix B). These were the ones encasing the xenoliths. When plotted on a TAS diagram they plotted on the boundary between the basalt and basaltic andesite fields with a total alkali wt% of 4.5-4.6 and a SiO_2 composition of 51.5-52.7wt%. Compared with primitive mantle, the trace element analysis shows the basalt contains more Ba than U and Th, also, depletion in HFSE and a very small LREE enrichment.

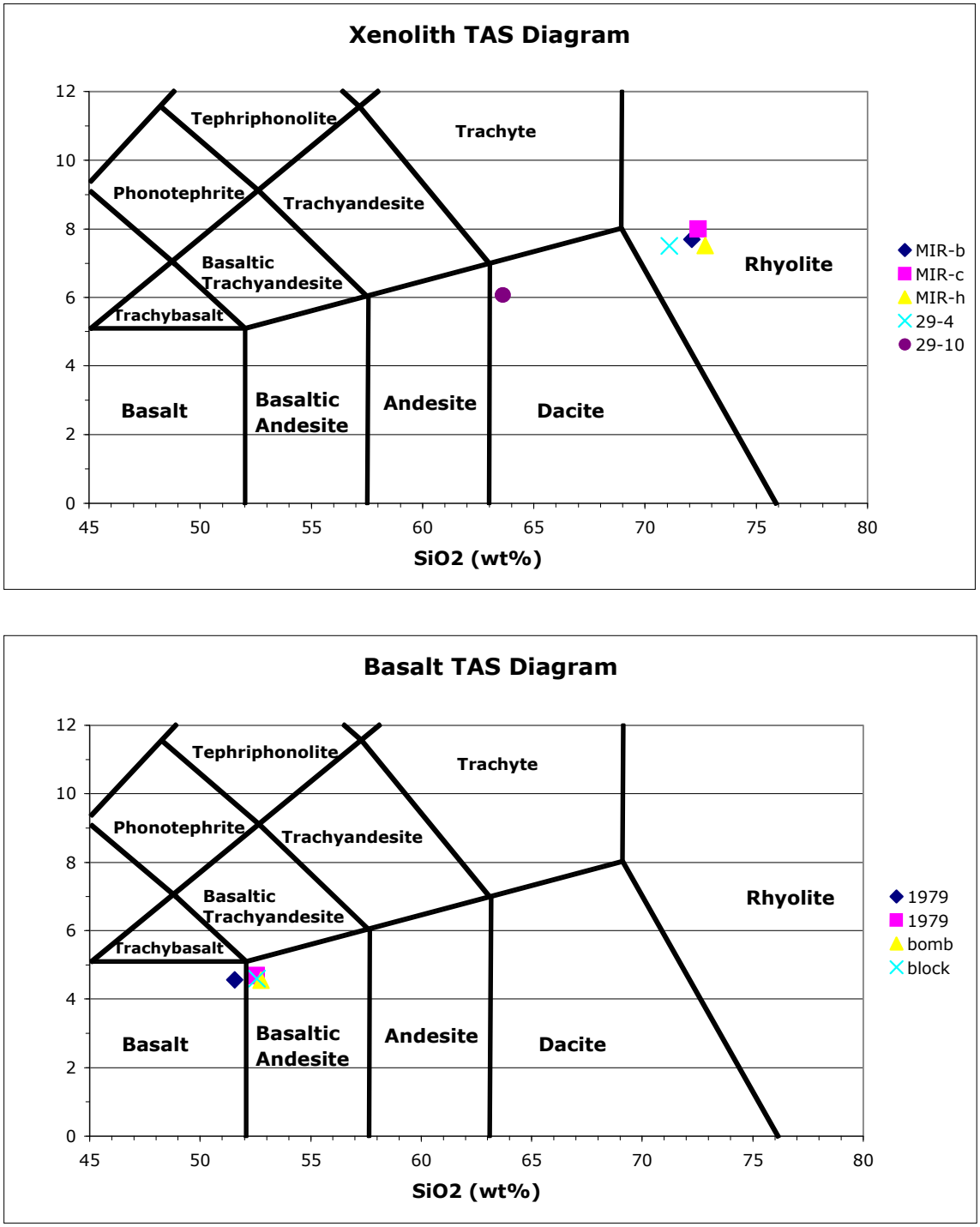

FIGURE 8: Total Alkali (Na_2O+K_2O) versus Silica (TAS) Diagrams for both the xenolith and the basalt in order to classify the type of igneous rock.

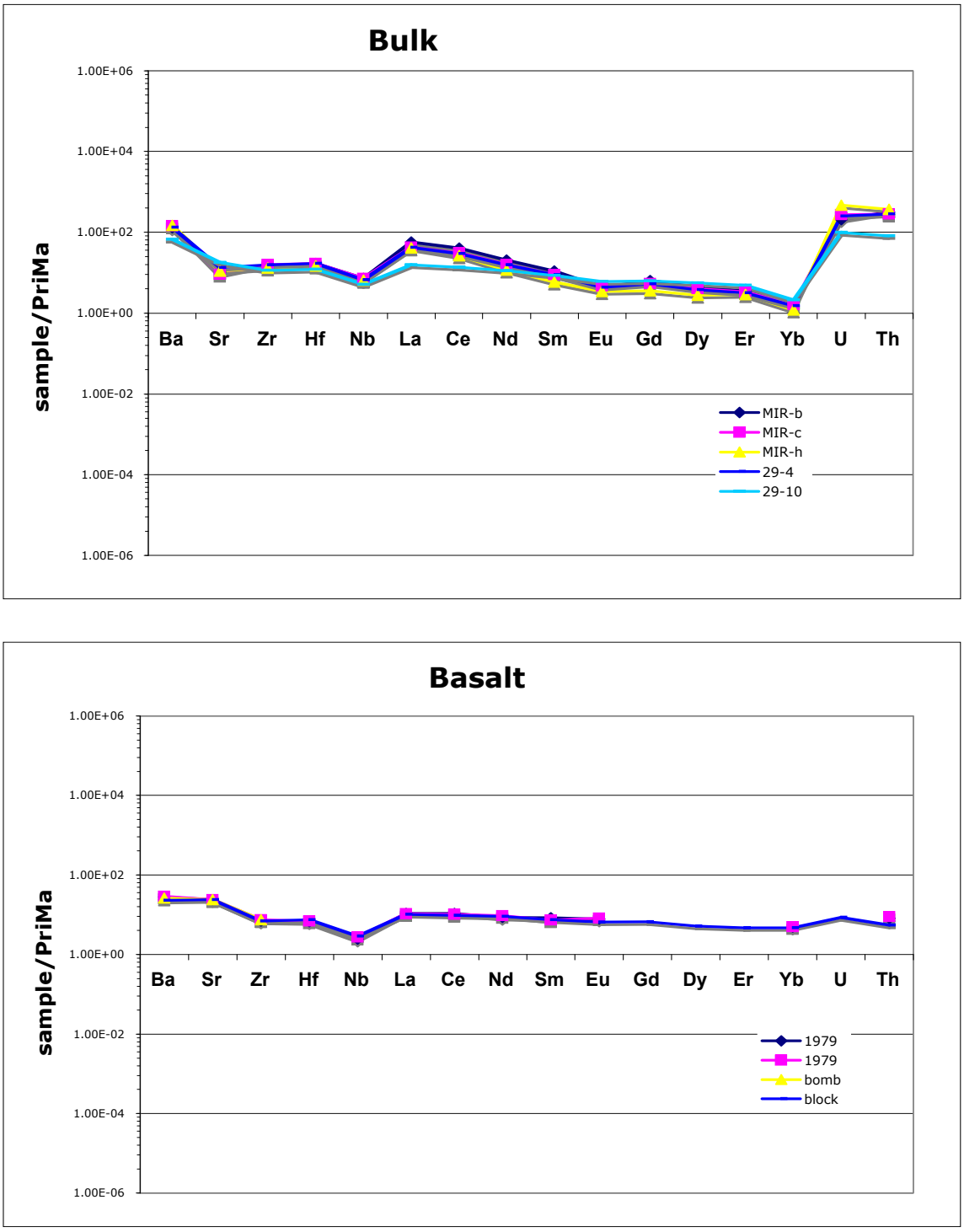

Figure 9: Multi-element plots normalized to primitive mantle (McDonough & Sun, 1995) for the crustal xenolith and basalt using the same scale throughout all the multi-element plots for consistency.

6b. Xenolith EPMA elemental maps

The EPMA elemental maps (Figure 10 and Appendix A) evaluate the concentrations of 9 major elements (Si, Al, K, Ca, Na, Mg, Fe, P, Ti and Mn) in a backscatter image. The elemental map includes an area ~200 μm x 200 μm. The criteria for the glass, as illustrated in figure 10, and also a more detailed Appendix A, were observed to be relatively homogenous in backscatter images along with a moderate abundance of Si (to avoid quartz), as well as K, Ca and Na (to avoid feldspar). Furthermore, a slightly higher abundance of Al relative to quartz and feldspar with minor Mg or Fe was indicative of glass via EPMA elemental maps. My choices for which spots to analyze chemically via EPMA and subsequently via ICP-MS were based on these criteria set up by the maps provided by the EPMA. Appendix A illustrates lasered spots chosen via the various elemental maps. They also show the in-situ chemical analysis spots done by the EPMA (in blue) and the spots ablated and analyzed by the ICP-MS (in red). Each number on the backscattered electron image for each elemental map correlates to the data shown in Appendix A. Figure 10 shows the high Si areas as being quartz; the high K areas as being potassium feldspar, the high Ti and Fe areas that overlap each other are the accessory mineral ilmenite.

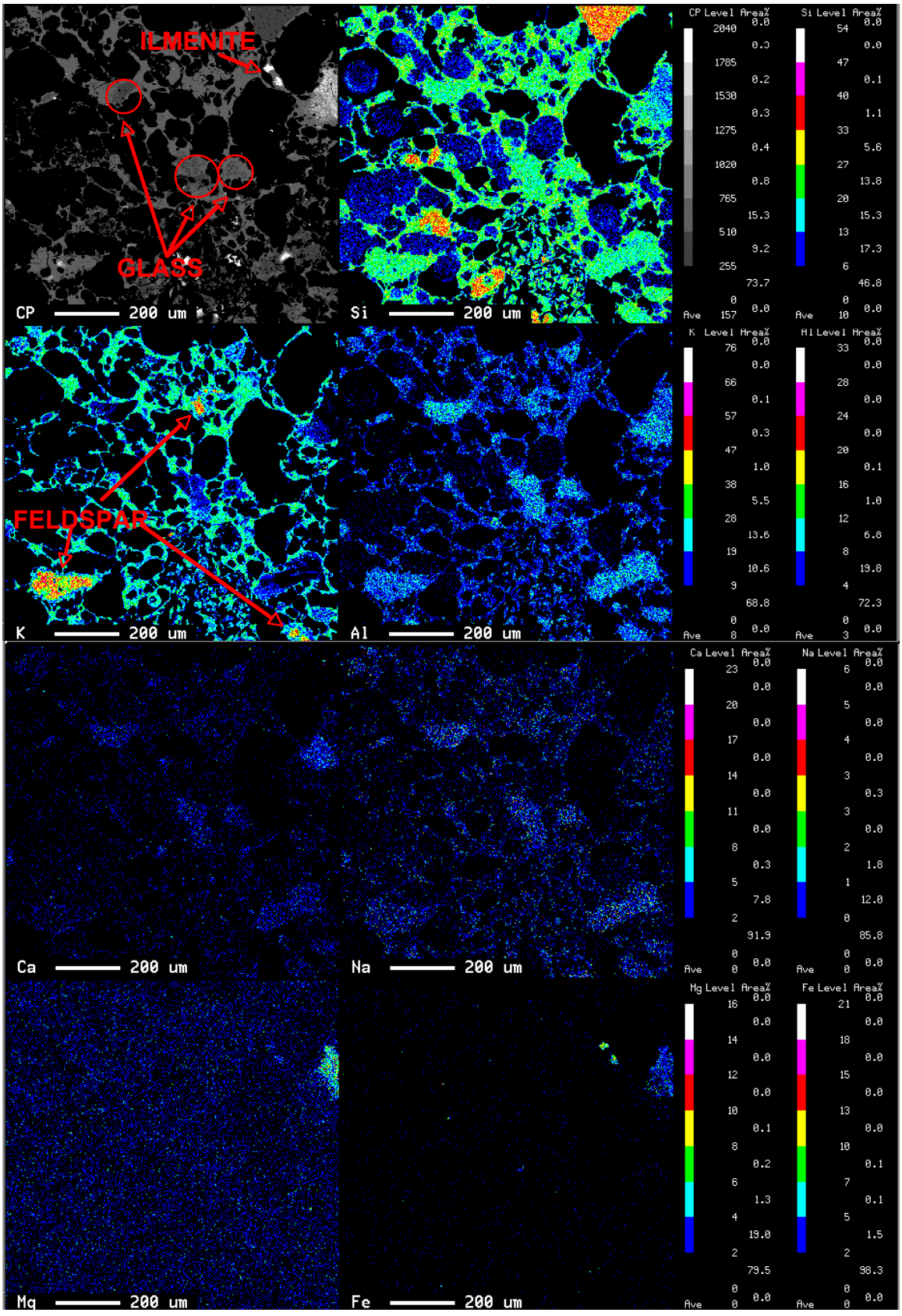
ILMENITE
GLASS
CP 200 um
Si 200 um
FELDSPAR
K 200 um
Al 200 um
Ca 200 um
Na 200 um
Mg 200 um
Fe 200 um

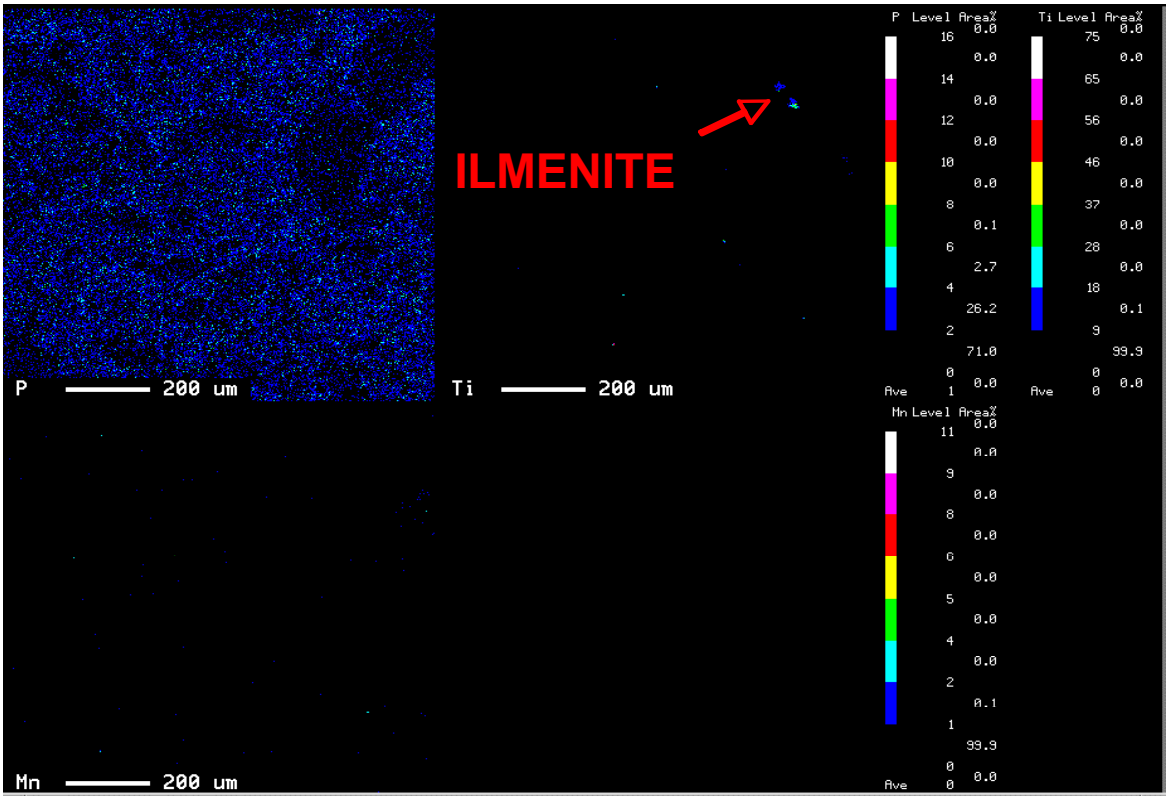

Figure 10: EPMA elemental maps of one of the samples (J-1-spot6b) from the Mirador Volcano (Chile). Backscattered electron image (first image) shows that the uniform colored areas ranging approximately between 510-765 CP level (composition image) are mainly the areas of glass (partial melt). The elemental map also shows levels of concentration of the following elements (Si, K, Al, Ca, Na, Mg, Fe, P, Ti and Mn) and is what is used for the preliminary detection of certain minerals (i.e. feldspars and ilmenite as noted in the figure).

6c. Xenolith EPMA chemical compositions

The EPMA data for glass and minerals is presented in Appendix B. Figure 11 illustrates Harker diagrams contrasting major element oxides with SiO_2 for the bulk xenolith, basalt and microprobed spots of thick sections from the xenolith. The highly potassic points on the graph have been identified as feldspars. Glass and feldspar were not always visibly distinguishable because the texture produced by melting made it difficult to differentiate certain minerals.

The xenolith has low abundances of MnO, MgO (with the exception of the diorite), TiO_2, FeO, Na_2O, CaO, low K_2O (2-4 wt%), low Al_2O_3 (14-16 wt%) relative to the thick sections and basalt analyzed and low P_2O_5 (0.06-0.14 wt%), however, it is still higher than most spots analyzed.

The major elemental chemical abundances for basalt are higher in MgO, FeO, P_2O_5 and TiO_2 than the bulk xenoliths or the microprobed glass spots; additionally, they contain moderate amounts of CaO (7.9-8.2 wt%) with low abundances of MnO, K_2O and Al_2O_3. The microprobed thick sections from the xenoliths overall had low abundances of MgO, TiO_2 and FeO. While there is a decrease in Al_2O_3 and CaO with increase in SiO_2, K_2O does the opposite and increases. There is a wide scatter in abundance of Na_2O and P_2O_5.

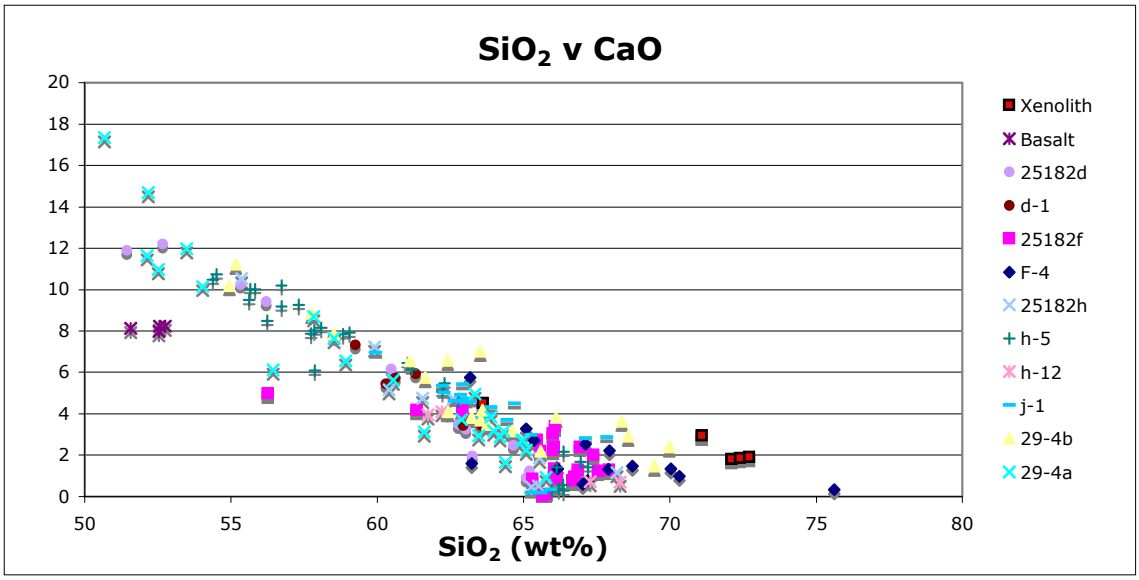
SiO2 v CaO
20
18
16
14
12
10
8
6
4
2
0
50
55
60
65
70
75
80
SiO2 (wt%)
Xenolith
Basalt
25182d
d-1
25182f
F-4
25182h
h-5
h-12
j-1
29-4b
29-4a

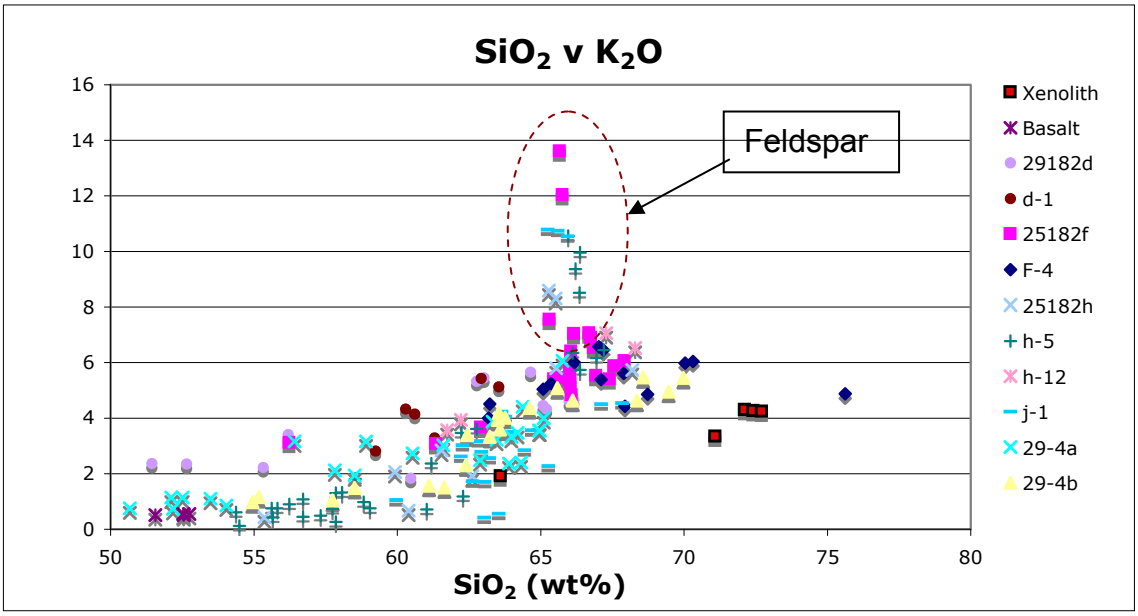
SiO2 v K2O
16
14
12
10
8
6
4
2
0
50
55
60
65
70
75
80
SiO2 (wt%)
Feldspar
Xenolith
Basalt
29182d
d-1
25182f
F-4
25182h
h-5
h-12
j-1
29-4a
29-4b

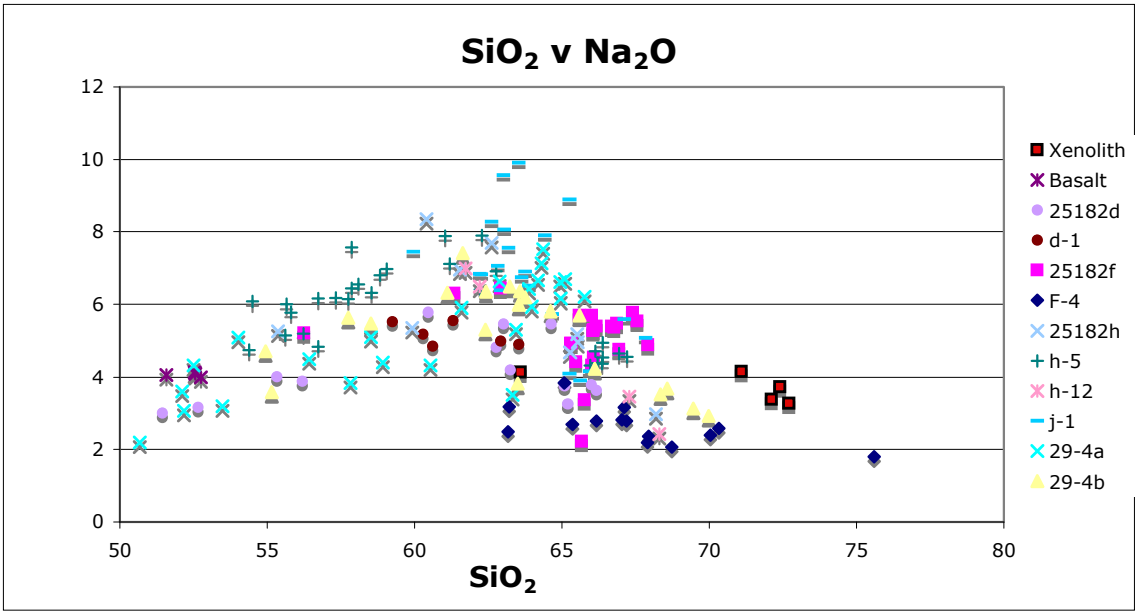
SiO2 v Na2O
12
10
8
6
4
2
0
50
55
60
65
70
75
80
SiO2
Xenolith
Basalt
25182d
d-1
25182f
F-4
25182h
h-5
h-12
j-1
29-4a
29-4b

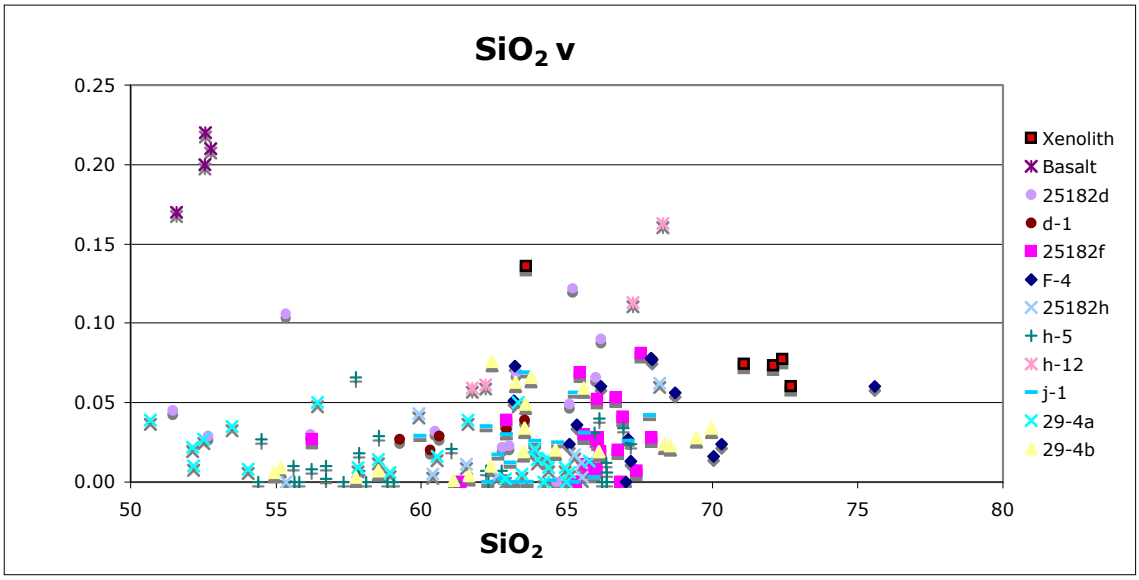
SiO2 v
0.25
0.20
0.15
0.10
0.05
0.00
50
55
60
65
70
75
80
SiO2
Xenolith
Basalt
25182d
d-1
25182f
F-4
25182h
h-5
h-12
j-1
29-4a
29-4b

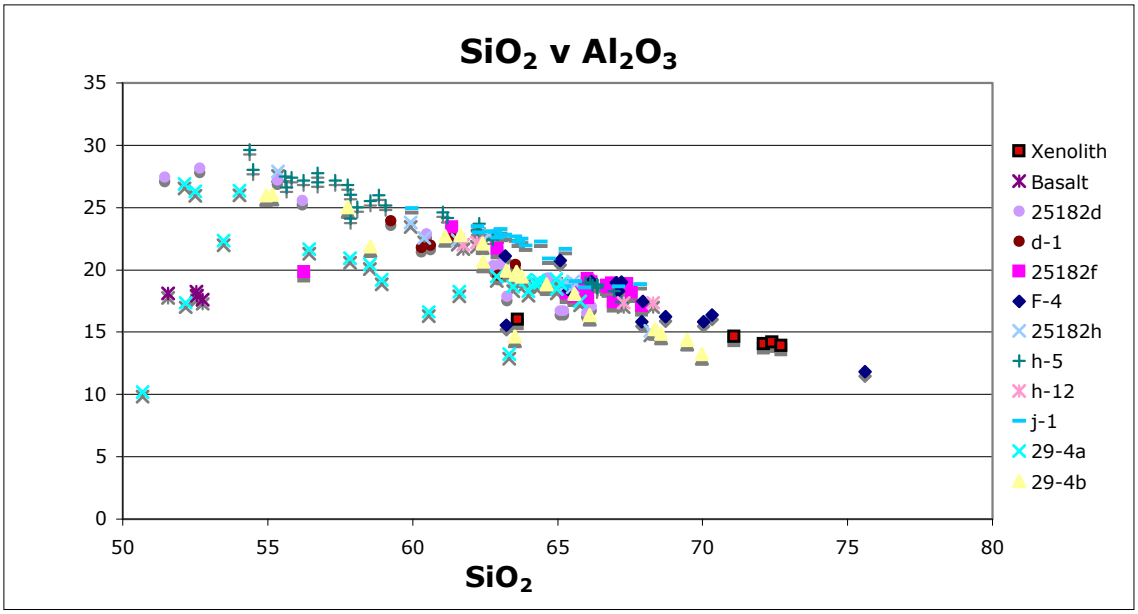
SiO2 v Al2O3
35
30
25
20
15
10
5
0
50
55
60
65
70
75
80
SiO2
Xenolith
Basalt
25182d
d-1
25182f
F-4
25182h
h-5
h-12
j-1
29-4a
29-4b

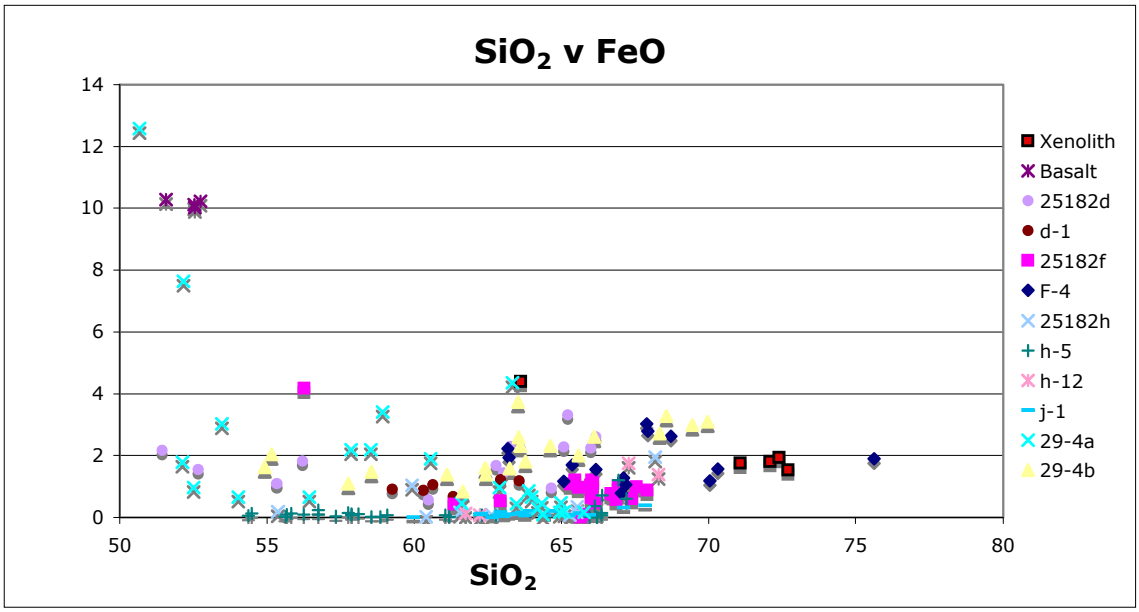
SiO2 v FeO
14
12
10
8
6
4
2
0
50
55
60
65
70
75
80
SiO2
Xenolith
Basalt
25182d
d-1
25182f
F-4
25182h
h-5
h-12
j-1
29-4a
29-4b

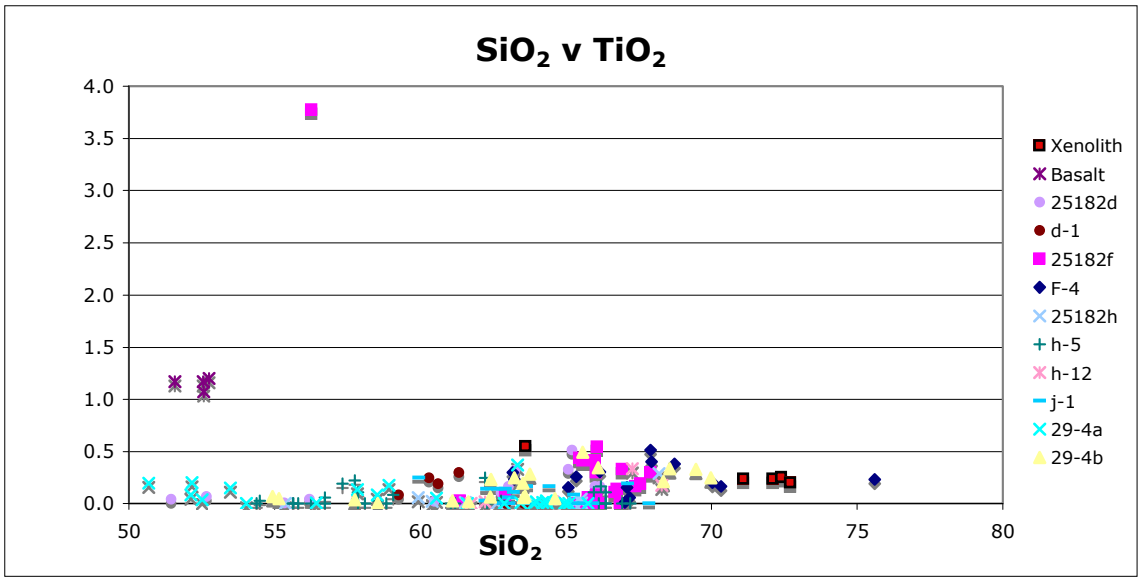
SiO2 v TiO2
4.0
3.5
3.0
2.5
2.0
1.5
1.0
0.5
0.0
50
55
60
65
70
75
80
SiO2
Xenolith
Basalt
25182d
d-1
25182f
F-4
25182h
h-5
h-12
j-1
29-4a
29-4b

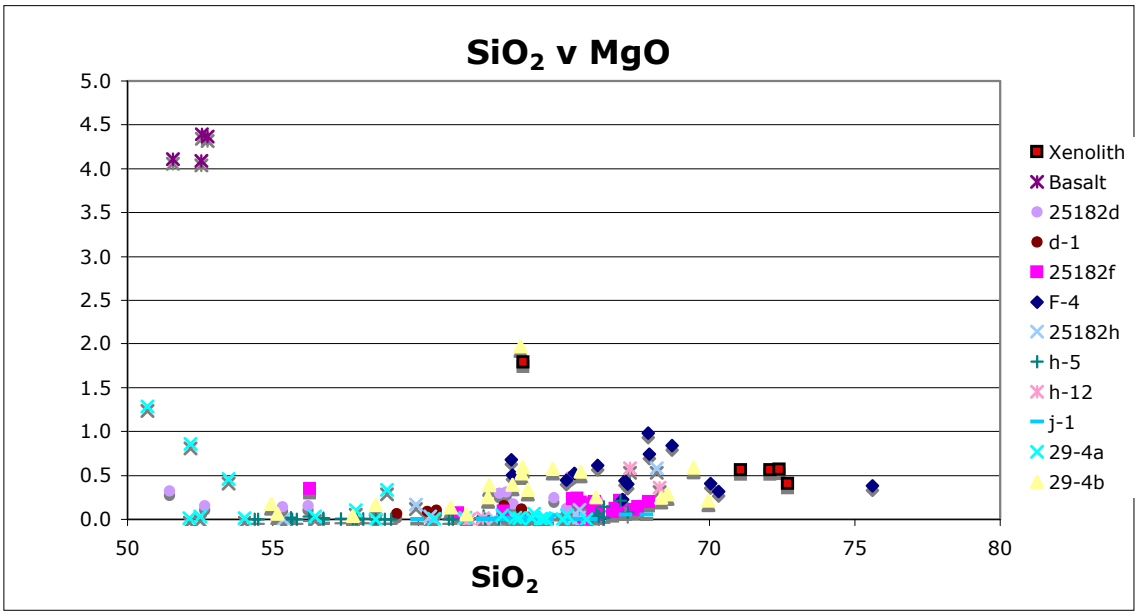
SiO2 v MgO
5.0
4.5
4.0
3.5
3.0
2.5
2.0
1.5
1.0
0.5
0.0
50
55
60
65
70
75
80
SiO2
Xenolith
Basalt
25182d
d-1
25182f
F-4
25182h
h-5
h-12
j-1
29-4a
29-4b

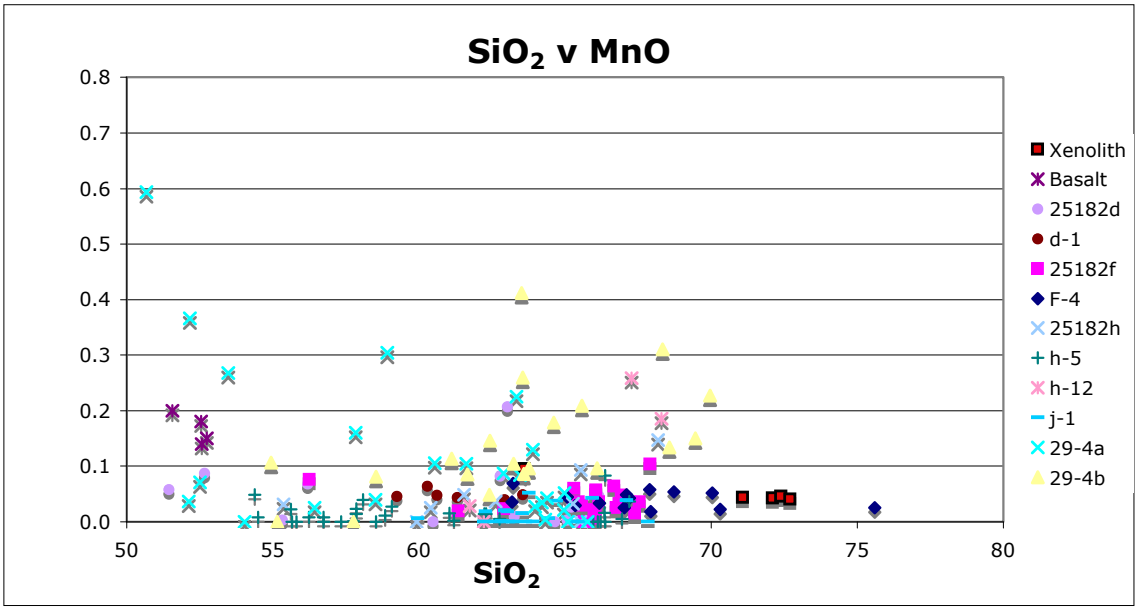

Figure 11: Harker diagrams for major elements for the bulk xenolith, basalt and microprobed spots. Glass and feldspar was not always distinguishable due to the texture produced by partial melting.

6d. LA-ICP-MS results

The LA-ICP-MS results are presented in Appendix B. Figure 12 shows multi-element diagrams for the lasered spots normalized to primitive mantle, on the same logarithmic scale and element order to that of the xenolith and basalt previously shown, to keep uniformity amongst appearance in trends. The diagrams are plotted in order of glass, feldspar and accessory minerals distinguished in alphabetical order. The last 2 plots are plots that seem to have similar trends however are intermediate mixtures of glass and minerals. The intermediate mixtures can be attributed to the 45 µm laser spot size versus the actual size of the certain minerals and/or glass being ablated. The size of the glass at times was smaller than the laser size, however, in order to keep accuracy and

precision high the spot size was not lowered which meant other material was being ablated simultaneously.

Phases were separated into patterns that closely mirrored one another. Published partition coefficients from GERM (earthref.org/GERM) were used to contrast the results from LA-ICP-MS and distinguish phases. The partition coefficients for trace elements (Table 5) of accessory phases found in andesites and rhyolites allowed for patterns within the spidergram to be discerned. The following accessory phases have been found within the xenolith glass regions: Allanite, Apatite, Ilmenite, Sphene and Zircon, as well as, the primary phase, Feldspar.

Partition Coefficients (K_d) of Andesitic and Rhyolitic liquids					
	Sphene	**Apatite**	**Ilmenite**	**Zircon**	**Allanite**
Ba	0.6	0.3	0.00034	nd	nd
Sr	nd	2.1 - 2.4	0.17 - 0.66	nd	1.8
Zr	nd	.636 - .906	1.98 - 10.4	nd	0.29
Hf	10.1	0.73 - 0.878	0.65	2645 - 3742	9.8 - 28
Nb	5.3 - 7.6	nd	65.5 - 144	nd	1.7
Y	nd	162	0.2 - 1.6	71.4	28.8 - 95.5
La	46	8 - 11.9	7.1	7.2 - 26.6	2362 - 2827
Ce	87	29.6	7.8	0.27 - 0.31	2063 - 2494
Nd	152	57.1	7.6	0.26 - 0.55	1400 - 1840
Sm	204	84.8	6.9	0.87 - 3.24	756 - 977
Eu	181	9.22	2.5	0.18 - 1.57	100 - 122
Gd	nd	21.7 - 95.6	nd	6.01	nd
Dy	206	246	4.9	25.2 - 105	123 - 150
Er	nd	275	nd	81.5 - 450	nd
Yb	104	232	4.1	178 - 890	nd
U	9.9	1.8 - 43.7	3.2	254	12 - 17
Th	17.1	17.1 - 41	7.5	22.1	283 - 648

Table 5: Published mineral partition coefficients for Andesitic and Rhyolitic liquids. (*Geochemical Earth Reference Model earthref.org/GERM*)

The glass has a higher Ba abundance with U being more abundant than Th, however, in some cases Th is more abundant. The glass also has very low abundances of HFSE with enrichment in LREE and a Eu anomaly. The feldspar has a high abundance

of Ba and Sr with no HFSE and very low, many under detection limit, abundances of the rare earths, however, an affinity to LREE over HREE. Furthermore feldspar has low abundances of U and Th.

In the accessory phases, allanite has LREE enrichment with an enrichment in Th over U and low abundances of HFSE. Apatite has a slight LREE enrichment and a slight U abundance over Th. Moreover, on the apatite multi-element diagram the upper (pink) pattern is a few orders of magnitude larger than the lower (blue) pattern. The upper pattern is believed to possibly be monazite because, like apatite, monazite is also a phosphate, however the LREE's and Th are in its chemical formula lending it to be comparatively very enriched in these elements. Ilmenite has a low abundance of HFSE with enrichment in Nb and low abundances of the rare earths with a very small affinity towards the LREE. Sphene has a positive Nb anomaly with a relatively horizontal rare earth pattern. Zircon has very high abundances of HFSE, HREE enrichment and an affinity for U over Th.

I also identified part feldspar and part glass mixes, this occurred while ablating, as in many of the ICP analyses, the product was not homogeneous due to the constraints on size of the laser spot versus size of the small fragment of material in the thick section. The mixture of part feldspar and part glass exhibits trace element behavior for both, high abundances in Ba with no HFSE and a positive Eu anomaly (as in the feldspar), however, LREE enrichment (as in the glass) with varying amounts of U and Th. Mixture 1 and mixture 2 are patterns detected that complement each other, however, do not match a certain known mineral pattern for trace elements and are comprised of glass mixtures with minerals.

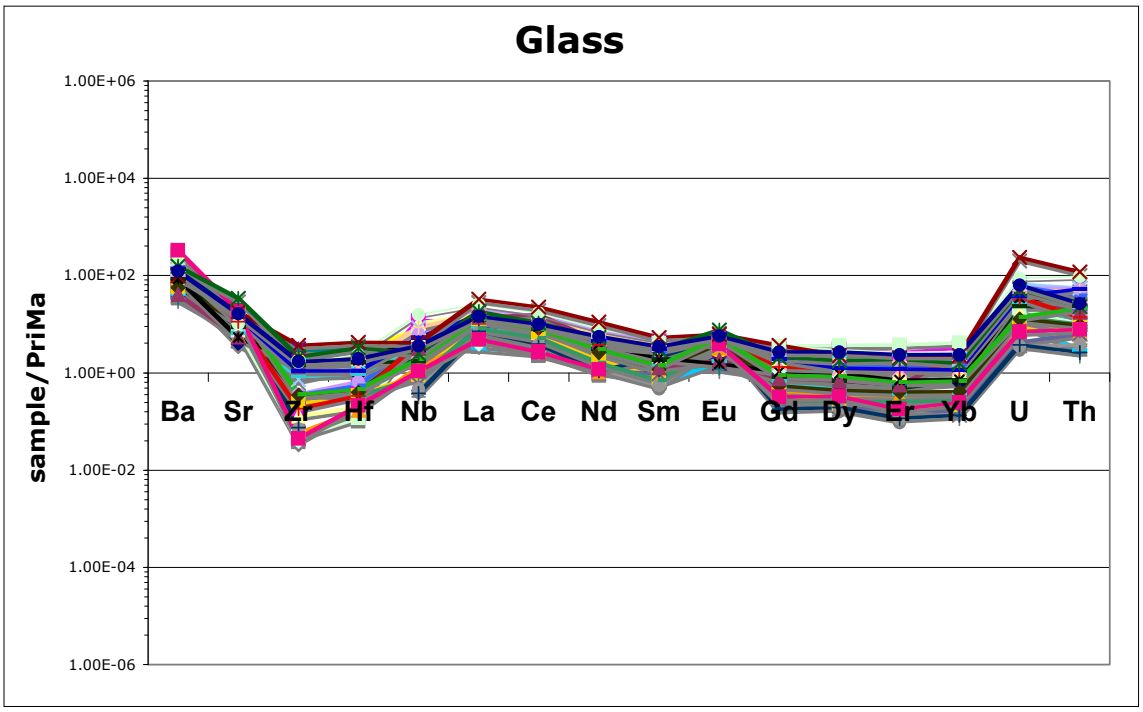
Glass
sample/PriMa
1.00E+06
1.00E+04
1.00E+02
1.00E+00
1.00E-02
1.00E-04
1.00E-06
Ba Sr Zr Hf Nb La Ce Nd Sm Eu Gd Dy Er Yb U Th

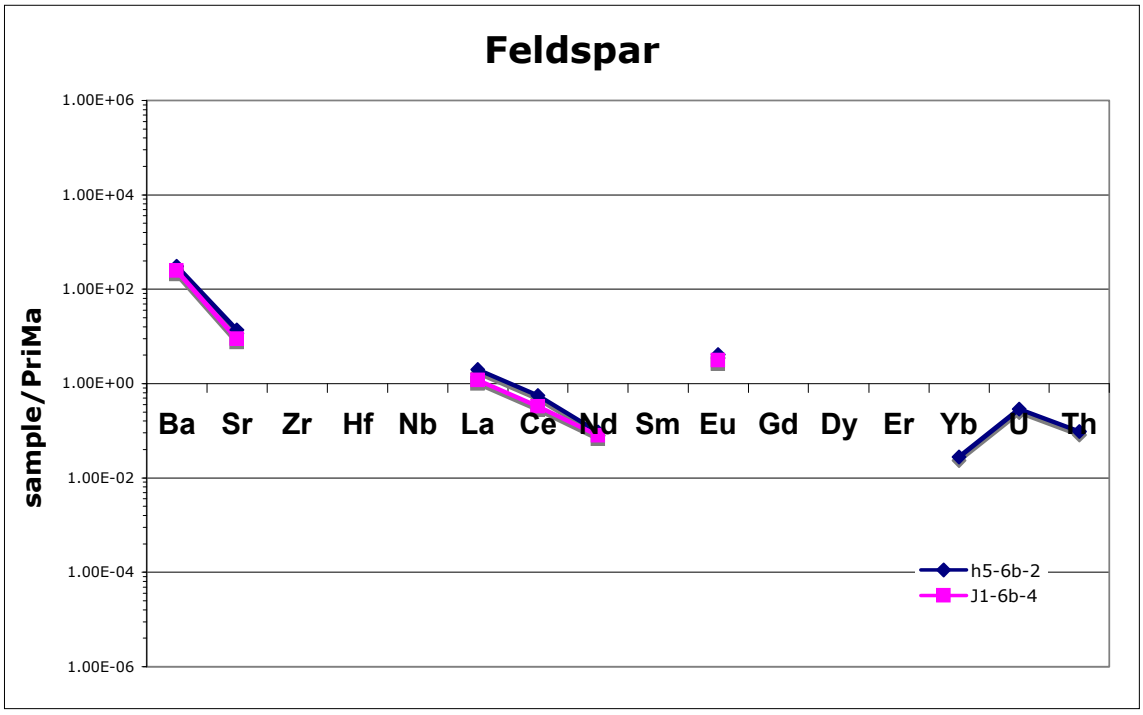
Feldspar
sample/PriMa
1.00E+06
1.00E+04
1.00E+02
1.00E+00
1.00E-02
1.00E-04
1.00E-06
Ba Sr Zr Hf Nb La Ce Nd Sm Eu Gd Dy Er Yb U Th
h5-6b-2
J1-6b-4

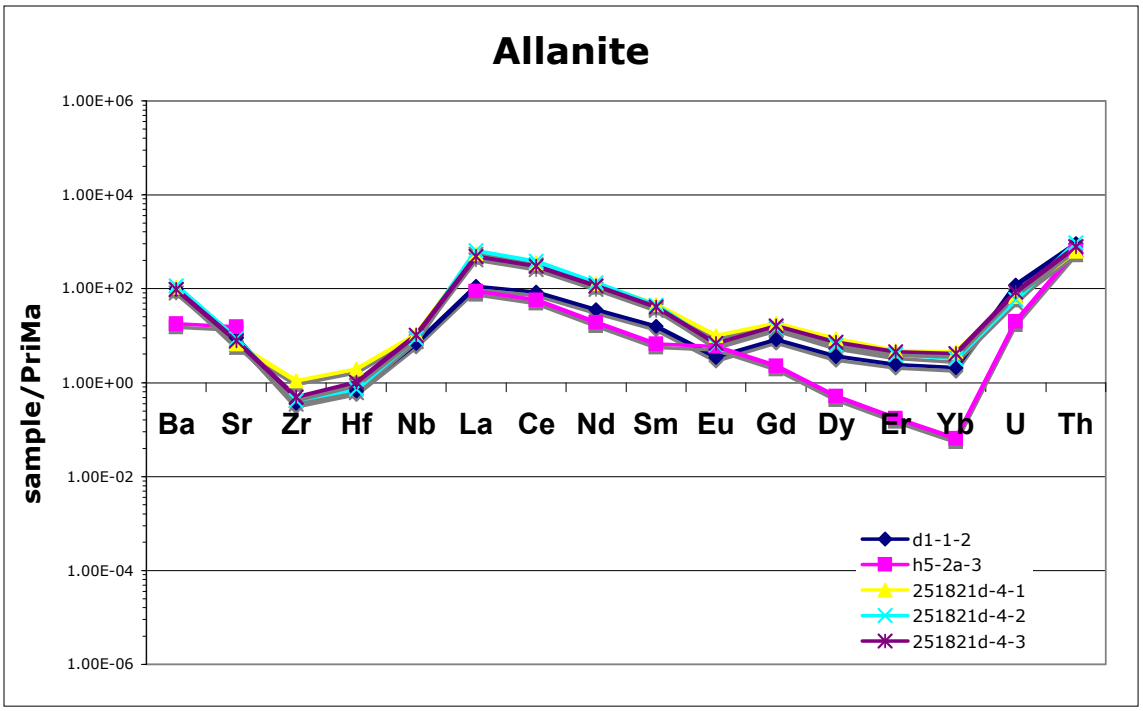
Allanite
1.00E+06
1.00E+04
1.00E+02
1.00E+00
1.00E-02
1.00E-04
1.00E-06
sample/PriMa
Ba Sr Zr Hf Nb La Ce Nd Sm Eu Gd Dy Er Yb U Th
d1-1-2
h5-2a-3
251821d-4-1
251821d-4-2
251821d-4-3

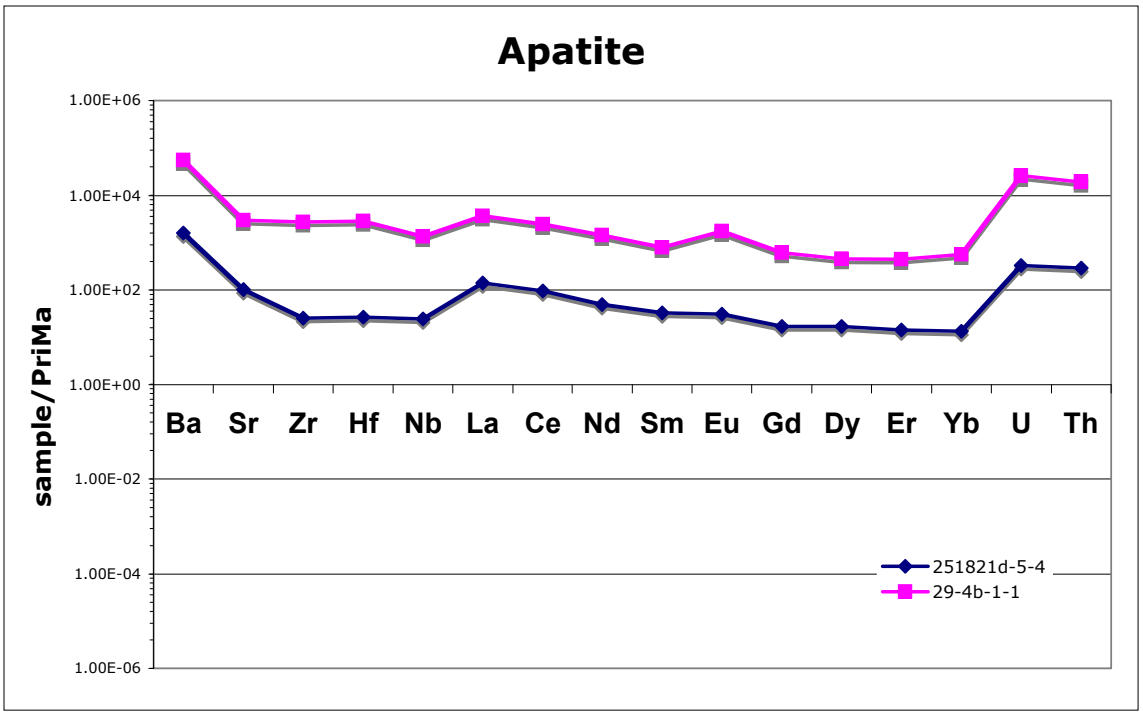
Apatite
1.00E+06
1.00E+04
1.00E+02
1.00E+00
1.00E-02
1.00E-04
1.00E-06
sample/PriMa
Ba Sr Zr Hf Nb La Ce Nd Sm Eu Gd Dy Er Yb U Th
251821d-5-4
29-4b-1-1

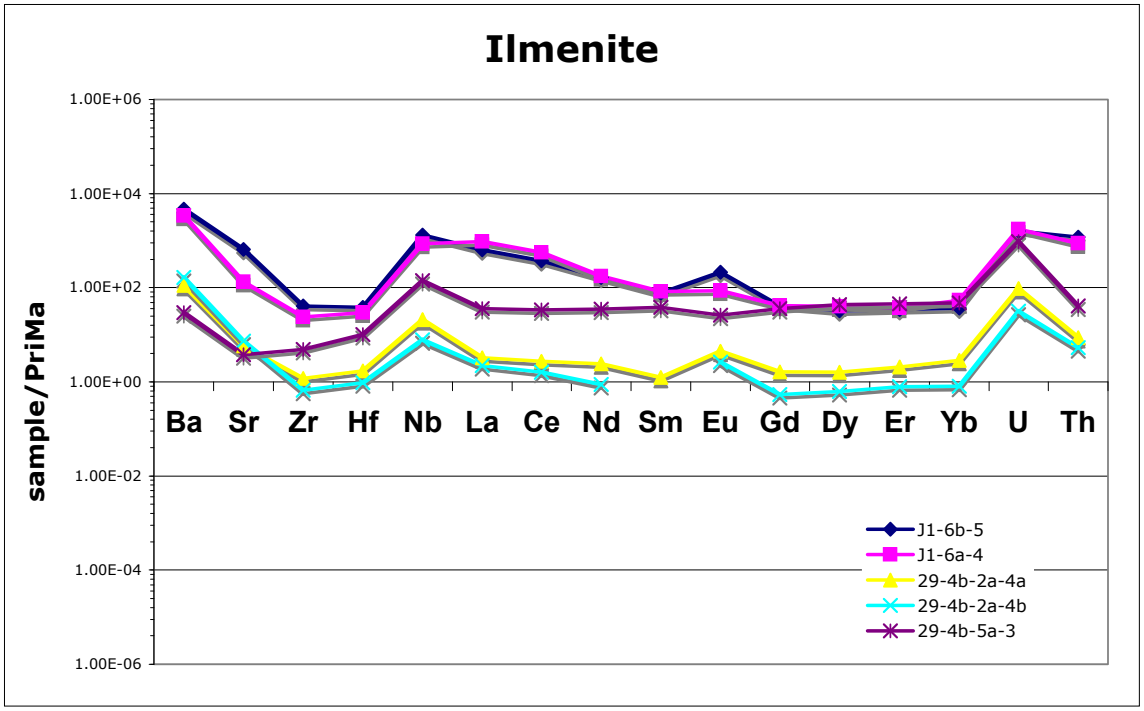
Ilmenite
sample/PriMa
1.00E+06
1.00E+04
1.00E+02
1.00E+00
1.00E-02
1.00E-04
1.00E-06
Ba Sr Zr Hf Nb La Ce Nd Sm Eu Gd Dy Er Yb U Th
J1-6b-5
J1-6a-4
29-4b-2a-4a
29-4b-2a-4b
29-4b-5a-3

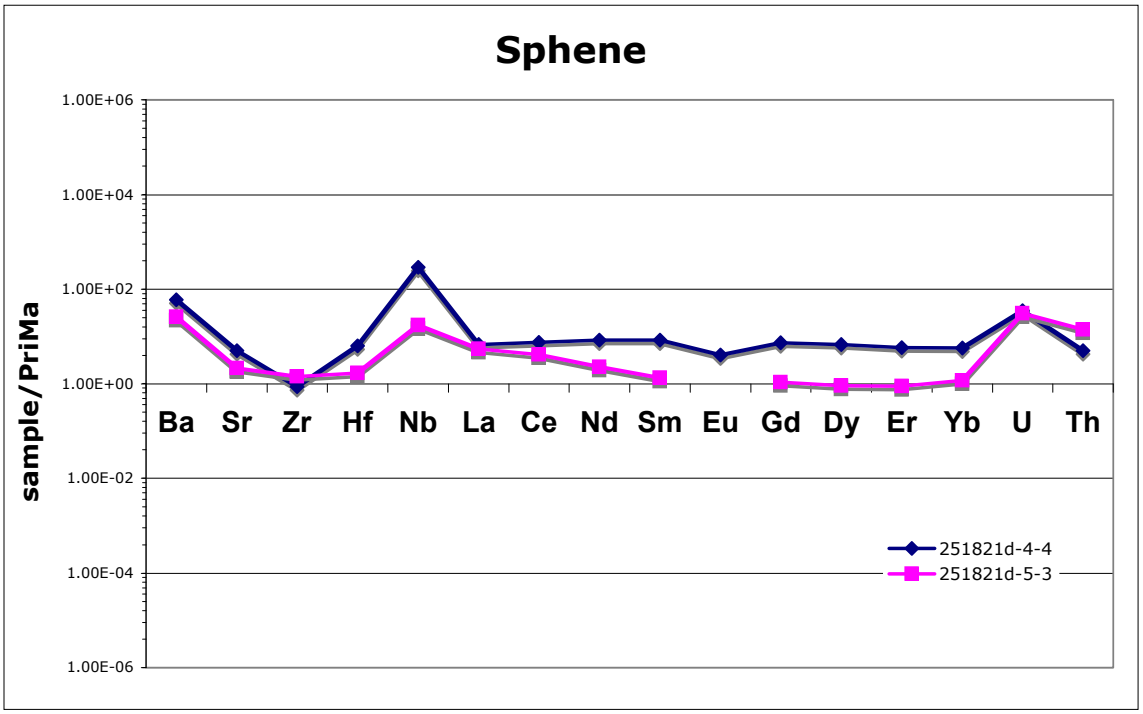
Sphene
sample/PriMa
1.00E+06
1.00E+04
1.00E+02
1.00E+00
1.00E-02
1.00E-04
1.00E-06
Ba Sr Zr Hf Nb La Ce Nd Sm Eu Gd Dy Er Yb U Th
251821d-4-4
251821d-5-3

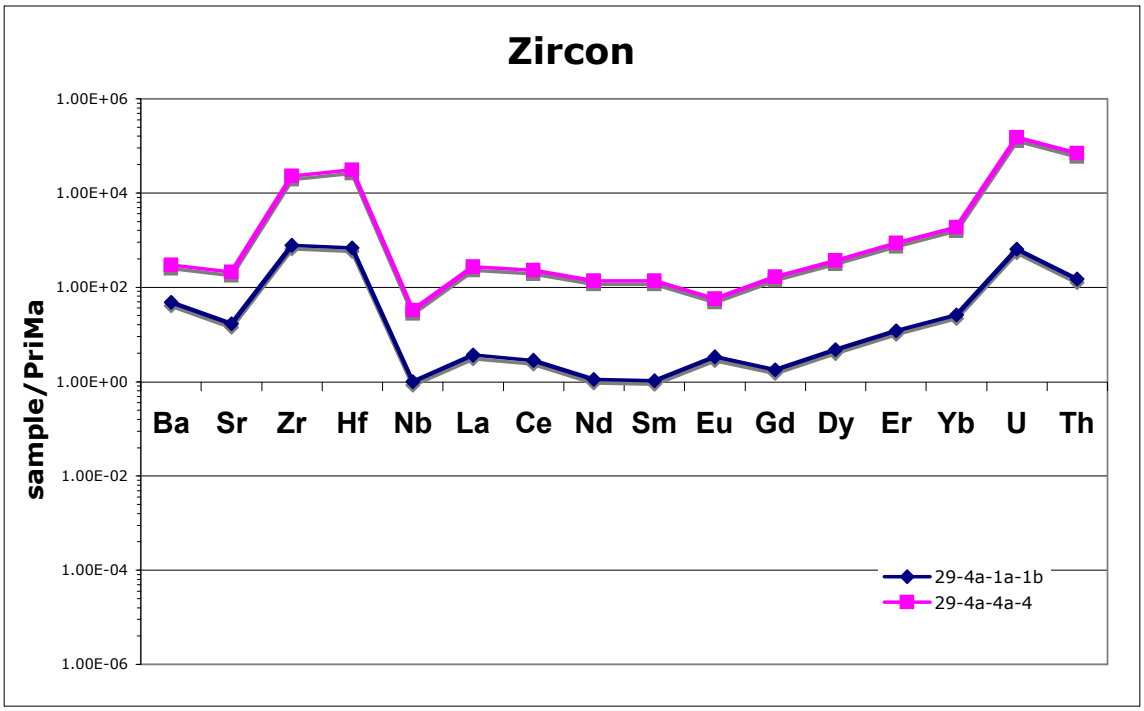
Zircon
1.00E+06
1.00E+04
1.00E+02
1.00E+00
1.00E-02
1.00E-04
1.00E-06
sample/PriMa
Ba Sr Zr Hf Nb La Ce Nd Sm Eu Gd Dy Er Yb U Th
29-4a-1a-1b
29-4a-4a-4

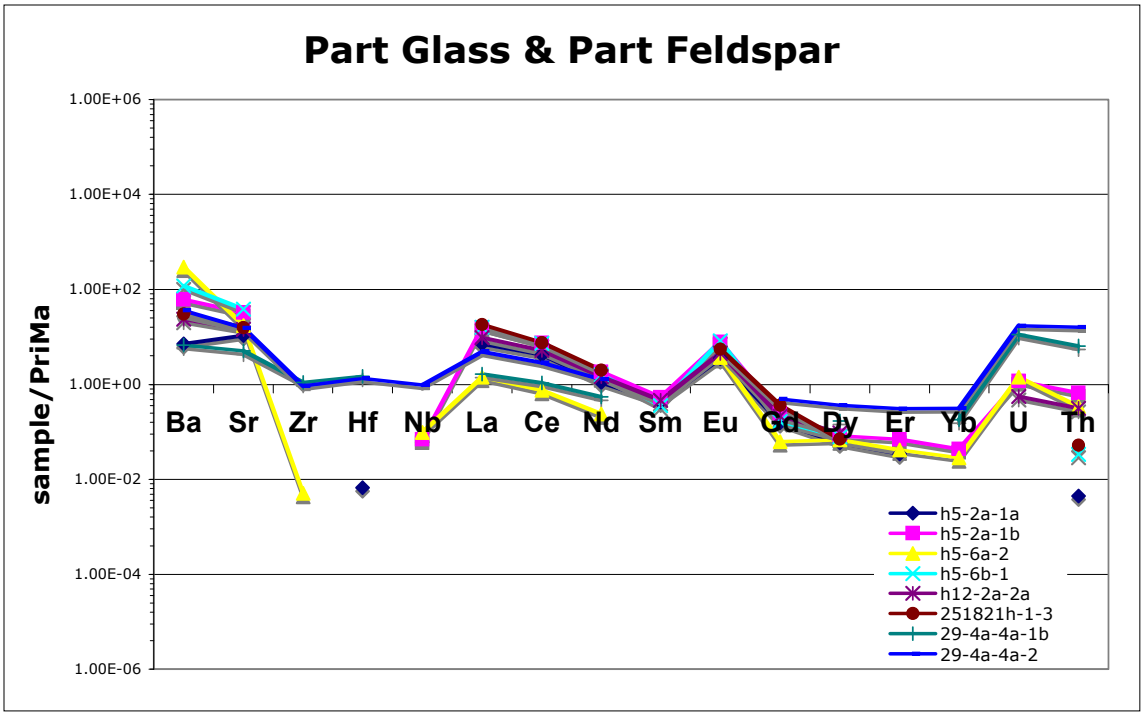
Part Glass & Part Feldspar
1.00E+06
1.00E+04
1.00E+02
1.00E+00
1.00E-02
1.00E-04
1.00E-06
sample/PriMa
Ba Sr Zr Hf Nb La Ce Nd Sm Eu Gd Dy Er Yb U Th
h5-2a-1a
h5-2a-1b
h5-6a-2
h5-6b-1
h12-2a-2a
251821h-1-3
29-4a-4a-1b
29-4a-4a-2

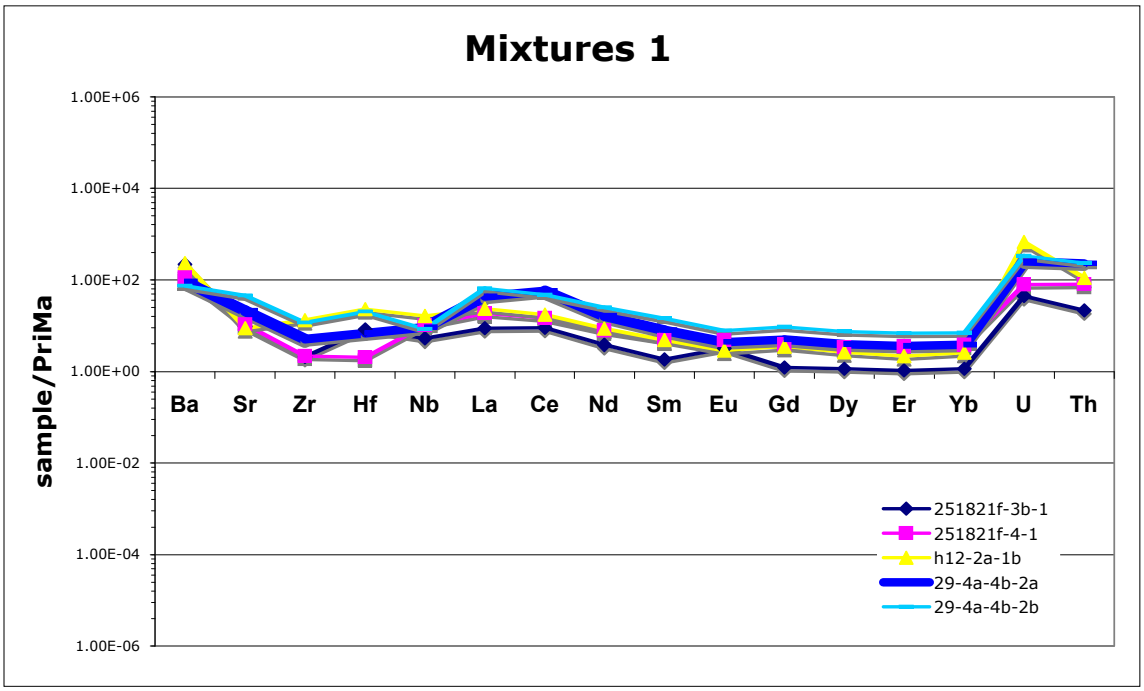

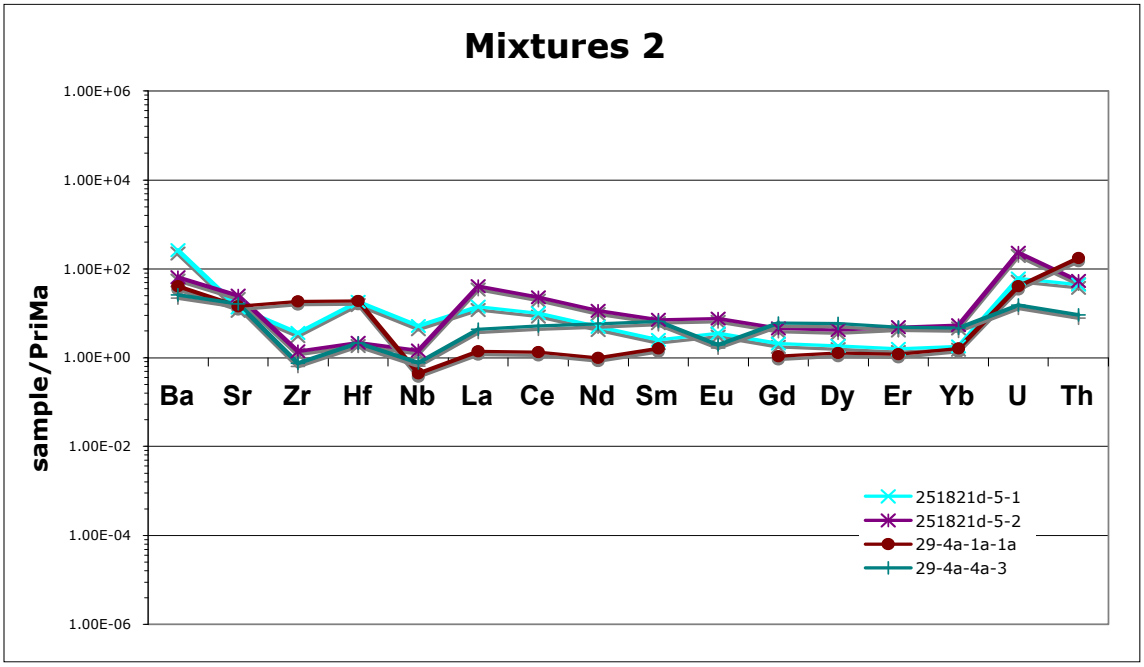

Figure 12: Multi-element diagram (Ba, Sr , REE, U, Th and HFSE) for the glass (partial melt), major mineral (feldspar) and accessory minerals. Analysis normalized to Primitive Mantle (PriMa) (McDonough & Sun, 1995). Mineral diagrams have been classified based on published partition coefficients (Kd) located on the Geochemical Earth Reference Model (GERM) database. Note: Unknown 1 & Unknown 2 represent multi-element diagram patterns that appear to be intermediates (mixtures with glass). Also, when ablating, glass was at times mixed with the accessory mineral due to size constraints.

VII. DISCUSSION

7a. LA-ICP-MS Results

The EPMA maps (Figure 10) allowed preliminary identification of mineral phases and glass (supplemented by optical microscopy), LA ICP-MS analysis of Ba, Sr, REE, U, Th and HFSE (Figure 12) further refined the identification of glass and accessory and major phases by comparison with published partition coefficients. Unfortunately, as a result of limitations on the laser spot size, in order to keep the accuracy of our analysis consistent, our spot size was not changed. Therefore, some of the accessory minerals were smaller than the spot size leading to inevitable glass mixing in many of the samples ablated. Moreover, since the EPMA elemental maps are only surficial to the sample and the laser ablates downward for a total of 2 minutes, it also ablated through other phases, not just the intended mineral phase chosen via the map. Consequently, once fully analyzed, areas once thought to be certain minerals proved to be others with some undistinguishable patterns emerging (Figure 12: Mixture 1 and Mixture 2).

7b. Interpretation of trace element ratios relative to the bulk xenolith

In Figure 13, Ba/Th v Th/U ratios in glass compared to bulk xenoliths are plotted (data in Table 6). The plot shows that partial melting has fractionated U, Th and Ba compared with the whole rock xenolith. Partial melts mostly display a U excess (and in some cases Th excess) and strong Ba excess. The results support the idea that partial melting can indeed play a role in altering the U-series signature of the ascending magma by altering the concentrations and contributing either U and/or Ba.

	Ba/Th	Th/U	Ba/Th (sample/WR)	Th/U (sample/WR)
XENOLITH			(based on rhyolitic xenolith average)	
MIR-b	33.10	4.00	0.91	1.00
MIR-c	41.80	3.61	1.15	0.90
MIR-h	32.81	4.17	0.90	1.04
29-4	38.14	4.27	1.05	1.06
29-10	66.34	2.71	1.82	0.67
Basalt				
1979	289.06	nd	nd	nd
1979	270.42	nd	nd	nd
bomb	nd	nd	nd	nd
block	406.00	2.53	11.14	0.63

Thick Sections	Ba/Th	Th/U	Ba/Th (sample/WR)	Th/U (sample/WR)
25182d-3-1	837.84	1.54	22.98	0.38
25182d-4-1	14.04	36.41	0.38	9.07
25182d-4-2	9.97	64.35	0.27	16.03
25182d-4-3	10.05	36.20	0.28	9.02
25182d-4-4	988.03	0.56	27.10	0.14
25182d-5-1	498.07	2.85	13.66	0.71
25182d-5-2	101.51	0.89	2.78	0.22
25182d-5-3	153.52	1.78	4.21	0.44
25182d-5-4	457.20	3.44	12.54	0.86
d1-1-1	201.14	3.22	5.52	0.80
d1-1-2	9.01	29.31	0.25	7.30
d1-1-3	284.72	2.65	7.81	0.66
d1-2-1	180.41	3.65	4.95	0.91
d1-2-2	289.45	3.87	7.94	0.96
d1-2-3	312.75	2.54	8.58	0.63
25182f-3a-1	238.45	4.51	6.54	1.12
25182f-3a-2	1160.48	1.03	31.83	0.26
25182f-3a-3	827.11	2.53	22.68	0.63
25182f-3b-1	856.12	1.91	23.48	0.48
25182f-3b-2	1103.41	1.59	30.26	0.40
25182f-3b-3	1589.26	1.28	43.59	0.32
25182f-4-1	117.94	3.97	3.23	0.99
f4-1-2	888.96	1.43	24.38	0.36
f4-1-3	416.03	1.93	11.41	0.48
f4-2-1	376.84	1.89	10.34	0.47
f4-2-2	291.65	2.35	8.00	0.59
f4-3-1	252.13	2.88	6.92	0.72
f4-3-2	291.85	0.97	8.00	0.24
f4-3-3	294.58	2.73	8.08	0.68

25182h-1-1a	486.80	5.99	13.35	1.49
25182h-1-1b	218.97	5.50	6.01	1.37
25182h-1-2	129.65	6.19	3.56	1.54
25182h-1-3	47083.33	-	1291.32	-
25182h-1-4	3599.51	4.27	98.72	1.07
h5-2a-1a	130277.78	-	3573.05	-
h5-2a-1b	7590.23	2.23	208.17	0.55
h5-2a-2	487.14	2.98	13.36	0.74
h5-2a-3	2.29	125.01	0.06	31.15
h5-2b-1	1894.33	3.03	51.95	0.75
h5-2b-2	481.87	4.70	13.22	1.17
h5-2b-3	3542.73	2.19	97.16	0.55
h5-6a-1	932.44	3.84	25.57	0.96
h5-6a-2	70765.09	0.94	1940.83	0.23
h5-6b-1	288570.37	-	7914.43	-
h5-6b-2	265264.47	1.31	7275.24	0.33
h12-2a-1	176.16	4.27	4.83	1.06
h12-2a-1b	173.44	0.65	4.76	0.16
h12-2a-2a	6091.63	2.20	167.07	0.55
J1-6a-1a	582.21	5.79	15.97	1.44
J1-6a-1b	2765.07	4.17	75.84	1.04
J1-6a-2a	4465.15	2.71	122.46	0.68
J1-6a-2b	590.68	2.78	16.20	0.69
J1-6a-3	296.13	4.02	8.12	1.00
J1-6a-4	321.16	1.98	8.81	0.49
J1-6b-1a	480.94	2.92	13.19	0.73
J1-6b-1b	312.28	2.00	8.56	0.50
J1-6b-2a	196.06	1.67	5.38	0.42
J1-6b-2b	144.13	0.79	3.95	0.20
J1-6b-3	252.88	3.15	6.94	0.78
J1-6b-4	-	-	-	-
J1-6b-5	324.70	2.90	8.91	0.72
29-4a-1a-1a	19.00	17.13	0.52	4.27
29-4a-1a-1b	26.34	0.92	0.72	0.23
29-4a-4a-1a	77.32	2.70	2.12	0.67
29-4a-4a-1b	86.40	2.27	2.37	0.57
29-4a-4a-2	183.63	3.67	5.04	0.92
29-4a-4a-3	232.25	2.35	6.37	0.59
29-4a-4a-4	0.35	1.84	0.01	0.46
29-4a-4b-2a	33.24	3.46	0.91	0.86
29-4a-4b-2b	26.81	2.71	0.74	0.67

29-4b-1-1	236.01	2.87	6.47	0.72
29-4b-2a-1	67.95	1.99	1.86	0.50
29-4b-2a-2a	553.44	1.76	15.18	0.44
29-4b-2a-2b	388.28	1.65	10.65	0.41
29-4b-2a-4a	1065.31	0.36	29.22	0.09
29-4b-2a-4b	2595.07	0.66	71.17	0.16
29-4b-3a-1	102.33	1.07	2.81	0.27
29-4b-3a-2	199.52	0.74	5.47	0.19
29-4b-5a-1	22.14	2.00	0.61	0.50
29-4b-5a-2	102.54	1.74	2.81	0.43
29-4b-5a-3	59.25	0.17	1.62	0.04
29-4b-5a-4	86.09	0.99	2.36	0.25

Table 6: Ba/Th and Th/U Ratios for the xenolith (bulk rock), basalt, and all the lasered spots on the thick sections. The spots correlate to the spots indicated in Appendix A.

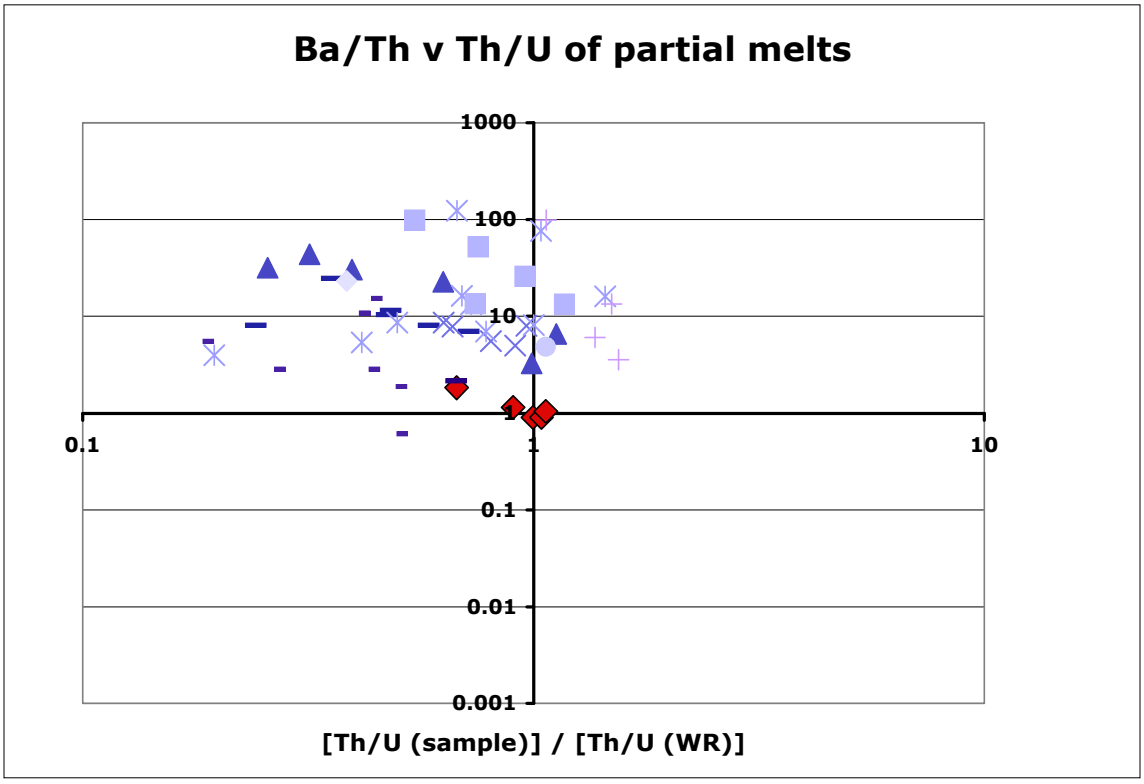

Figure 13: Ba/Th v Th/U ratios for partial melts (sample) compared with the whole rock (WR).

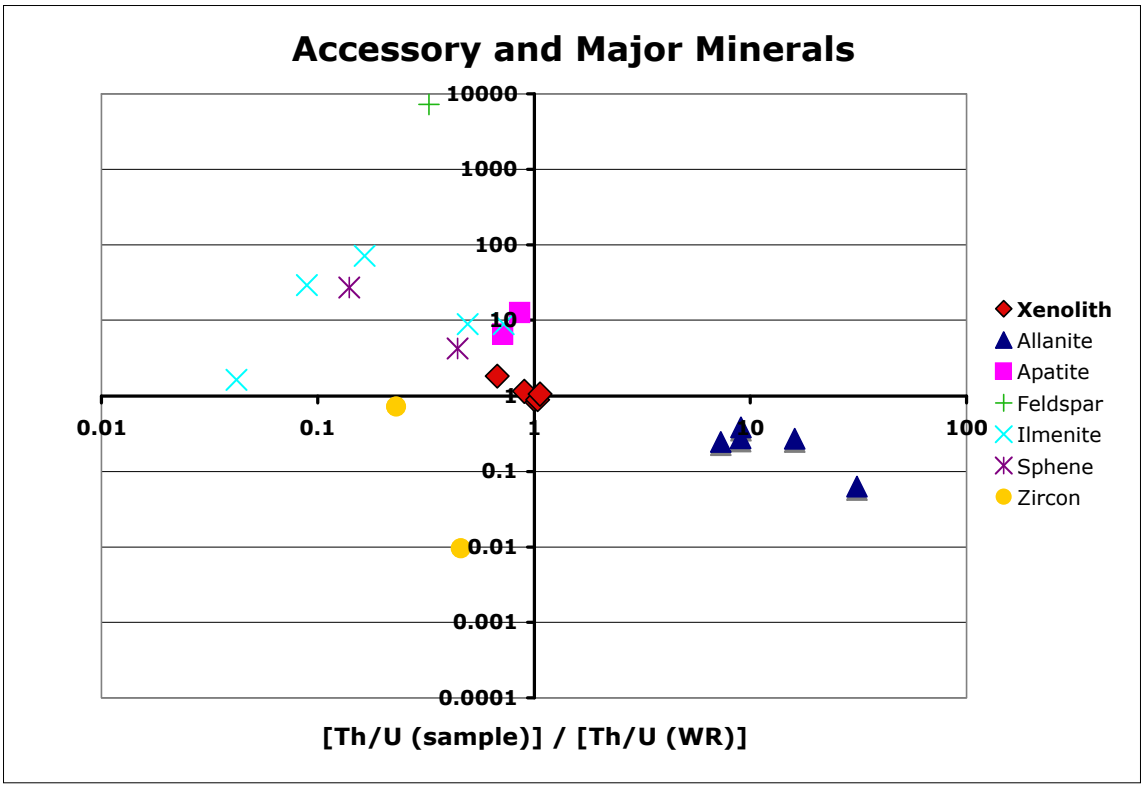

Figure 14: Ba/Th v Th/U ratios for identified accessory minerals and the major mineral (feldspar) compared with the whole rock. Ba/Th and Th/U ratios of the whole rock are an average of the xenoliths, shown as red diamonds.

Accessory minerals show variable effects as 'restite', with Allanite having a large Th excess and Zircon having a U excess (Figure 14). Other minerals mentioned plot in the U excess and Ba excess field much like the partially melted glass. The foremost accessory minerals that are responsible for the fractionation also provide insight on the macroscopic scale of fractionation. Depending on what accessory mineral is present and its abundance relative to the others (i.e. allanite abundance v zircon abundance) it can be inferred where the partial melt will be fractionating and what type of excess will be imparted on the magma. Melting near allanite would leave the partial melt with U and Ba excesses. Alternatively, Zircon, with its affinity for U, causes the opposite reaction in the partial melt leaving it with a Th excess.

7c. Potential impact of fractionation during crustal assimilation

The volcanic suites from the Mirador Volcano are mafic in composition, however, they were not in the crust long enough to mix completely with the partially melted crustal xenoliths. Instead the xenoliths partially melted but remained largely intact. As seen in Figure 7, mixing had already begun occurring in some of the samples collected, while others were completely intact; this was the onset of a separation of the xenolith partial melt from the xenolith. The analyzed glass was melted within the xenolith, while the 'restite' or accessory minerals remained largely intact. Thus, assimilation of a partial melt of granite will alter the U-series signature of magma toward a U-excess, although in fewer circumstances toward a Th-excess, and toward a Ba-excess, so long as the melt and restite can be separated.

The potential for separation of the liquid from the xenolith could be examined with computer modeling. Possible variables are the average pore space created by the vesicles, viscosity and rate at which a partial melt could migrate out of the xenolith without having the xenolith be completely assimilated into the magma. To quantify the amount of disequilibrium that can be imparted by the partial melts onto the magma we must first consider how to separate the melt into the magma. According to Wickham (1987) the upper limit of the critical melt fraction is 50%, in a non-hydrous melt, at which point the viscosity of the melt becomes that of the liquids and assimilation via convection occurs. However, the numerous vesicles in the partially melted xenoliths, in contrast to the non-vesicular nature of the xenoliths not partially melted, implies that there was hydrous melting occurring. Therefore, the melt viscosity will be lower (Huppert and Sparks, 1988) and assimilation will occur at a lower critical melt fraction. Some of the

samples support this idea with the semi-ductile flow of basalt into the perimeter of the xenolith. Bacon (1992) clarifies the possible way in which melt could be extracted out of the xenolith. Since the partial melt from the xenolith has not dissociated from the xenolith under static conditions, a quick depressurization of highly melted rocks could force tensile fractures from which the melt can then separate out of the xenolith.

As highlighted in this section modeling can be done contrasting the rate of eruption with the rate of separation of the partial melts to find out how much can successfully migrate out of the xenolith prior to eruption or complete assimilation. Given these constraints, i.e., the quantity of partial melt and the volume of the magma in the chamber, it can be quantified how much of a U and/or Ba excess the partial melt will impart on the magma chamber. These conditions should be taken into consideration but are beyond the scope of this research.

VIII. CONCLUSIONS AND FUTURE DIRECTIONS

LA-ICP-MS analysis shows that quenched partial melts do indeed have ratios of U, Th and Ba that are different from the bulk granitic xenoliths, thus establishing that partial melting causes fractionation of these elements. The amount of fractionation varies and could be influenced by proximity to accessory minerals that contain excesses of either element. Moreover, accessory minerals are the slower minerals to dissolve into the melt given their chemistry and abundance throughout the xenolith relative to the glass. Partial melts, like the ones analyzed in this study, and accessory minerals should display disequilibrium among U-series isotopes, such as ^{238}U, ^{230}Th and ^{226}Ra (assuming Ba-like behavior), and selective assimilation or mixing of melt or restite into magma could result in U-series disequilibrium effects on the contaminated magma.

Potential future research directions could include using a Secondary Ion Mass Spectrometer (SIMS) to further improve analyses for trace elements because of its much smaller spot size compared to the LA-ICP-MS. The smaller spot size could afford more homogenous selection of areas to analyze. Also, deconvolution of the mixed analyses should be done to figure out what minerals are in the mixtures. Finally, a detailed modeling of the conditions needed to separate melt and the restite including pore space along with rate of migration and viscosity can be done.

REFERENCES

Bacon, C.R., 1992. Partially melted granodiorite and related rocks ejected from Crater Lake caldera, Oregon. Trans Royal Society of Edinburgh: Earth Sciences 83, 27-43.

Berlo, K., Turner, S., Blundy, J., Hawkesworth, C., 2004. The extent of U-series disequilibria produced during partial melting of the lower crust with implications for the formation of the Mount St. Helens dacites. Contrib Mineral Petrol 148, 122-130.

Blundy, J., Wood, B., 2003. Mineral-melt partitioning of uranium, thorium and their daughters. In: Bourdon, B., Henderson, G., Lundstrom, C., Turner, S., (eds), 2003. Introduction to U-series Geochemistry. Reviews in Mineralogy and Geochemistry 52, 59-123.

Bourdon, B., Worner, G., Zindler, A., 2000. U-series evidence for crustal involvement and magma residence times in the petrogenesis of Parinacota volcano, Chile. Contrib Mineral Petrol 139, 458-469.

Cembrano, J., Lavenu, A., Yañez, G., Riquelme, R., Garcia, M., Gonzalez, G., Herail, G., 2007. Neotectonics, 231-262. In: Moreno, T., Gibbons, W. The Geology of Chile. UK: The Geological Society, 2007.

Charlier, B., Zellmer, G., 2000. Some remarks on U-Th mineral ages from igneous rocks with prolonged crystallization histories. Earth and Planetary Science Letters 183, 457-469.

Davidson, J., Tepley III, F., Palaczb, Z., Meffan-Mainb, S., 2001. Magma recharge, contamination and residence times revealed by in situ laser ablation isotopic analysis of feldspar in volcanic rocks. Earth and Planetary Science Letters 184, 427-442.

Dickin, A.P., Radiogenic Isotope Geology. Cambridge University Press, 1997: 325.

Faure, G., Mensing, T.M. Isotopes: principles and applications 3rd ed. John Wiley & Sons, Inc., 2005.

Garrison, J., Davidson, J., Reid., M., Turner, S., 2006. Source versus differentiation controls on U-series disequilibria: Insights from Cotopaxi Volcano, Ecuador. Earth and Planetary Science Letter 244, 548-565.

Hermann, J., 2002. Allanite: thorium and light rare earth element carrier in subducted crust. Chemical Geology 192, 289-306.

Huang, F., Gao, L., Lundstrom, G.C., 2008. The effect of assimilation, fractional crystallization, and ageing on U-series disequilibria in subduction zone lavas. Geochimica et Cosmochimica Acta 72, 4136-4145.

Huppert, H.E., Sparks, R.S., 1998. The fluid dynamics of crustal melting by injection of basaltic sills. Trans Royal Society of Edinburgh: Earth Sciences 79, 237-243.

Klemme, S., Dalpé, C., 2003. Trace-element partitioning between apatite and carbonatite melt. Am Miner 88, 639-646.

Knesel, K.M., Turner, S.P., Davidson, J.P., in prep. U-series isotopic disequilibrium produced during experimental melting of granitic upper crust: implications for shallow-level crustal assimilation and pluton remobilization. Earth and Planetary Science Letters.

Lopez-Escobar, L., Moreno, H., 1981. Erupcion de 1979 del volcan Mirador, Andes del Sur, 40 degrees 21'S.; Caracteristicas geoquimica de las lavas y xenolitos graniticos. Eruption in 1979 of the Mirador Volcano, Southern Andes; geochemical characteristics of the lavas and granitic inclusions. Revista Geologica de Chile 13 & 14,17-33.

McDonough, W.F., Sun, S. -s., 1995. The composition of the Earth. Chemical Geology 120, 223-253.

Munizaga, F., Herve, F., Drake, R., Pankhurst, R.J., Brook, M., 1988. Geochronology of the Lake region of South Central Chile (39°-42°S): Preliminary results. Journal of South American Earth Sciences 1, N°3, 309-316.

Snyder, D.C., Widom, E., Pietruszka, A.J., Carlson, R.W., Schmincke, H., 2007. Time scales of formation of zoned magma chambers: U-series disequilibria in the Fogo A and 1563 A.D. trachyte deposits, Sao Miguel, Azores. Chemical Geology 239, 138-155.

Stern, R.J., 2002. Subduction Zones. Revue of Geophysics 40, 4.

Stern, R.J., Moreno, H., Lopez-Escobar, L., Clavero, J.E., Lara, L.E., Naranjo, J.A., Parada, M.A., Skewes, M.A., 2007. Chilean volcanoes, 147-178. In: Moreno, T., Gibbons, W. The Geology of Chile. UK: The Geological Society, 2007.

Tiepolo, M., Oberti, R., Vannucci, R., 2002. Trace-element incorporation in titanite: constraints from experimentally determined solid/liquid partition coefficients. Chemical Geology 191: 105-119.

Turner, S., Bourdon, B., Gill, J., 2003. U-series isotopes and magma genesis at convergent margins. Rev Mineral Geochem 52, 255-315.

Turner, S., Evans, P., Hawkesworth, C., 2001. Ultrafast source-to-surface movement of melt at island arcs from ^{226}Ra-^{230}Th systematics. Science 292, 1363-1366.

von Huene, R., Scholl, D.W., 1991. Observations at convergent margins concerning sediment subduction, subduction erosion, and the growth of continental crust. Revue of Geophysics 29, 279-316.

White, K., 1988. “Residence” time of Mirador xenoliths in magma. Unpublished Undergraduate Research Project (supervised by Dr. Rosemary Hickey), Department of Geology, Florida International University.

Wickham, S.M., 1987. The segregation and emplacement of granitic magmas. Journal of Geological Society London 144, 281-297.

Appendix A - Electron Microprobe Maps with chosen spots for chemical in situ analysis (blue spots) and Laser Ablation ICP-MS (red spots)

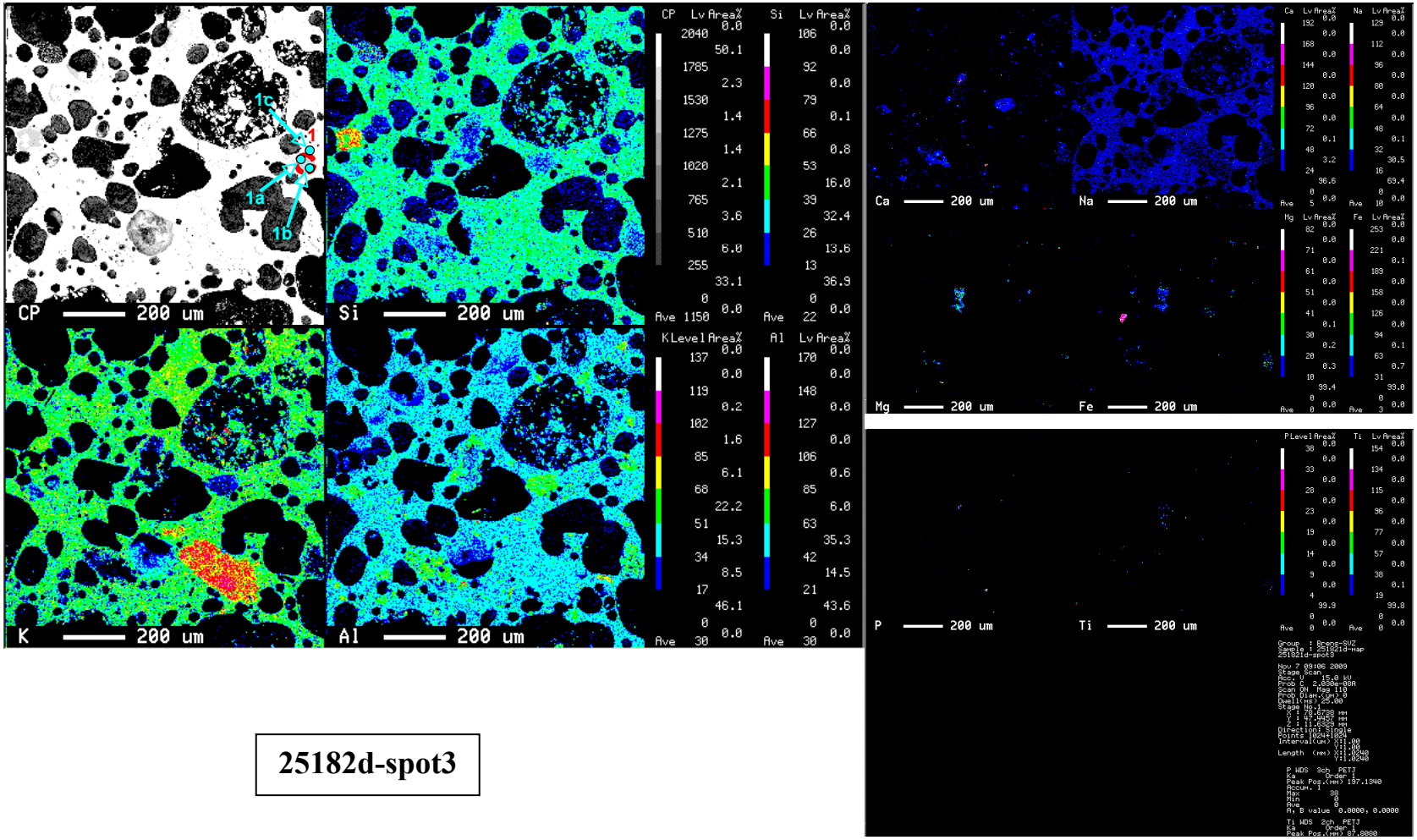

25182d-spot3

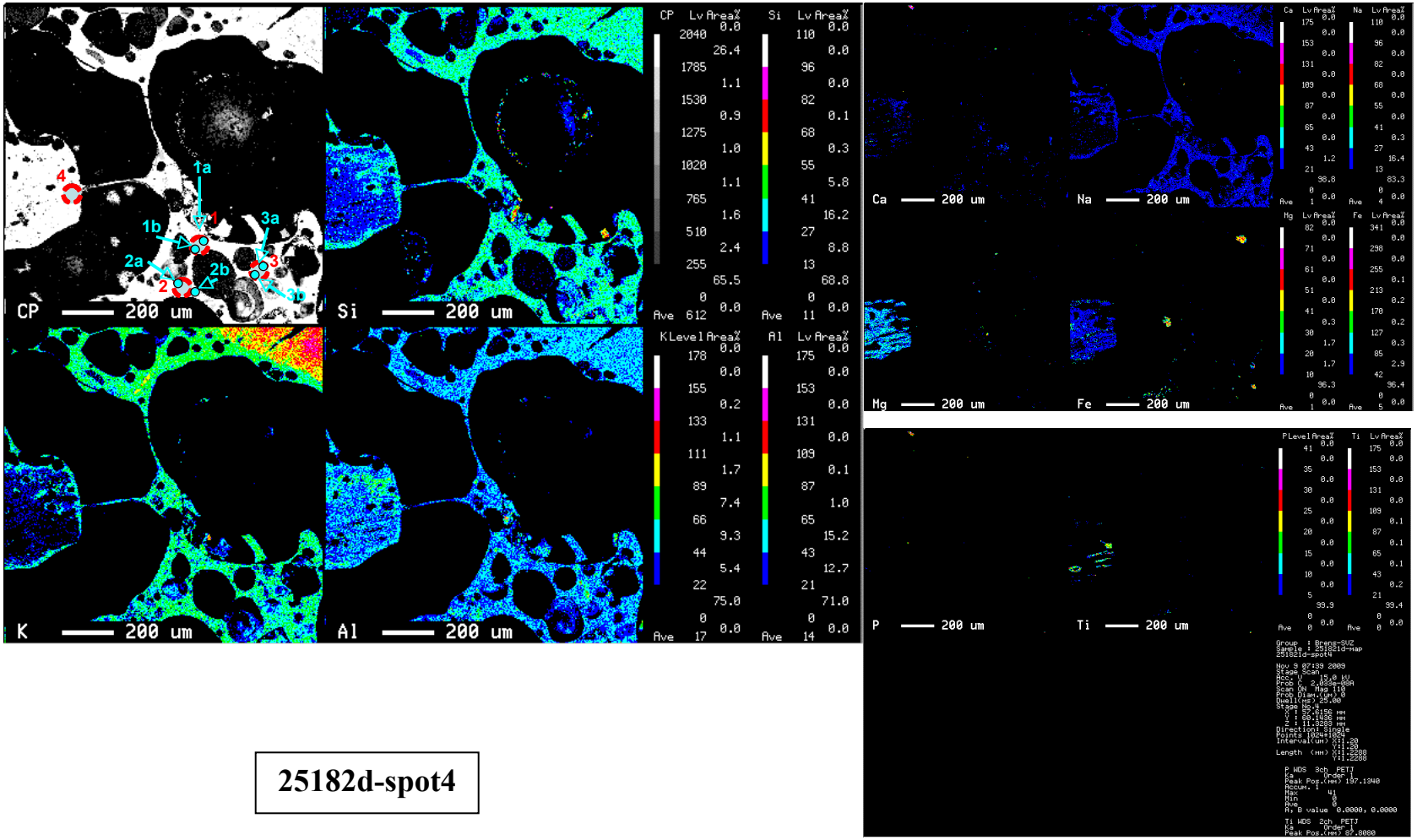

25182d-spot4

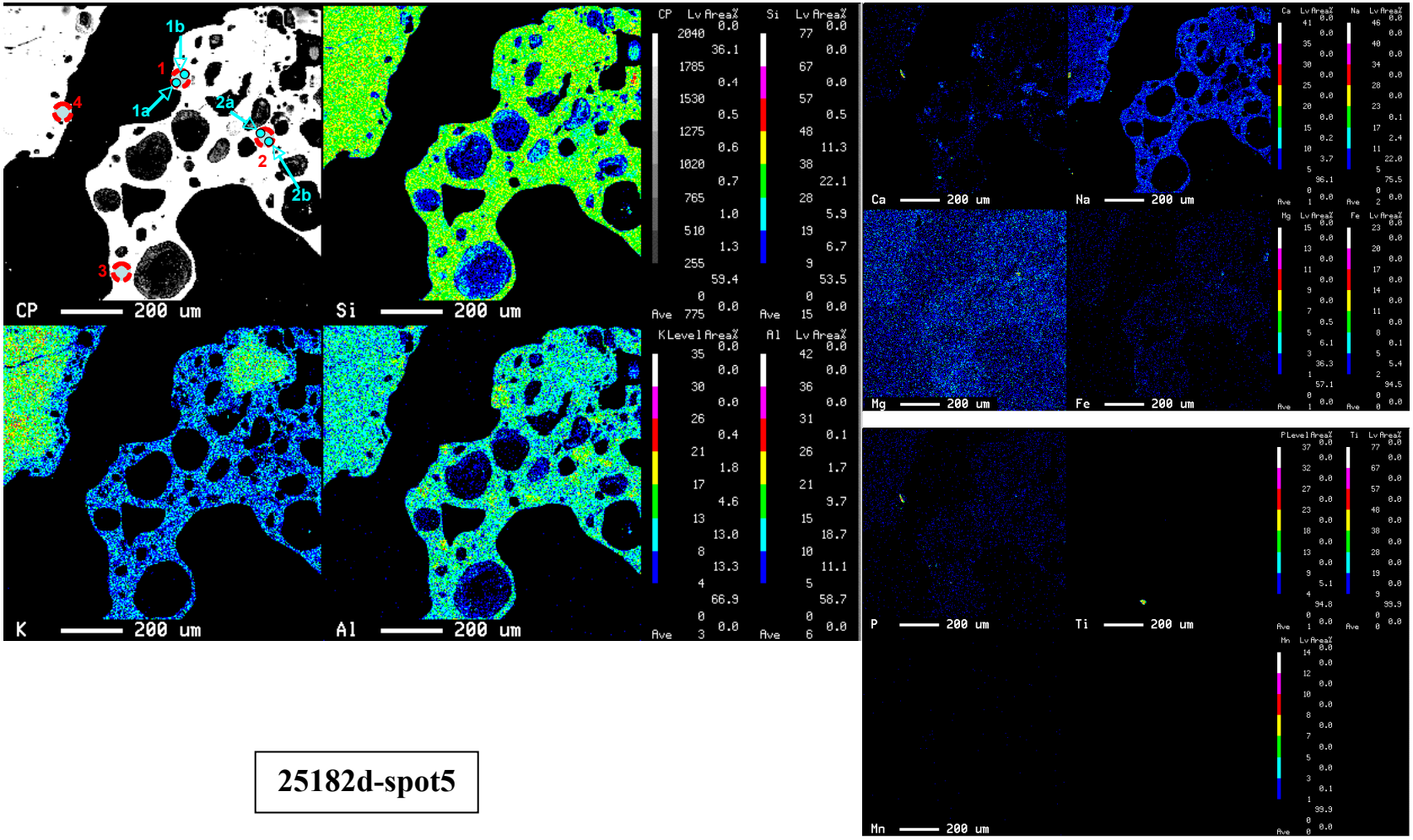

25182d-spot5

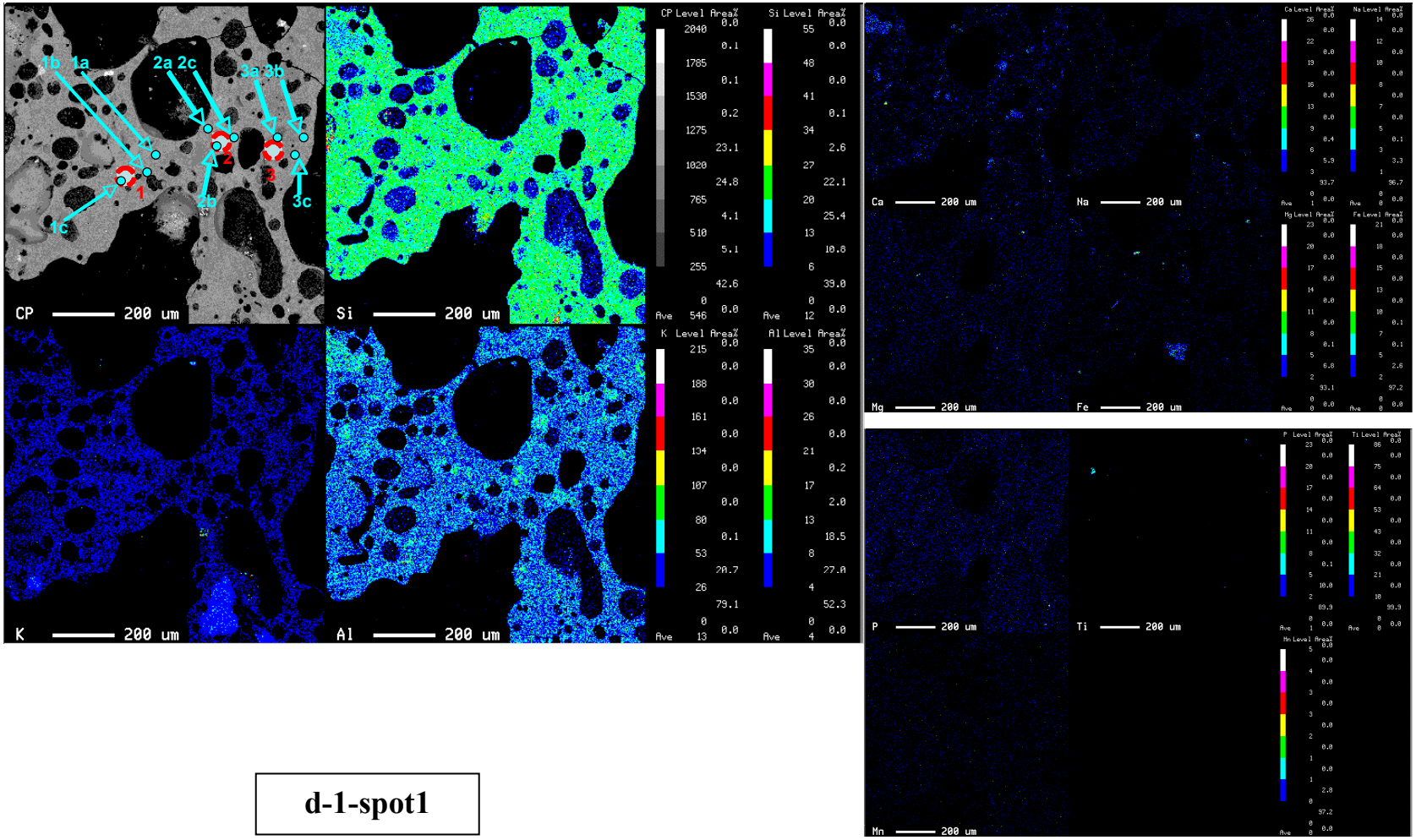
1b 1a
2a 2c
3a 3b
1c
2b
3c
CP 200 um
Si 200 um
K 200 um
Al 200 um
Ca 200 um
Na 200 um
Mg 200 um
Fe 200 um
P 200 um
Ti 200 um
Mn 200 um

d-1-spot1

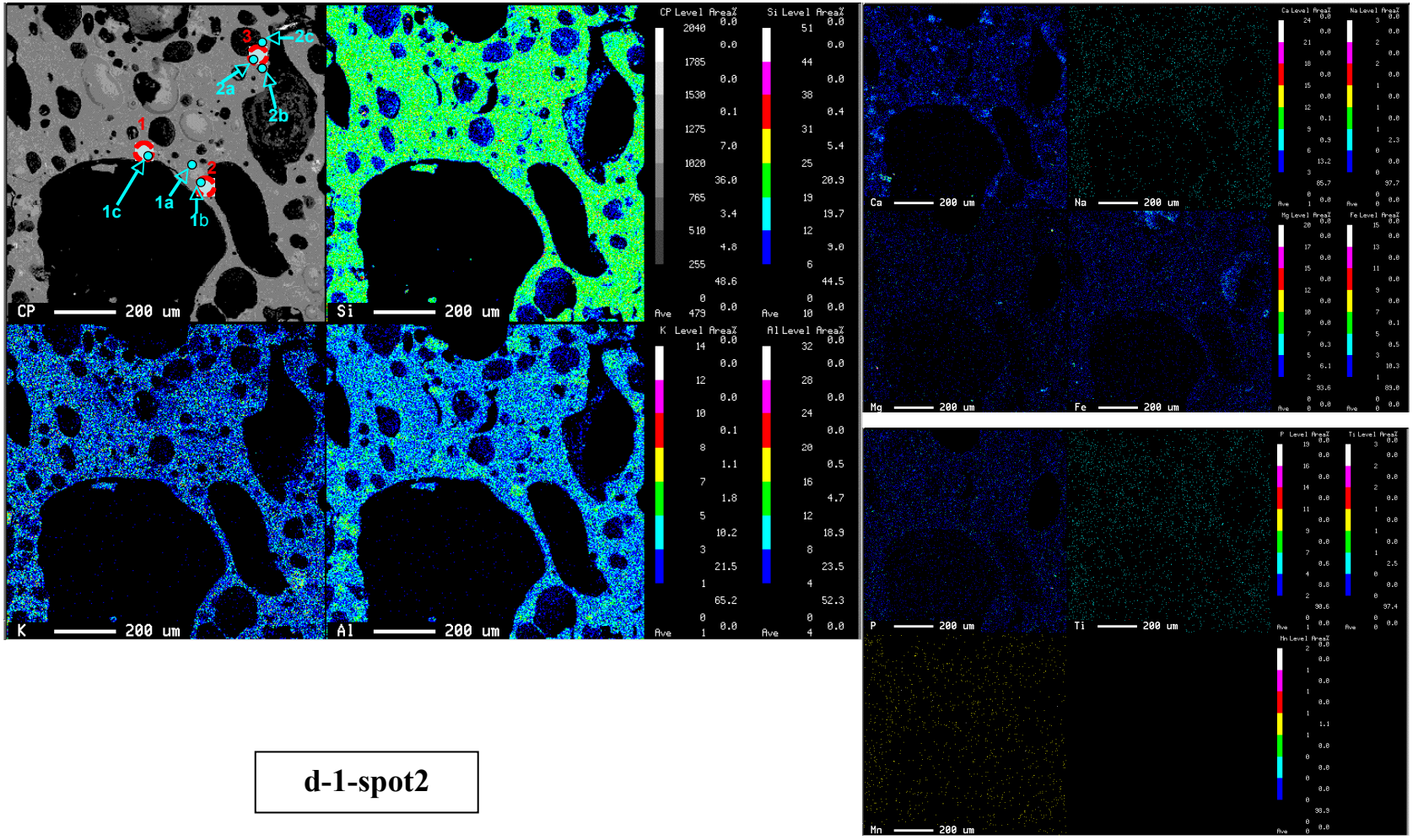
CP
200 um
Si
200 um
K
200 um
Al
200 um
Ca
200 um
Na
200 um
Mg
200 um
Fe
200 um
P
200 um
Ti
200 um
Mn
200 um
1
1a
1b
1c
2
2a
2b
2c
3

d-1-spot2

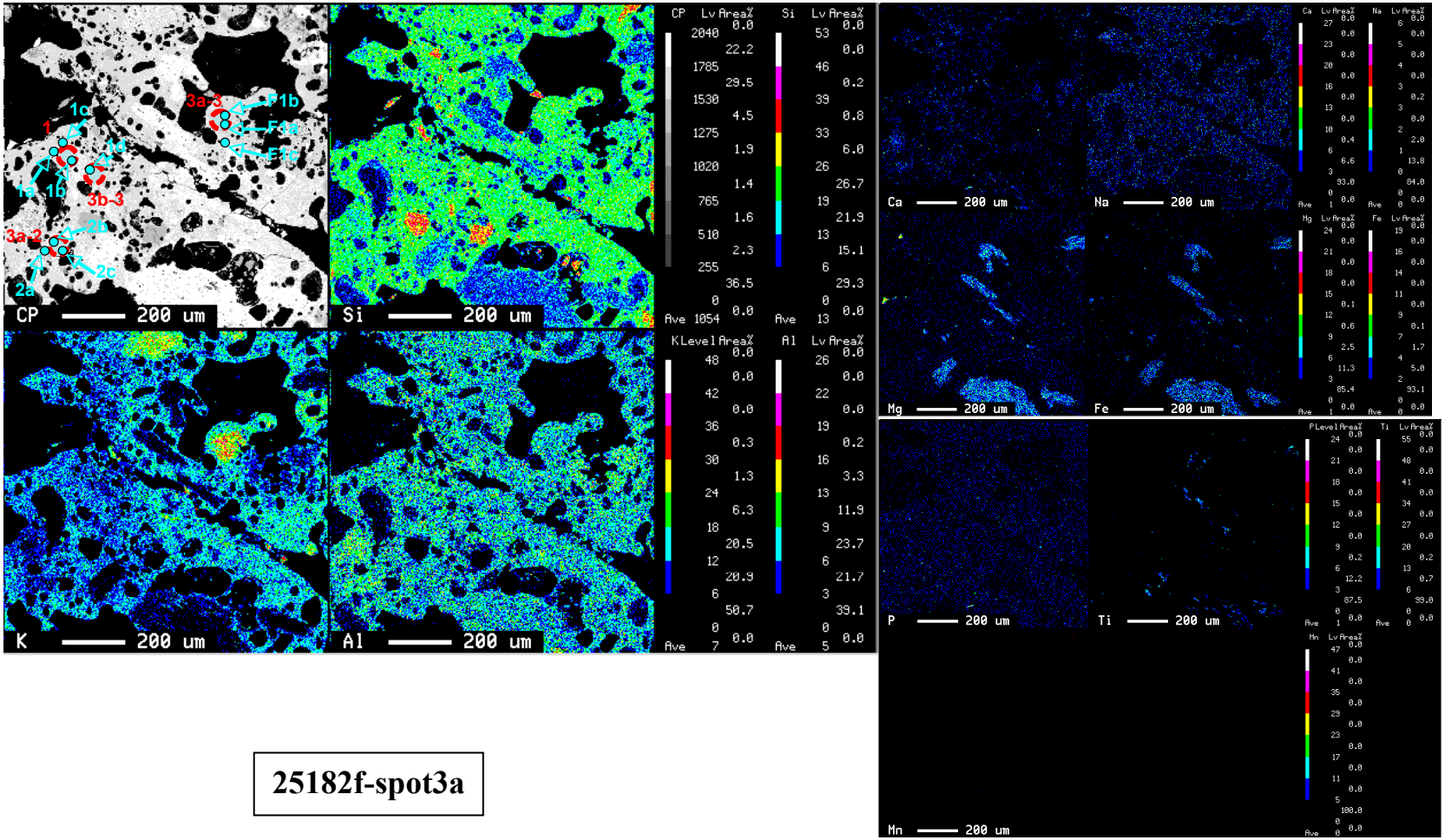

25182f-spot3a

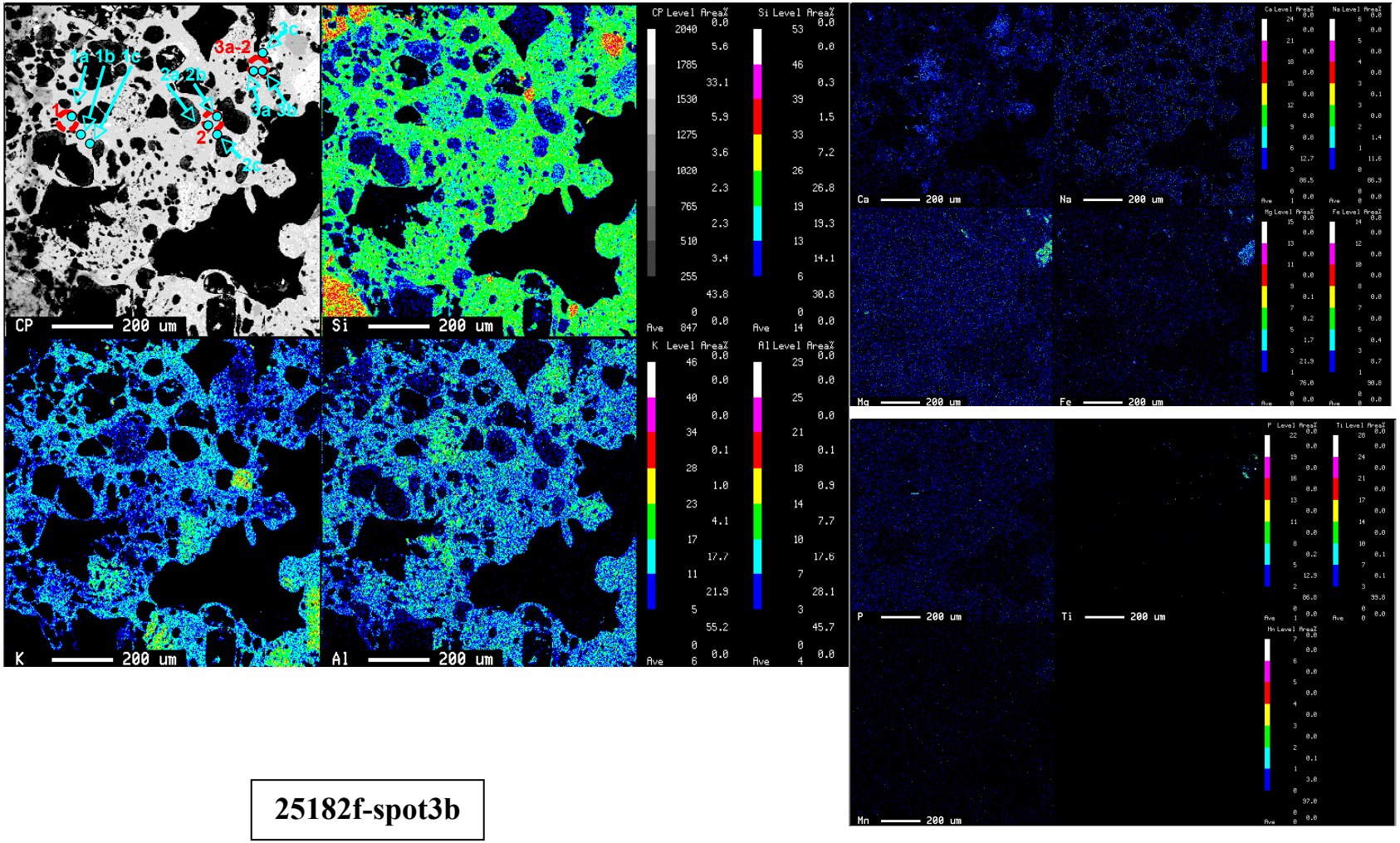

25182f-spot3b

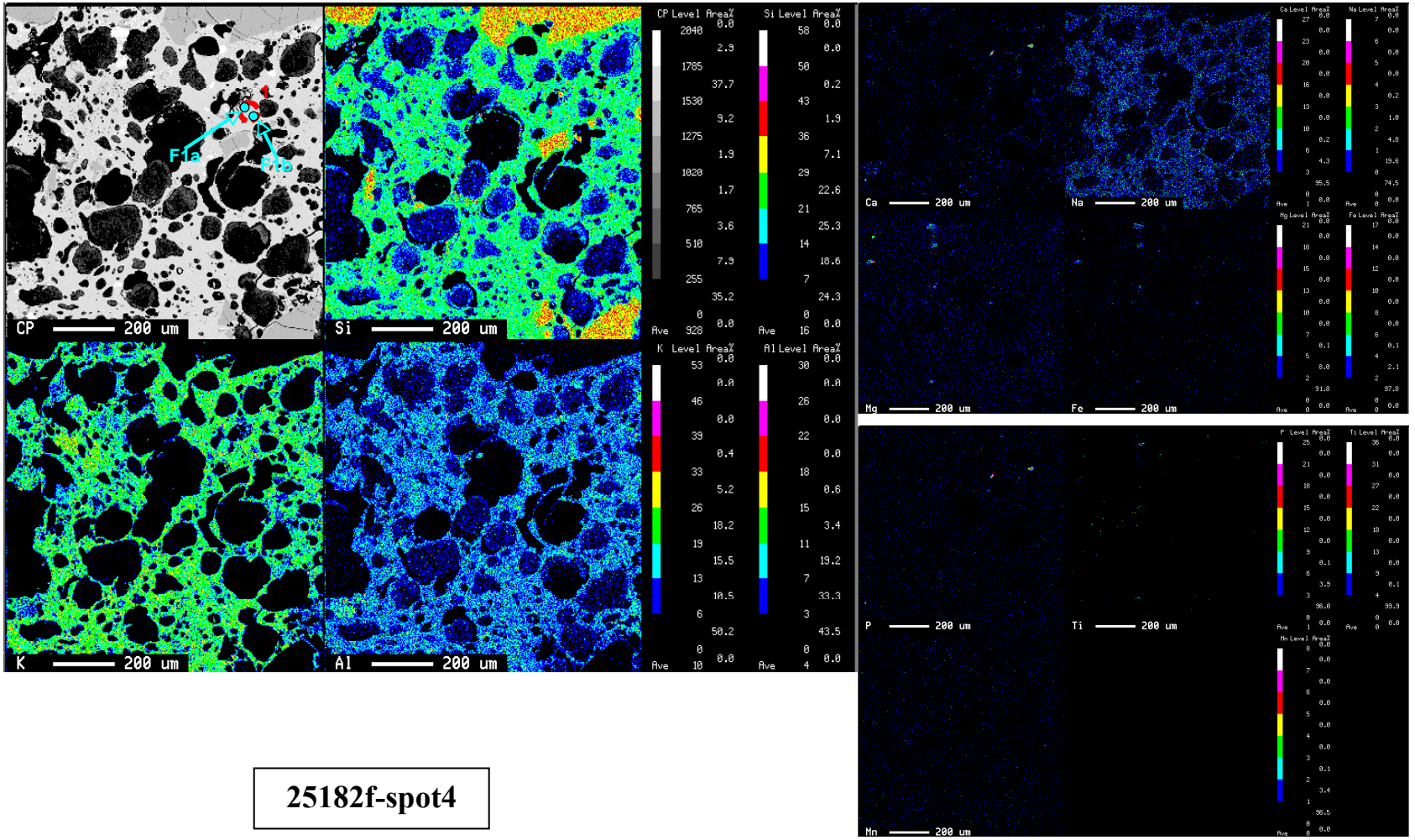

25182f-spot4

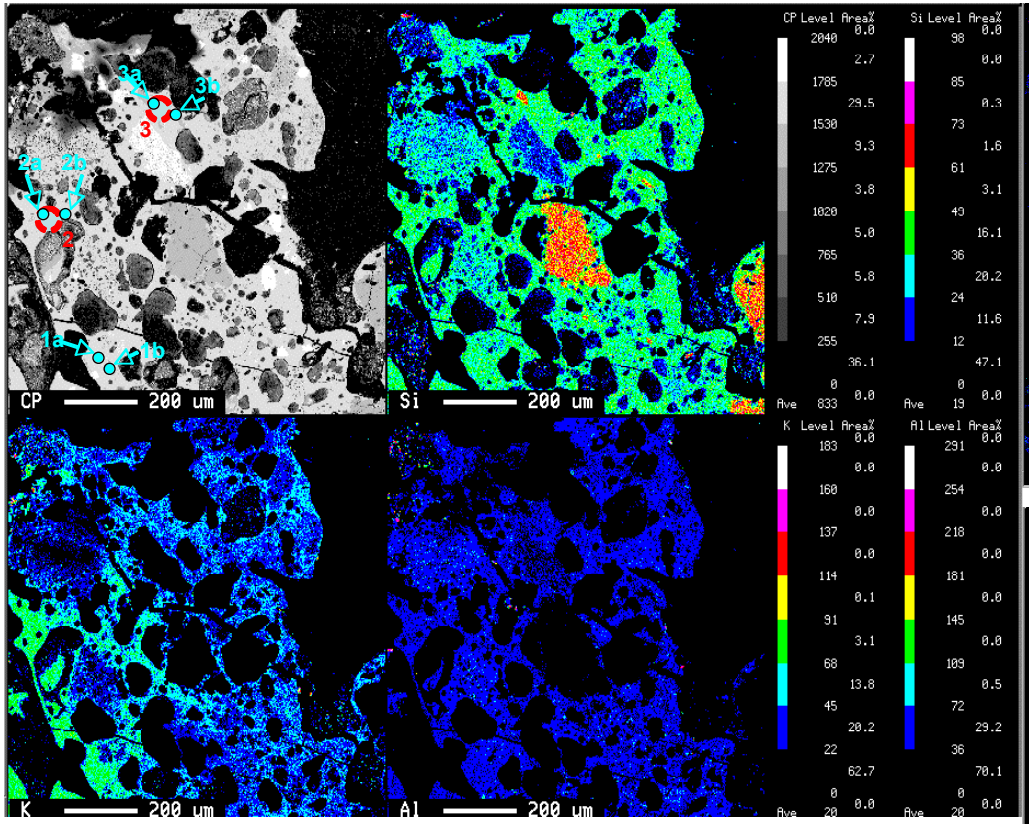
3a
3b
3
2a
2b
2
1a
1b
CP
200 um
Si
200 um
K
200 um
Al
200 um

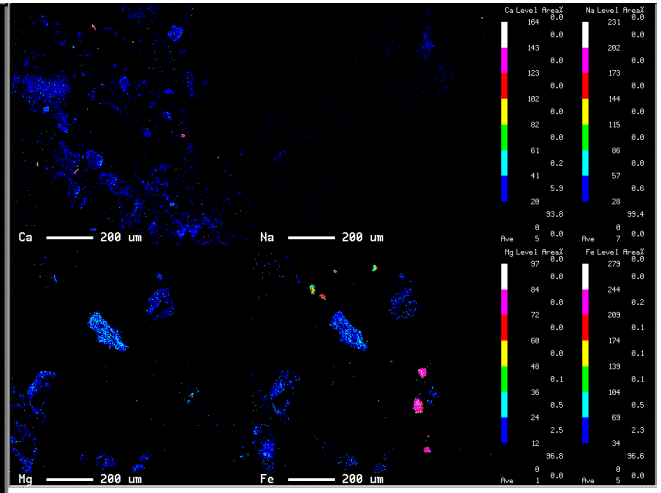
Ca
200 um
Na
200 um
Mg
200 um
Fe
200 um

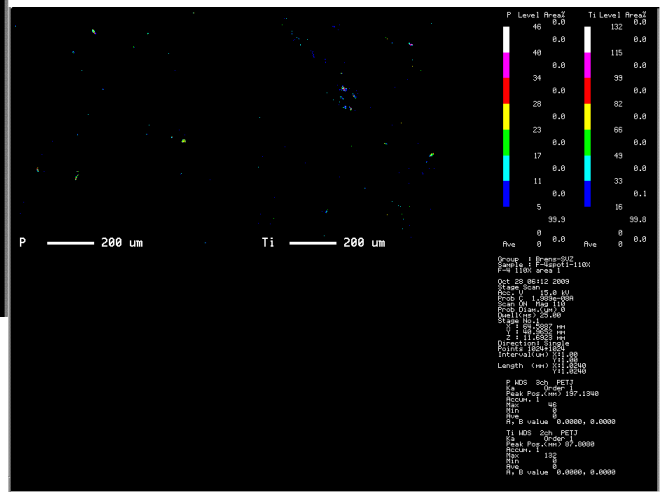
P
200 um
Ti
200 um

F-4-spot1

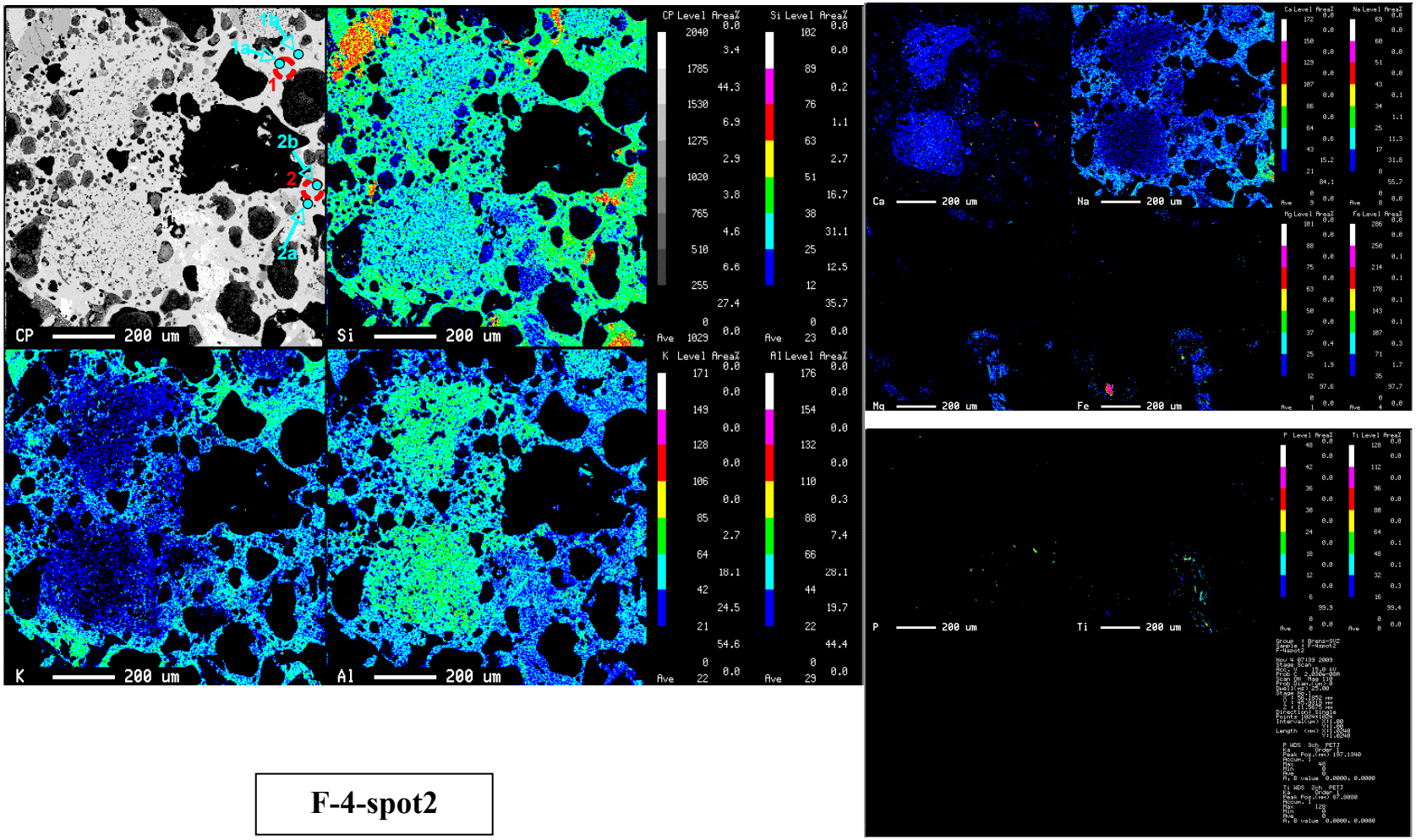
1b
1a
1
2b
2
2a
CP 200 um
Si 200 um
K 200 um
Al 200 um
Ca 200 um
Na 200 um
Mg 200 um
Fe 200 um
P 200 um
Ti 200 um

F-4-spot2

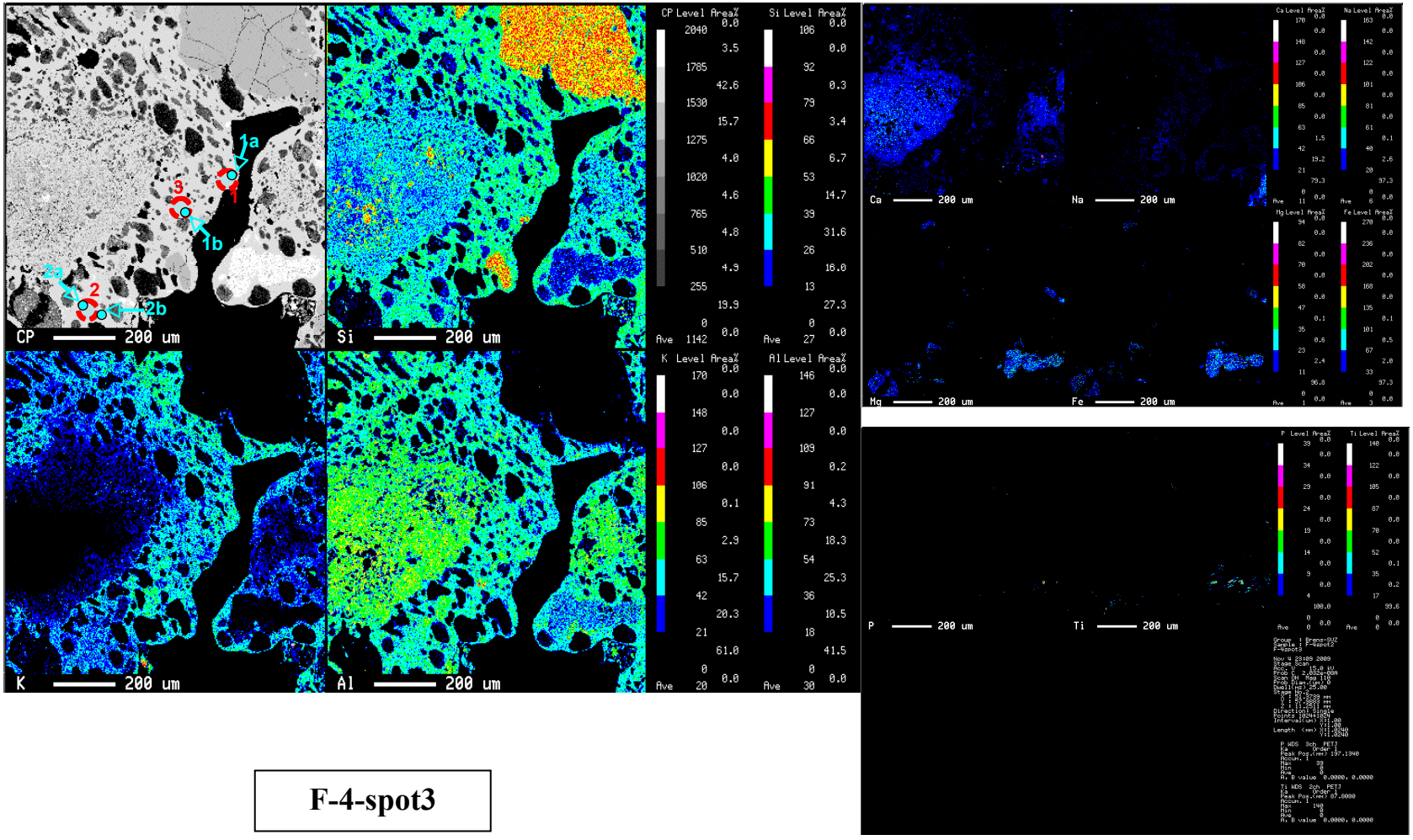
1a
1
3
1b
2a
2
2b
CP 200 um
Si 200 um
K 200 um
Al 200 um
Ca 200 um
Na 200 um
Mg 200 um
Fe 200 um
P 200 um
Ti 200 um

F-4-spot3

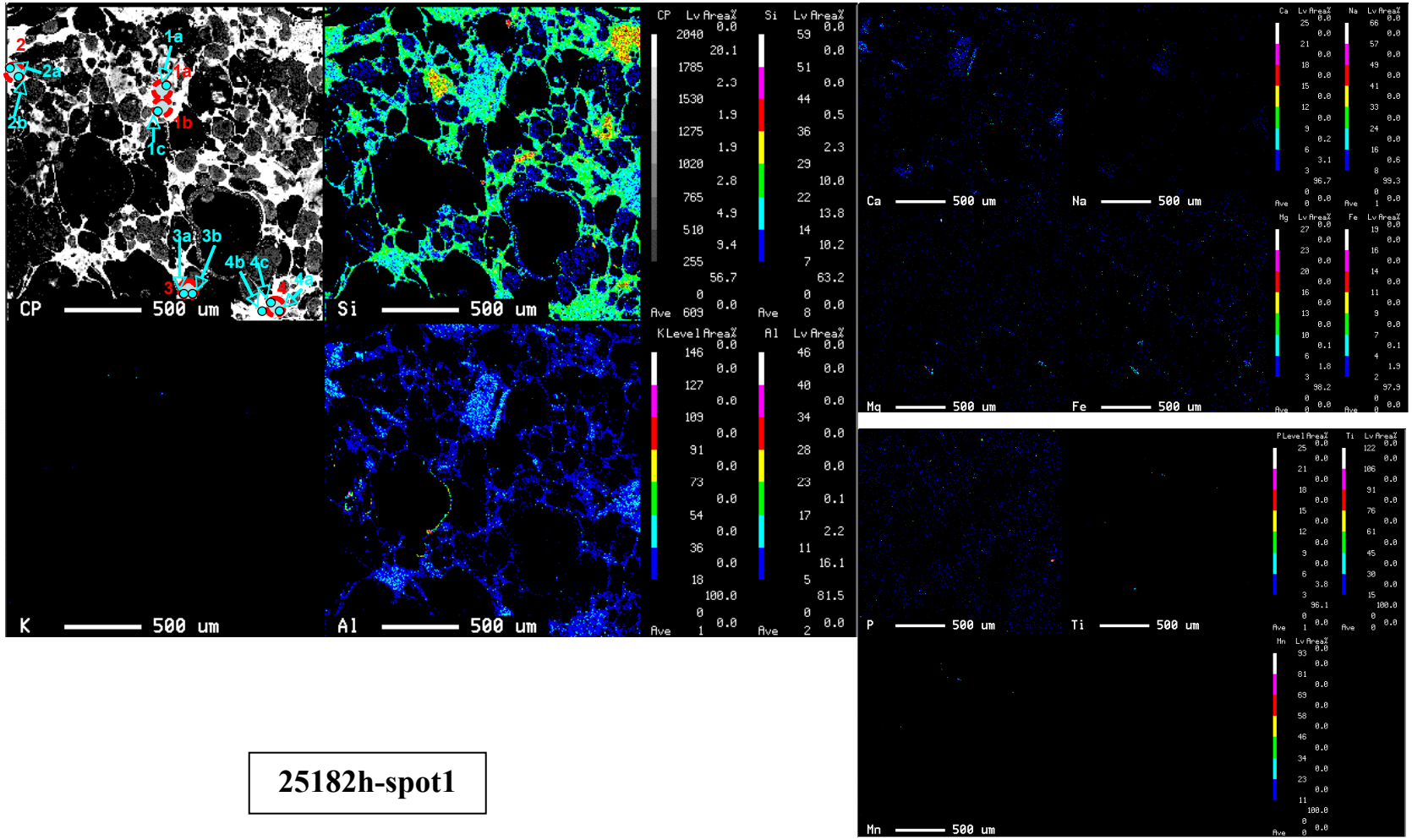

25182h-spot1

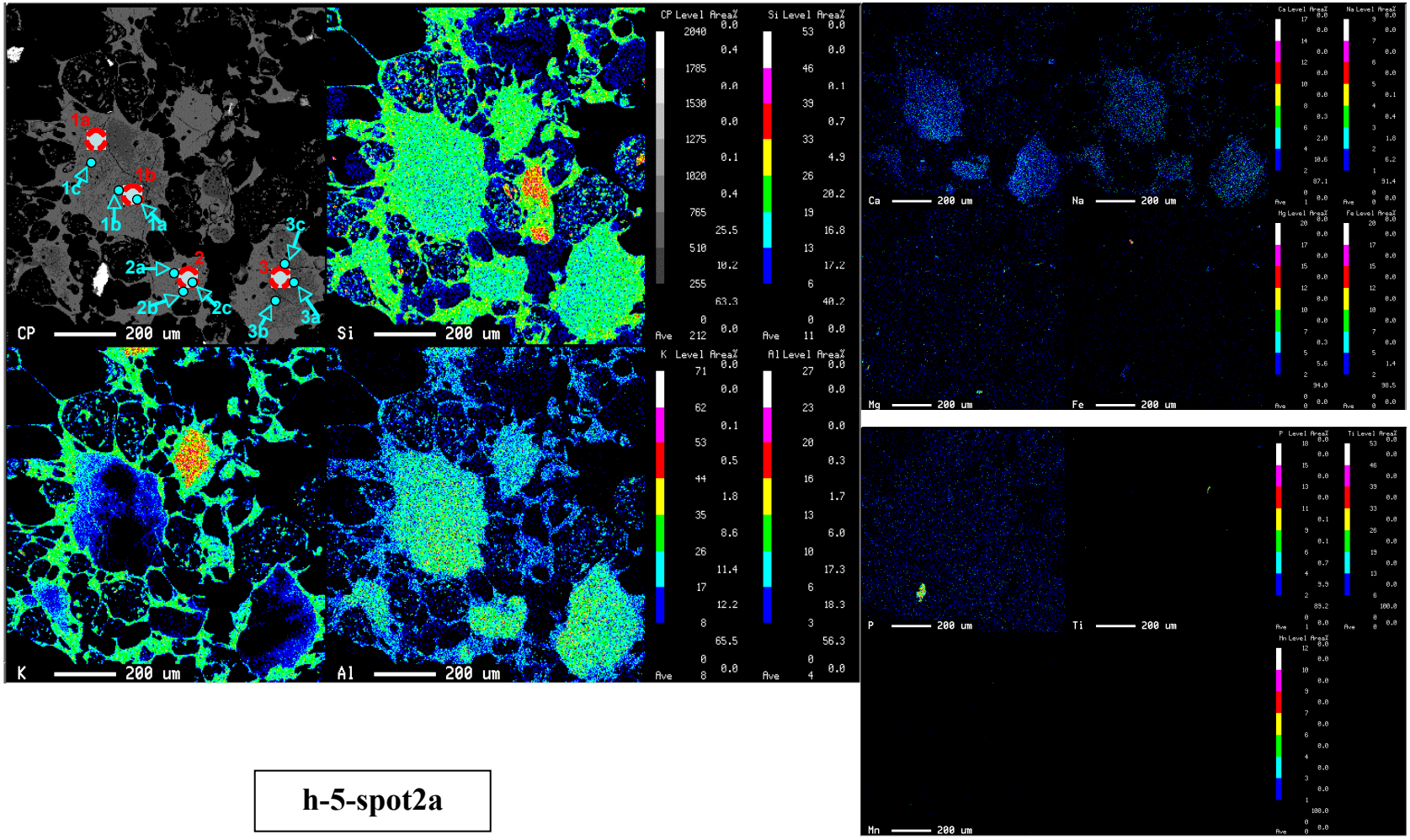
1a
1c
1b
1b
1a
2a
2
2b
2c
3c
3
3b
3a
CP 200 um
Si 200 um
K 200 um
Al 200 um
Ca 200 um
Na 200 um
Mg 200 um
Fe 200 um
P 200 um
Ti 200 um
Mn 200 um

h-5-spot2a

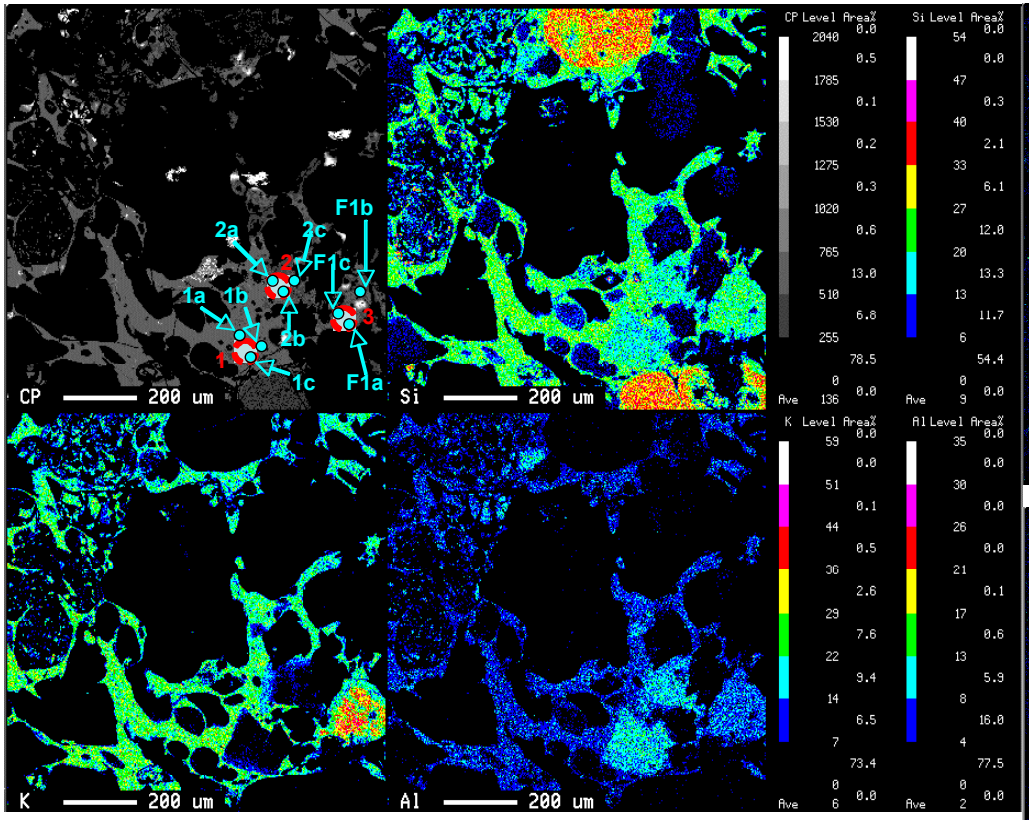
CP
200 um
2a
2c
F1b
F1c
1a
1b
2b
1c
F1a
Si
200 um
K
200 um
Al
200 um

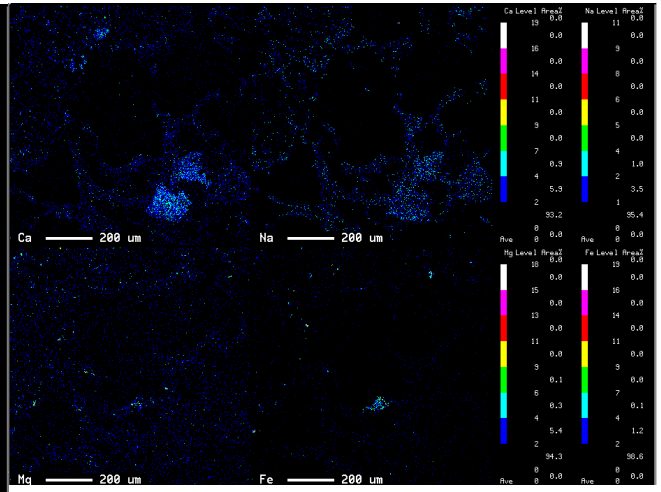
Ca
200 um
Na
200 um
Mg
200 um
Fe
200 um

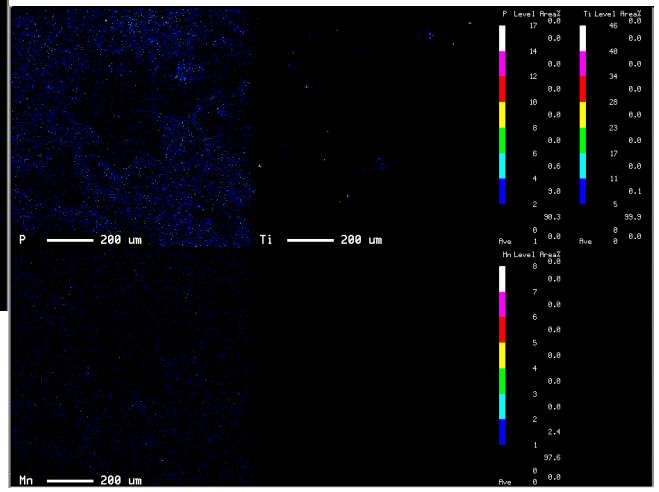
P
200 um
Ti
200 um
Mn
200 um

h-5-spot2b

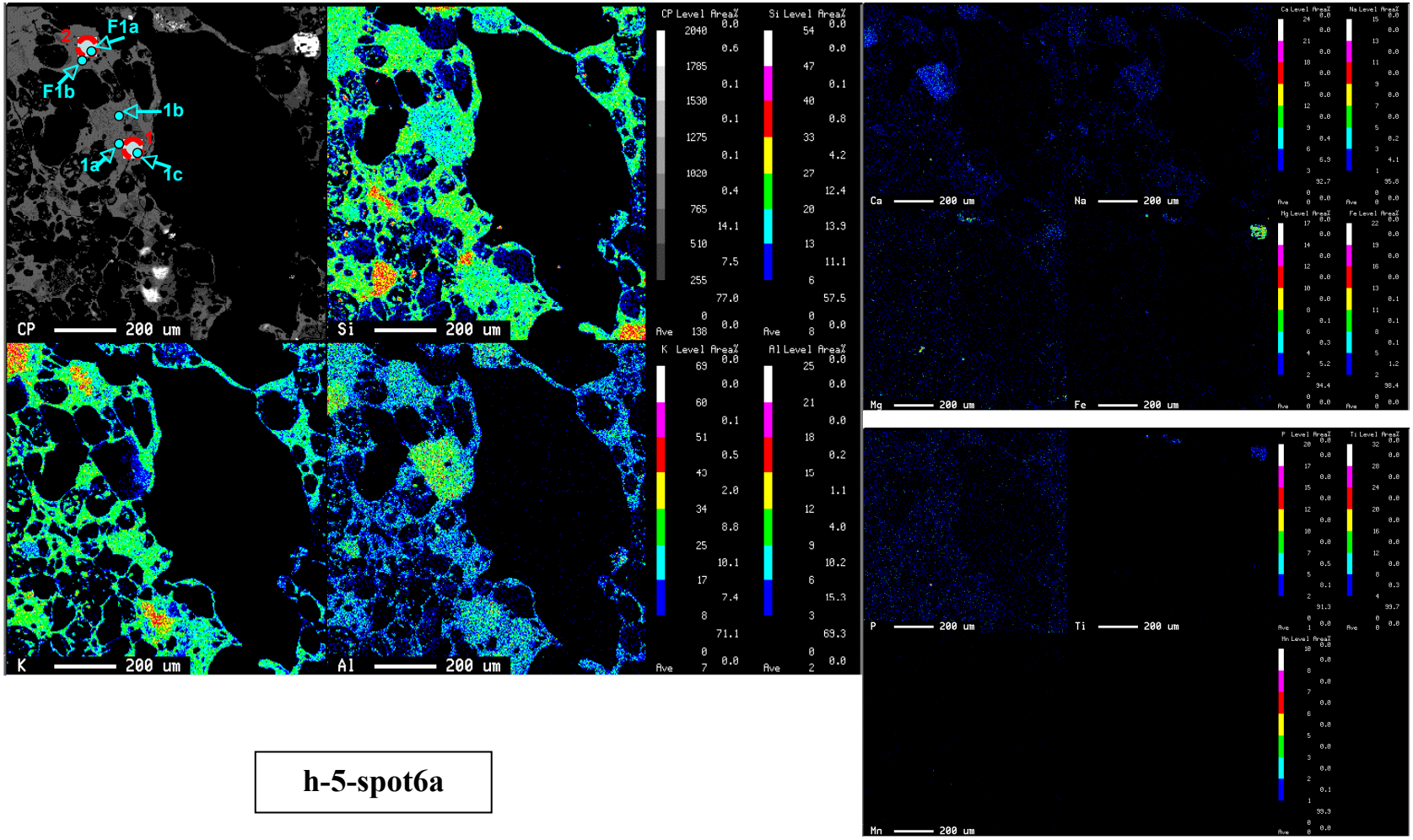
F1a
F1b
1b
1a
1c
CP 200 um
Si 200 um
K 200 um
Al 200 um
Ca 200 um
Na 200 um
Mg 200 um
Fe 200 um
P 200 um
Ti 200 um
Mn 200 um

h-5-spot6a

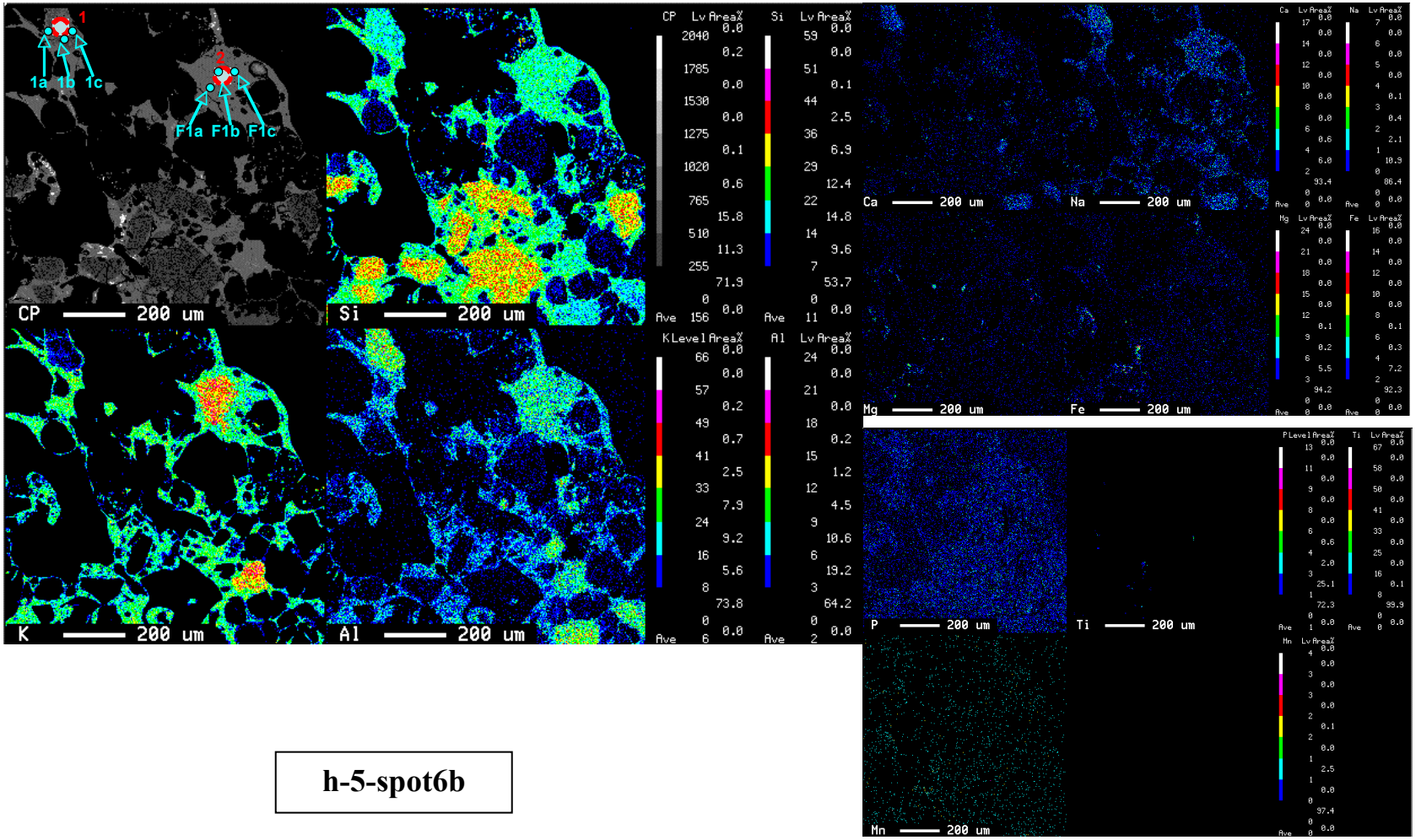
1
1a 1b 1c
2
F1a F1b F1c
CP 200 um
Si 200 um
K 200 um
Al 200 um
Ca 200 um
Na 200 um
Mg 200 um
Fe 200 um
P 200 um
Ti 200 um
Mn 200 um

h-5-spot6b

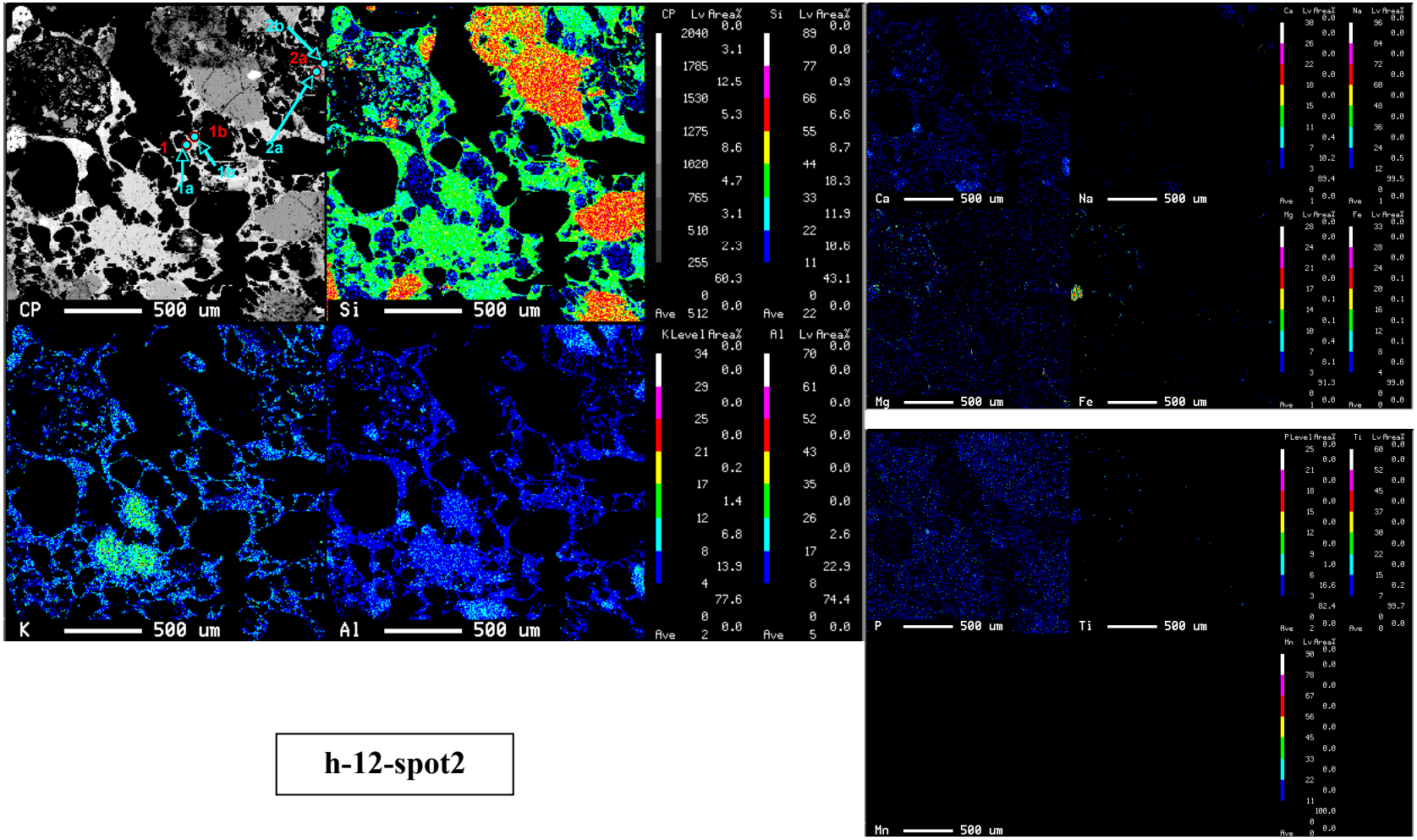
1b
2a
1
1b
2a
1a
CP 500 um
Si 500 um
K 500 um
Al 500 um
Ca 500 um
Na 500 um
Mg 500 um
Fe 500 um
P 500 um
Ti 500 um
Mn 500 um

h-12-spot2

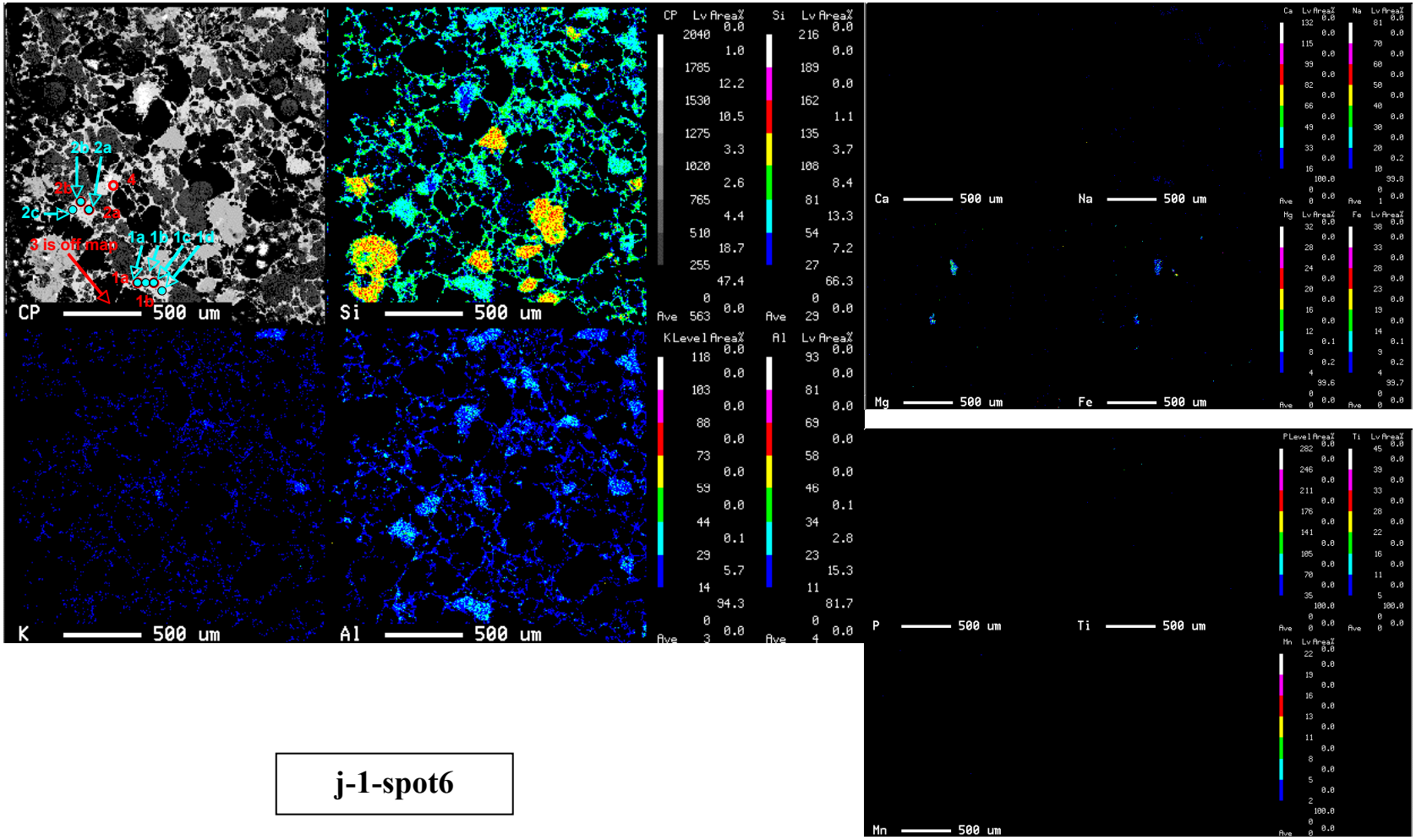
2b 2a
2b
4
2c
2a
3 is off map
1a 1b 1c 1d
1a
1b
CP 500 um
Si 500 um
K 500 um
Al 500 um
Ca 500 um
Na 500 um
Mg 500 um
Fe 500 um
P 500 um
Ti 500 um
Mn 500 um

j-1-spot6

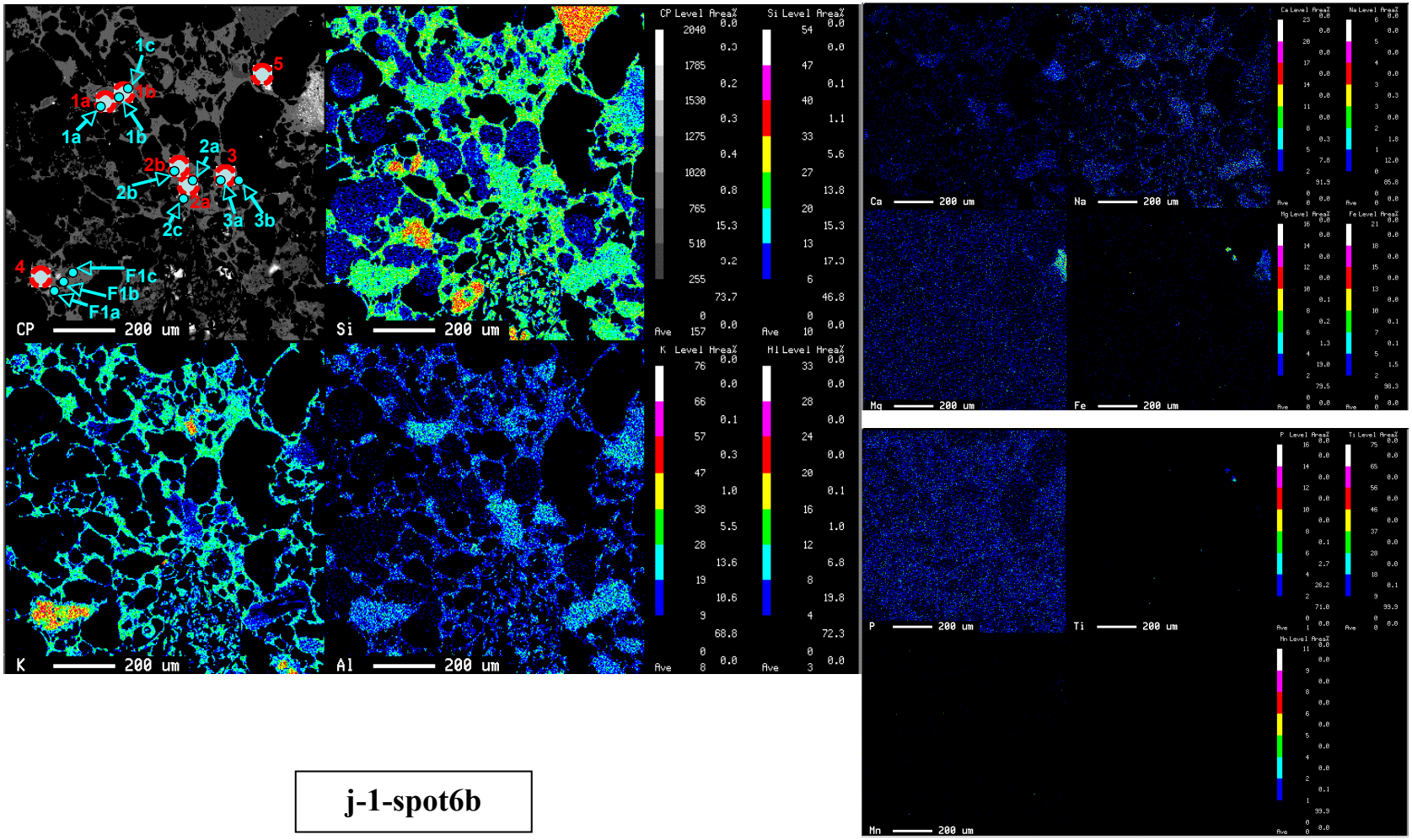
1c
1a
1b
1a
1b
5
2a
3
2b
2b
2a
2c
3a
3b
4
F1c
F1b
F1a
CP 200 um
Si 200 um
K 200 um
Al 200 um
Ca 200 um
Na 200 um
Mg 200 um
Fe 200 um
P 200 um
Ti 200 um
Mn 200 um

j-1-spot6b

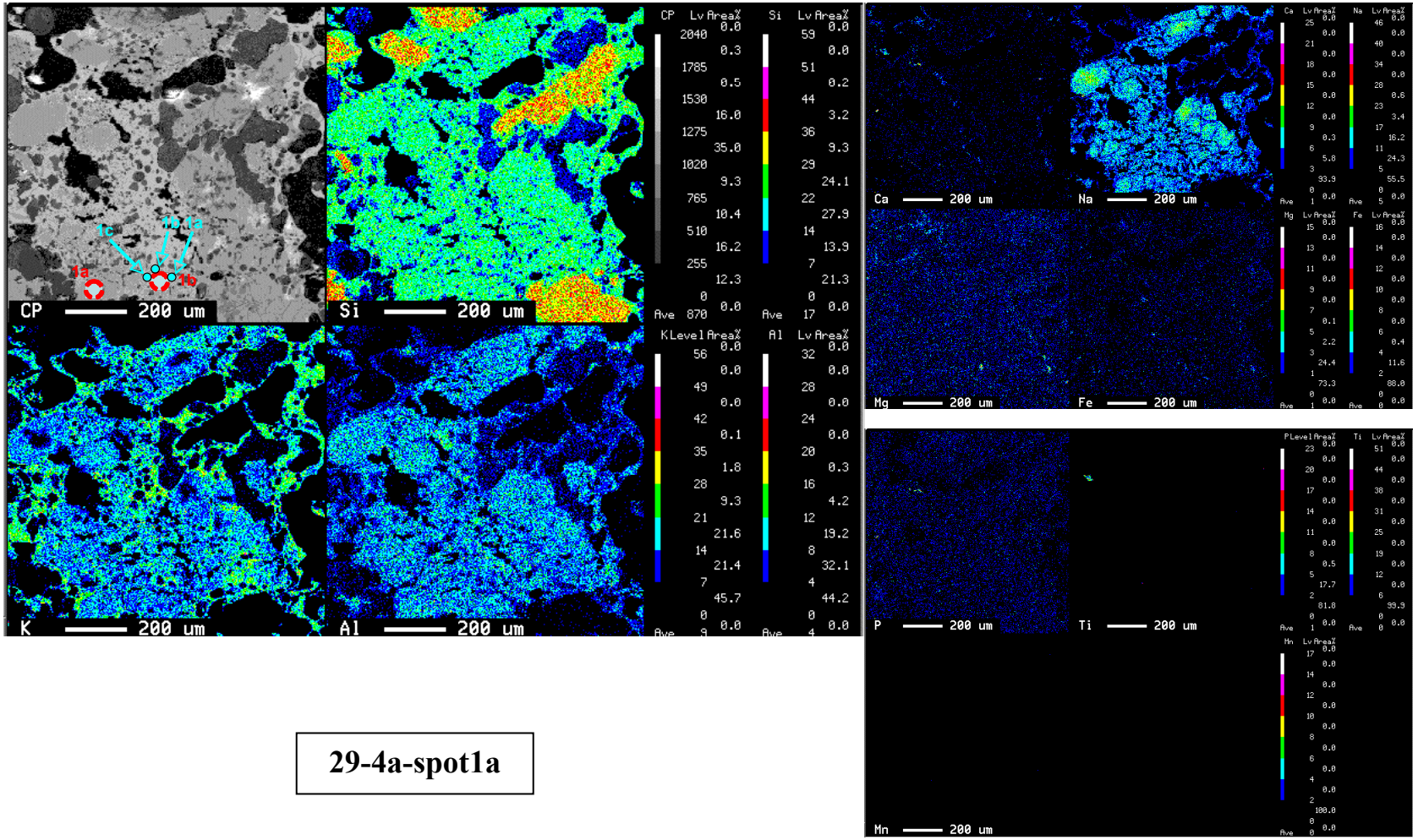
1c
1b
1a
2a
2b
CP 200 um
Si 200 um
K 200 um
Al 200 um
Ca 200 um
Na 200 um
Mg 200 um
Fe 200 um
P 200 um
Ti 200 um
Mn 200 um

29-4a-spot1a

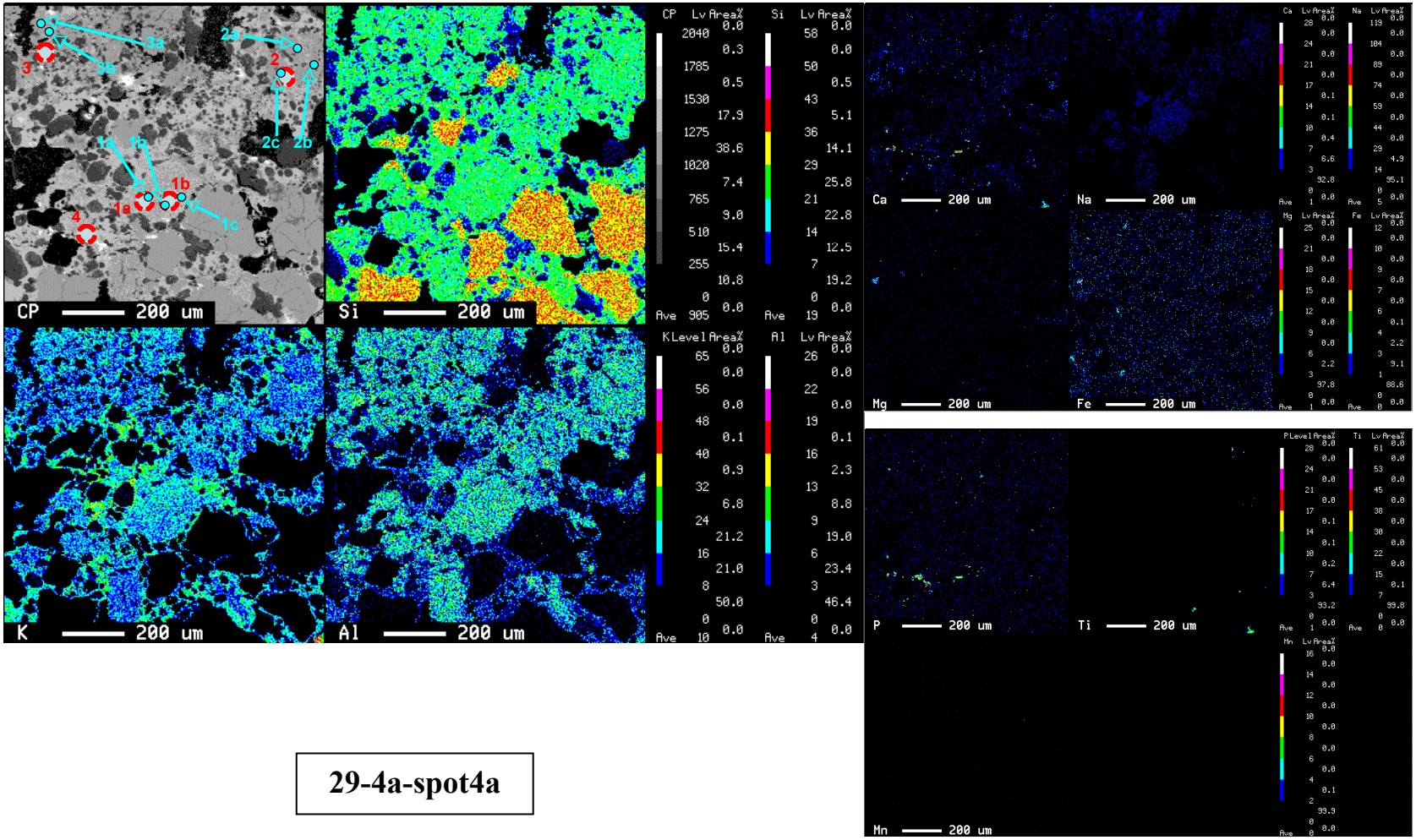
CP 200 um
Si 200 um
K 200 um
Al 200 um
Ca 200 um
Na 200 um
Mg 200 um
Fe 200 um
P 200 um
Ti 200 um
Mn 200 um

29-4a-spot4a

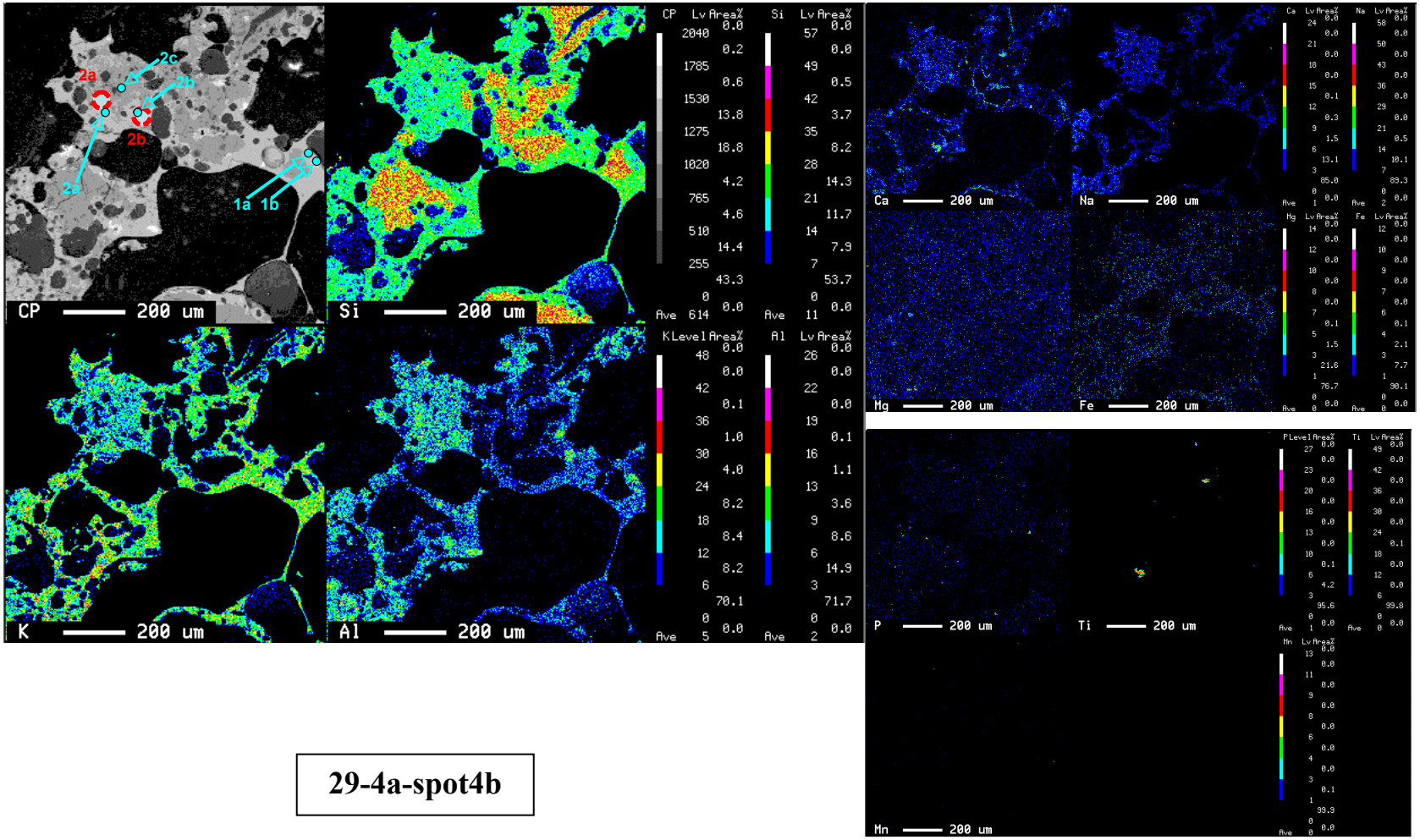
2a
2c
2b
2b
2a
1a
1b
CP 200 um
Si 200 um
K 200 um
Al 200 um
Ca 200 um
Na 200 um
Mg 200 um
Fe 200 um
P 200 um
Ti 200 um
Mn 200 um

29-4a-spot4b

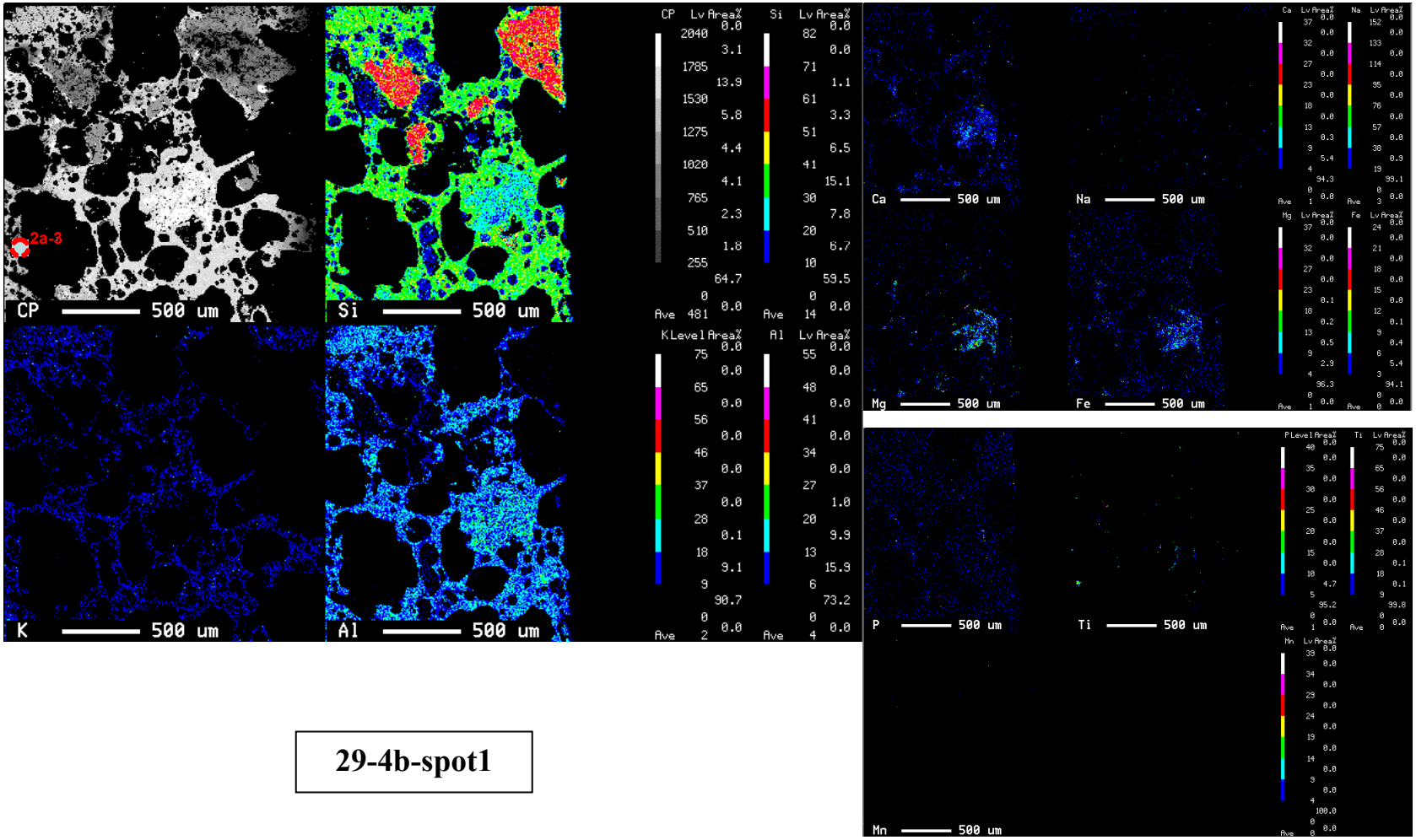
2a-3
CP 500 um
Si 500 um
K 500 um
Al 500 um
Ca 500 um
Na 500 um
Mg 500 um
Fe 500 um
P 500 um
Ti 500 um
Mn 500 um

29-4b-spot1

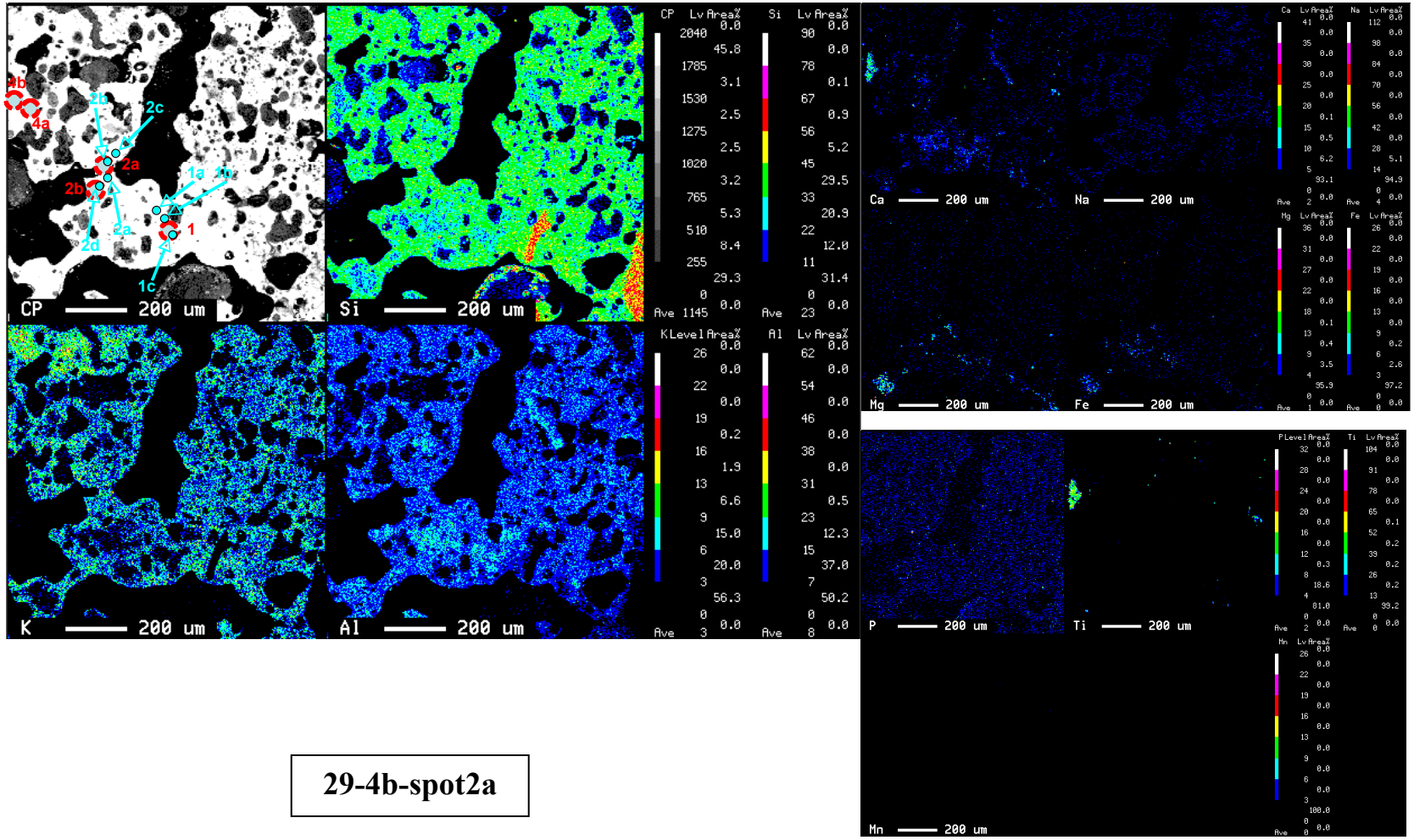
CP 200 um
Si 200 um
K 200 um
Al 200 um
Ca 200 um
Na 200 um
Mg 200 um
Fe 200 um
P 200 um
Ti 200 um
Mn 200 um
4b
4a
2b
2c
2a
1a
1
1c
2d

29-4b-spot2a

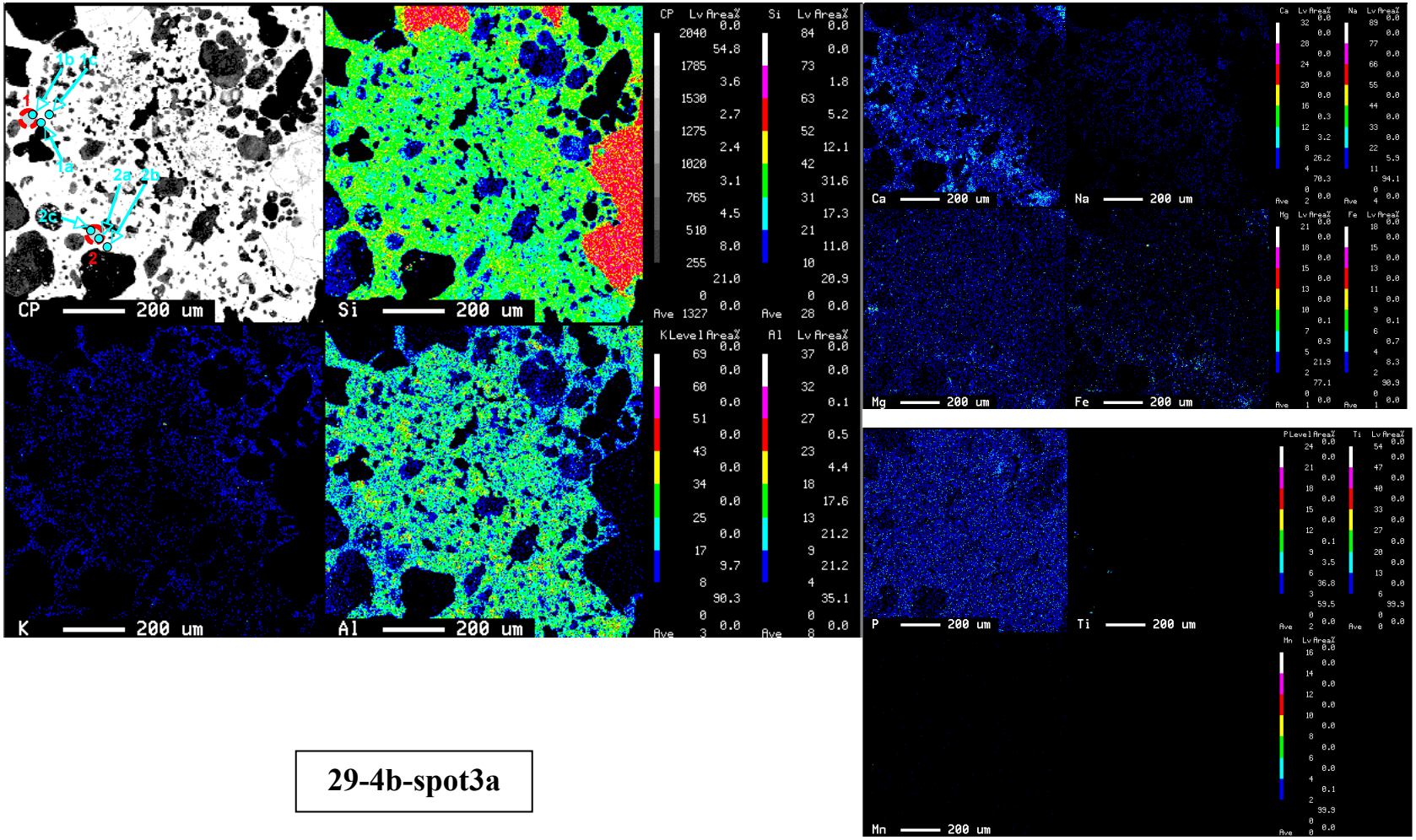
1b
1c
1
1a
2a
2b
2c
2
CP 200 um
Si 200 um
K 200 um
Al 200 um
Ca 200 um
Na 200 um
Mg 200 um
Fe 200 um
P 200 um
Ti 200 um
Mn 200 um

29-4b-spot3a

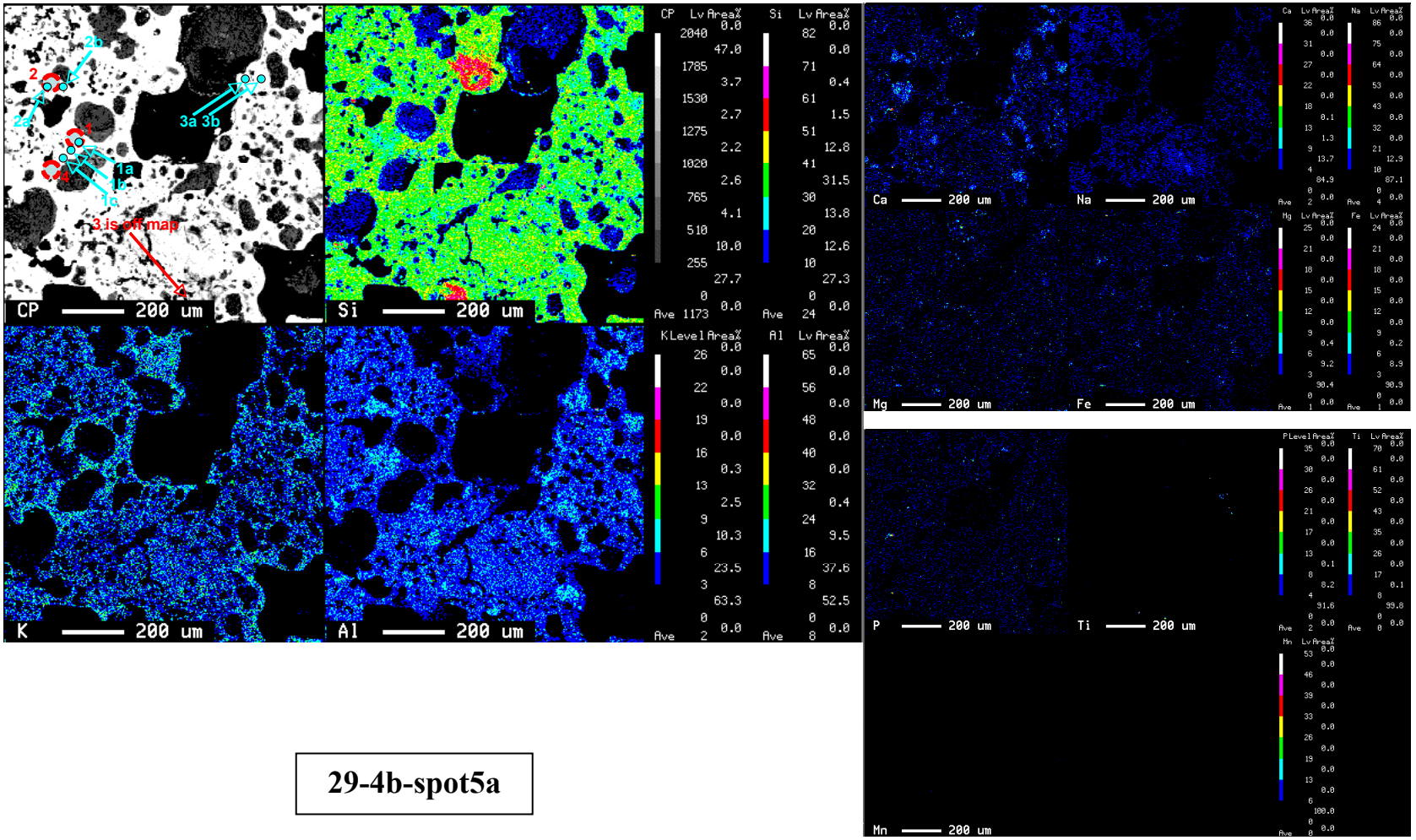
CP 200 um
Si 200 um
K 200 um
Al 200 um
Ca 200 um
Na 200 um
Mg 200 um
Fe 200 um
P 200 um
Ti 200 um
Mn 200 um
3 is off map

29-4b-spot5a

Appendix B – Geochemical Data for Major elements and Trace Elements

Supplementary Table: Major element chemical composition for Xenolith											
XENOLITH	**SiO2**	**CaO**	**K2O**	**Na2O**	**P2O5**	**Al2O3**	**FeO**	**TiO2**	**MgO**	**MnO**	**Total**
MIR-b	72.10	1.81	4.30	3.39	0.073	14.06	1.82	0.237	0.56	0.042	98.40
MIR-c	72.40	1.86	4.27	3.74	0.077	14.20	1.93	0.252	0.57	0.046	99.33
MIR-h	72.70	1.90	4.24	3.27	0.060	13.92	1.53	0.200	0.41	0.040	98.28
29-4	71.08	2.94	3.36	4.15	0.074	14.63	1.75	0.236	0.56	0.044	98.83
29-10	63.61	4.50	1.93	4.14	0.136	15.98	4.41	0.550	1.79	0.096	97.14

Supplementary Table: Trace Elements (ppm) for Xenolith									
XENOLITH	**Rb**	**Sr**	**Y**	**Zr**	**Nb**	**Ba**	**La**	**Ce**	**Nd**
MIR-b	207.0	207	16.10	158	4.70	854	37.03	67.65	25.48
MIR-c	186.2	180	14.91	166	4.71	950	27.83	51.22	19.79
MIR-h	197.8	218	11.00	138	4.26	975	26.66	43.87	14.54
29-4	132.0	268	14.09	163	4.36	864	26.96	49.53	19.36
29-10	77.9	357	20.64	119	3.38	439	10.16	22.95	14.06

	Sm	**Eu**	**Gd**	**Dy**	**Er**	**Yb**	**Hf**	**Pb**	**Th**	**U**
MIR-b	4.47	0.67	3.49	2.97	1.57	1.56	4.76	20.78	26.85	4.23
MIR-c	3.60	0.72	2.91	2.69	1.46	1.47	4.76	19.31	22.16	5.48
MIR-h	2.41	0.53	1.93	1.86	1.11	1.27	4.19	26.76	29.23	9.43
29-4	3.60	0.67	2.86	2.52	1.40	1.39	4.74	21.00	23.77	5.09
29-10	3.45	0.93	3.44	3.72	2.19	2.13	3.43	7.38	6.97	1.99

Origin of the basalt and xenolith data is from Lopez et al. (2008) and Hickey-Vargas (unpublished). The EPMA in-situ chemical analysis (microprobed spots) and LA-ICP-MS data is all original to this work.

Supplementary Table: Major element chemical composition for Basalt											
BASALT - CARRAN	**SiO2**	**CaO**	**K2O**	**Na2O**	**P2O5**	**Al2O3**	**FeO**	**TiO2**	**MgO**	**MnO**	**TOTAL**
Vn. Mirador 1979 (2)	51.570	8.110	0.510	4.050	0.170	18.130	10.279	1.170	4.110	0.200	98.299
Vn. Mirador 1979 (3)	52.540	7.970	0.550	4.130	0.200	18.260	10.117	1.170	4.090	0.180	99.207
Vn. Mirador bomb	52.750	8.220	0.550	4.000	0.210	17.630	10.225	1.200	4.370	0.150	99.305
Vn Mirador block	52.560	8.210	0.510	4.090	0.220	17.950	10.018	1.070	4.390	0.140	99.158

Supplementary Table: Trace Elements (ppm) for Basalt									
Basalt	**Rb**	**Sr**	**Y**	**Zr**	**Nb**	**Ba**	**La**	**Ce**	**Nd**
1979	9.75	478	21.700	72.200	1.6	185	7.060	18.1	10.8
1979	8.53	478	21.800	77.800	1.8	192	6.860	17.2	11.7
bomb	8	474	21.000	79.000	nd	173	nd	nd	nd
block	9	479	18.000	72.000	1.92	152	6.630	16.1	11.4

Basalt	**Sm**	**Eu**	**Gd**	**Dy**	**Er**	**Yb**	**Hf**	**Pb**	**Th**	**U**
1979	3.41	1.2	nd	nd	nd	2.17	1.9	nd	0.64	nd
1979	2.97	1.26	nd	nd	nd	2.18	1.96	nd	0.71	nd
bomb	nd	nd	nd	nd	nd	nd	nd	nd	nd	nd
block	3.06	1	3.610	3.520	2.06	2.06	2.1	5.55	0.44	0.174

Supplementary Table: Major element chemical composition for Microprobed Spots											
25182d	**SiO2**	**CaO**	**K2O**	**Na2O**	**P2O5**	**Al2O3**	**FeO**	**TiO2**	**MgO**	**MnO**	**Total**
25182d-spot3-1a	64.652	2.484	5.661	5.473	0	19.353	0.944	0.03	0.244	0	98.841
25182d-spot3-1b	55.328	10.262	2.219	4.016	0.106	27.243	1.1	0.004	0.143	0.003	100.424
25182d-spot3-1c	62.78	3.472	5.334	4.82	0.022	20.378	1.681	0.102	0.299	0.082	98.97
25182dspot4-1a	65.207	1.246	4.338	3.265	0.122	16.729	3.331	0.512	0.485	0.026	95.261
25182dspot4-1b	60.475	6.17	1.84	5.782	0.032	22.892	0.557	0.02	0.026	0	97.794
25182dspot4-2a	63.257	1.966	3.974	4.199	0.069	17.896	2.304	0.32	0.176	0.009	94.17
25182dspot4-2b	65.083	0.901	4.452	3.764	0.049	16.739	2.288	0.326	0.124	0.003	93.729
25182dspot4-3a	65.997	1.354	4.588	3.795	0.066	16.56	2.236	0.164	0.202	0.009	94.971
25182dspot4-3b	66.165	0.908	4.669	3.642	0.09	17.106	2.612	0.162	0.213	0.047	95.614
25182d-spot5-1a	52.658	12.206	2.358	3.17	0.029	28.179	1.543	0.069	0.154	0.087	100.453
25182d-spot5-1b	63.027	3.255	5.452	5.474	0.023	20.516	1.451	0.165	0.311	0.207	99.881
25182d-spot5-2a	51.441	11.902	2.372	3.01	0.045	27.437	2.176	0.04	0.323	0.058	98.804
25182d-spot5-2b	56.201	9.406	3.422	3.884	0.03	25.593	1.819	0.043	0.157	0.068	100.623
d-1	**SiO2**	**CaO**	**K2O**	**Na2O**	**P2O5**	**Al2O3**	**FeO**	**TiO2**	**MgO**	**MnO**	**Total**
d-1-spot1-1a	64.473	2.507	5.994	5.162	0.023	19.52	1.136	0	0.148	0.007	98.97
d-1-spot1-1b	64.297	1.82	6.762	5.369	0.051	18.334	1.43	0.326	0.21	0.033	98.632
d-1-spot1-2a	62.496	3.298	5.192	5.826	0.054	19.791	1.03	0	0.117	0.009	97.813
d-1-spot1-2b	62.495	2.039	6.071	5.261	0.034	18.965	1.372	0.217	0.178	0.03	96.662
d-1-spot1-2c	63.836	3.057	5.229	5.632	0.045	20.18	1.088	0.245	0.162	0.008	99.482
d-1-spot1-3a	65.455	1.447	6.154	5.243	0	18.499	1.341	0	0.155	0	98.294
d-1-spot1-3b	63.195	3.307	4.975	5.605	0.045	20.262	1.104	0.326	0.106	0.021	98.946
d-1-spot1-3c	63.768	2.795	5.521	5.903	0	20.066	0.898	0.136	0.077	0.014	99.178
d-1-spot2-1a	60.297	5.449	4.335	5.19	0.02	21.805	0.883	0.245	0.091	0.064	98.379
d-1-spot2-1b	62.933	3.423	5.432	4.991	0.033	19.578	1.217	0	0.154	0.039	97.8
d-1-spot2-1c	59.252	7.318	2.819	5.528	0.027	23.953	0.91	0.082	0.063	0.046	99.998
d-1-spot2-2a	60.619	5.718	4.144	4.853	0.029	22.019	1.053	0.191	0.101	0.048	98.775
d-1-spot2-2b	61.319	5.921	3.288	5.565	0	22.747	0.684	0.3	0.059	0.044	99.927
d-1-spot2-2c	63.553	3.415	5.138	4.911	0.039	20.448	1.195	0	0.119	0.049	98.867

25182f	SiO2	CaO	K2O	Na2O	P2O5	Al2O3	FeO	TiO2	MgO	MnO	Total
25182f-spot3a-1a	65.583	2.2	5.456	5.706	0.03	17.859	0.972	0.408	0.194	0.029	98.437
25182f-spot3a-1b	66.005	3.04	5.382	4.329	0.028	18.55	1.049	0.408	0.175	0.021	98.987
25182f-spot3a-1c	67.909	1.295	6.069	4.884	0.028	17.086	0.871	0.299	0.199	0.103	98.743
25182f-spot3a-1d	66.071	3.379	4.844	4.537	0.026	19.137	1.121	0.544	0.203	0.057	99.919
25182f-spot3a-2a	56.259	4.962	3.121	5.222	0.027	19.865	4.187	3.773	0.351	0.076	97.843
25182f-spot3a-2b	61.359	4.17	3.079	6.291	0	23.457	0.428	0.027	0.071	0.019	98.901
25182f-spot3a-2c	66.04	2.405	5.275	5.284	0.052	17.756	1.209	0.299	0.193	0.021	98.534
25182f-spot3b-1a	66.019	2.242	5.724	5.7	0.008	19.307	0.645	0	0.106	0.006	99.757
25182f-spot3b-1b	66.857	1.297	6.539	5.483	0	18.958	0.563	0	0.116	0.032	99.845
25182f-spot3b-1c	66.06	1.352	6.414	5.311	0.028	18.999	0.968	0.082	0.168	0.055	99.437
25182f-spot3b-2a	66.757	0.941	6.9	5.379	0.02	18.655	0.732	0.136	0.122	0.025	99.667
25182f-spot3b-2b	66.681	0.772	7.07	5.408	0.053	18.772	0.76	0.109	0.086	0.064	99.775
25182f-spot3b-2c	66.156	0.868	7.056	5.397	0.019	19.062	0.461	0	0.052	0.035	99.106
25182f-spot3b-3a	66.93	2.408	5.531	4.77	0.041	17.421	1.025	0.327	0.212	0.048	98.713
25182f-spot3b-3b	62.923	4.14	3.682	6.444	0.039	21.725	0.533	0.082	0.092	0.023	99.683
25182f-spot3b-3c	65.464	2.729	5.424	4.423	0.069	18.18	1.207	0.435	0.24	0.035	98.206
25182f-spot3a-F1a	65.769	0.099	12.028	3.361	0.008	18.512	0.09	0.055	0	0	99.922
25182f-spot3a-F1b	65.657	0.038	13.617	2.217	0.011	18.502	0	0	0	0	100.042
25182f-spot3a-F1c	65.312	0.863	7.569	4.939	0	18.139	1.076	0	0.235	0.06	98.193
25182f-spot4-F1a	67.556	1.226	5.875	5.544	0.081	18.244	0.979	0.19	0.141	0.035	99.871
25182f-spot4-F1b	67.396	1.998	5.413	5.762	0.007	18.904	0.608	0.163	0.109	0.015	100.375
F-4	**SiO2**	**CaO**	**K2O**	**Na2O**	**P2O5**	**Al2O3**	**FeO**	**TiO2**	**MgO**	**MnO**	**Total**
F-4-spot1-1a	65.086	3.275	5.042	3.832	0.024	20.774	1.16	0.155	0.448	0.045	99.841
F-4-spot1-1b	66.17	1.332	6.002	2.786	0.06	19.11	1.555	0.301	0.614	0.033	97.963
F-4-spot1-2a	67.192	0.771	6.451	2.796	0.013	19.048	1.064	0.055	0.4	0.043	97.833
F-4-spot1-2b	67.029	0.585	6.582	2.824	0	18.986	0.789	0.009	0.223	0.025	97.052
F-4-spot1-3a	67.937	2.206	4.44	2.361	0.077	17.515	2.785	0.401	0.741	0.018	98.481
F-4-spot1-3b	68.726	1.48	4.869	2.073	0.056	16.236	2.622	0.377	0.84	0.054	97.333
F-4-spot2-1a	65.356	2.694	5.246	2.693	0.036	18.442	1.7	0.258	0.526	0.029	96.98
F-4-spot2-1b	70.317	0.975	6.058	2.584	0.024	16.351	1.575	0.165	0.316	0.022	98.387
F-4-spot2-2a	63.224	1.593	4.513	3.185	0.073	15.545	1.926	0.231	0.504	0.069	90.863
F-4-spot2-2b	75.602	0.337	4.889	1.804	0.06	11.825	1.9	0.231	0.382	0.025	97.055
F-4-spot3-1a	70.037	1.332	5.988	2.402	0.016	15.797	1.186	0.198	0.408	0.052	97.416
F-4-spot3-1b	67.107	2.516	5.395	3.169	0.027	18.322	1.275	0.152	0.441	0.049	98.453
F-4-spot3-2a	63.185	5.75	3.997	2.498	0.051	21.159	2.235	0.298	0.678	0.035	99.886
F-4-spot3-2b	67.904	1.315	5.61	2.189	0.078	15.807	3.032	0.511	0.982	0.058	97.486

25182h	SiO2	CaO	K2O	Na2O	P2O5	Al2O3	FeO	TiO2	MgO	MnO	Total
25182h-spot1-1a	60.405	5.152	0.674	8.355	0.005	22.594	0.016	0.018	0.033	0.025	97.277
25182h-spot1-1c	68.191	1.147	5.752	2.979	0.062	15.081	1.955	0.286	0.583	0.147	96.183
25182h-spot1-2a	59.924	7.216	2.055	5.359	0.043	23.817	1.034	0.054	0.166	0	99.668
25182h-spot1-2b	55.363	10.554	0.436	5.259	0	27.909	0.185	0	0	0.031	99.737
25182h-spot1-3a	62.618	4.713	1.916	7.696	0.004	22.859	0.096	0	0.006	0.036	99.944
25182h-spot1-3b	61.548	4.745	2.842	6.951	0.011	22.412	0.16	0.009	0	0.049	98.727
25182h-spot1-4a	65.518	0.523	8.303	5.18	0.012	18.651	0.167	0.041	0.019	0	98.414
25182h-spot1-4b	65.279	0.474	8.577	4.691	0.017	18.878	0.07	0	0	0.032	98.018
25182h-spot1-4c	65.538	1.845	5.813	4.97	0.003	19.069	0.345	0.004	0.107	0.093	97.787
h-5	SiO2	CaO	K2O	Na2O	P2O5	Al2O3	FeO	TiO2	MgO	MnO	Total
h-5-spot2a-1a	57.863	8.009	0.275	7.569	0.018	26.031	0.078	0	0	0.014	99.857
h-5-spot2a-1b	58.841	7.847	0.971	6.796	0	26.002	0.026	0	0	0.011	100.494
h-5-spot2a-1c	62.232	5.057	3.466	6.406	0.007	23.191	0.078	0.245	0.036	0.014	100.732
h-5-spot2a-2a	55.816	10.037	0.751	5.782	0	27.431	0.121	0	0	0	99.938
h-5-spot2a-2b	55.651	10.024	0.434	6.001	0	26.65	0.09	0	0	0	98.85
h-5-spot2a-2c	57.333	9.241	0.489	6.169	0	27.197	0.036	0.191	0.006	0	100.662
h-5-spot2a-3a	62.3	5.459	1.179	7.893	0	23.727	0.073	0	0	0.014	100.645
h-5-spot2a-3b	61.042	6.445	0.713	7.882	0.021	24.639	0.067	0	0	0.015	100.824
h-5-spot2a-3c	59.064	7.909	0.754	6.978	0	25.192	0.073	0.082	0	0.027	100.079
h-5-spot2b-1a	56.728	9.179	1.089	4.848	0.01	27.767	0.246	0	0.016	0.008	99.891
h-5-spot2b-1b	54.378	10.483	0.604	4.754	0	29.64	0.051	0	0	0.049	99.959
h-5-spot2b-1c	55.617	9.488	0.753	5.161	0.01	27.5	0.027	0	0.017	0.022	98.595
h-5-spot2b-2a	57.755	7.866	0.73	6.143	0.066	26.833	0.155	0.218	0	0.001	99.767
h-5-spot2b-2b	57.865	6.072	1.314	6.431	0.007	24.124	0.102	0.109	0.007	0.023	96.054
h-5-spot2b-2c	56.241	8.469	0.904	5.197	0.008	27.161	0.091	0	0.03	0.008	98.109
h-5-spot6a-1a	54.498	10.759	0.126	6.083	0.027	28.059	0.123	0.027	0	0.008	99.71
h-5-spot6a-1b	56.728	10.218	0.455	6.161	0.002	27.05	0.085	0.055	0	0	100.754
h-5-spot6a-1c	62.77	4.595	3.622	6.907	0.007	22.465	0.056	0.027	0	0.005	100.454
h-5-spot6b-1a	61.19	6.128	2.369	7.107	0	24.177	0.023	0	0	0.002	100.996
h-5-spot6b-1b	58.539	7.756	1.815	6.319	0.029	25.532	0.026	0.027	0	0	100.043
h-5-spot6b-1c	58.098	8.134	1.334	6.546	0	25.036	0.107	0	0.009	0.04	99.304
h-5-spot2b-F1a	66.357	0.556	8.494	4.368	0.012	18.871	0.076	0	0.02	0.016	98.77
h-5-spot2b-F1b	66.126	1.419	6.346	4.716	0.04	18.992	0.356	0	0.063	0	98.058
h-5-spot2b-F1c	66.207	0.359	9.356	4.387	0	18.789	0	0.164	0.031	0	99.293
h-5-spot6a-F1a	66.373	2.17	5.737	4.95	0	18.787	0.718	0	0.144	0.083	98.962
h-5-spot6a-F1b	67.2	1.42	6.462	4.553	0.024	17.446	0.6	0	0.079	0.036	97.82
h-5-spot6b-F1a	65.962	0.266	10.553	4.328	0.031	19	0.027	0.109	0	0	100.276
h-5-spot6b-F1b	66.367	0.292	9.947	4.544	0.006	18.576	0.138	0.109	0.012	0	99.991
h-5-spot6b-F1c	66.942	1.666	6.161	4.657	0.034	18.305	1.208	0	0.21	0.005	99.188

h-12	SiO2	CaO	K2O	Na2O	P2O5	Al2O3	FeO	TiO2	MgO	MnO	Total
h-12-spot2a-1a	67.279	0.715	7.065	3.469	0.113	17.365	1.757	0.333	0.581	0.258	98.935
h-12-spot2a-1b	68.293	0.697	6.536	2.428	0.163	17.348	1.389	0.175	0.364	0.185	97.578
h-12-spot2a-2a	61.746	3.948	3.569	6.988	0.059	22.049	0.133	0	0	0.028	98.52
h-12-spot2a-2b	62.219	4.092	3.942	6.48	0.061	22.222	0.08	0.014	0.016	0	99.126
j-1	**SiO2**	**CaO**	**K2O**	**Na2O**	**P2O5**	**Al2O3**	**FeO**	**TiO2**	**MgO**	**MnO**	**Total**
j-1-spot6a-1a	63.541	3.801	0.549	9.908	0.069	22.672	0.105	0	0	0.015	100.66
j-1-spot6a-1b	62.843	4.897	3.167	7.056	0.002	23.038	0.049	0	0.014	0.001	101.067
j-1-spot6a-1c	65.261	2.966	2.269	8.89	0.056	21.674	0.066	0.082	0	0	101.264
j-1-spot6a-1d	64.689	4.475	3.562	5.732	0.025	20.891	0.203	0	0.047	0.037	99.661
j-1-spot6a-2a	63.648	3.926	4.24	6.737	0	22.261	0.153	0.164	0.012	0	101.141
j-1-spot6a-2b	64.427	3.688	2.832	7.897	0.001	22.292	0.055	0.163	0	0.006	101.361
j-1-spot6a-2c	67.847	2.849	4.533	5.074	0.042	18.871	0.39	0	0.052	0	99.658
j-1-spot6a-3a	62.226	5.337	2.614	6.825	0.035	23.505	0.089	0.027	0	0	100.658
j-1-spot6a-3b	62.283	4.996	3.026	6.812	0	23.011	0.114	0.137	0.005	0.018	100.402
j-1-spot6a-3c	62.927	5.401	2.789	6.375	0.03	22.585	0.168	0.137	0.01	0.02	100.442
j-1-spot6b-1a	59.96	6.923	1.038	7.446	0.029	24.975	0	0.246	0	0.006	100.623
j-1-spot6b-1b	62.632	4.607	1.716	8.276	0.017	23.072	0	0.136	0	0	100.456
j-1-spot6b-1c	63.032	4.532	0.41	9.55	0	23.284	0.028	0.054	0	0.018	100.908
j-1-spot6b-2a	63.201	4.575	2.551	7.555	0	22.798	0.092	0.109	0	0	100.881
j-1-spot6b-2b	63.893	4.293	3.495	6.496	0.026	21.939	0.195	0	0.009	0	100.346
j-1-spot6b-2c	63.758	3.981	4.037	6.892	0.018	22.492	0.055	0	0	0.052	101.285
j-1-spot6b-3a	67.11	2.799	4.498	5.593	0.026	18.689	0.313	0.191	0.05	0.038	99.307
j-1-spot6b-3b	63.053	4.729	1.703	8.057	0.012	22.739	0.072	0	0	0	100.365
j-1-spot6b-F1a	65.931	0.33	10.516	4.147	0.003	18.569	0.066	0	0	0.043	99.605
j-1-spot6b-F1b	65.251	0.174	10.771	4.085	0	18.689	0.058	0	0	0	99.028
j-1-spot6b-F1c	65.61	0.185	10.727	3.9	0.031	19.079	0.123	0	0	0	99.655

29-4a	SiO2	CaO	K2O	Na2O	P2O5	Al2O3	FeO	TiO2	MgO	MnO	Total
29-4a-spot1a-1a	63.895	3.836	2.371	6.429	0.021	19.235	0.852	0	0.013	0.13	96.782
29-4a-spot1a-1b	62.89	3.718	2.487	6.632	0.002	19.488	0.963	0	0.042	0.087	96.309
29-4a-spot1a-1c	64.322	3.133	2.416	7.125	0.015	19.195	0.45	0.027	0.016	0.004	96.703
29-4a-spot2a-1a	56.434	6.118	3.167	4.501	0.05	21.69	0.663	0.004	0.031	0.025	92.683
29-4a-spot2a-1b	65.769	0.939	6.072	6.209	0.013	17.512	0.169	0	0	0	96.683
29-4a-spot2a-2a	52.508	10.974	1.14	4.318	0.027	26.333	0.968	0.036	0.035	0.071	96.41
29-4a-spot2a-2b	54.026	10.147	0.863	5.094	0.008	26.35	0.657	0.002	0.013	0	97.16
29-4a-spot2a-3a	38.635	11.72	0.38	2.462	0.03	15.906	21.503	0.222	1.639	0.708	93.205
29-4a-spot2a-3b	43.834	16.927	0.155	1.691	0.02	26.65	6.681	0.118	0.478	0.297	96.851
29-4a-spot2a-4a	47.253	10.806	1.235	3.052	0.022	24.817	9.938	0.439	0.174	0.33	98.066
29-4a-spot2a-4b	58.928	6.545	3.174	4.405	0.006	19.246	3.405	0.174	0.336	0.304	96.523
29-4a-spot2a-4c	52.124	11.642	1.154	3.608	0.022	26.921	1.793	0.083	0.016	0.036	97.399
29-4a-spot3a-1a	44.553	15.242	0.354	2.058	0.014	25.68	6.894	0.229	0.364	0.26	95.648
29-4a-spot3a-1b	57.839	8.682	2.135	3.844	0.009	20.941	2.198	0.135	0.105	0.16	96.048
29-4a-spot3a-1c	53.48	11.977	1.096	3.194	0.035	22.346	3.029	0.148	0.458	0.267	96.03
29-4a-spot4a-1a	64.98	2.729	3.555	6.163	0	18.501	0.466	0	0	0.052	96.446
29-4a-spot4a-1b	64.203	2.885	3.469	6.665	0	19.02	0.286	0.009	0.005	0.034	96.576
29-4a-spot4a-1c	64.952	2.708	3.547	6.611	0.009	19.276	0.172	0	0	0.021	97.296
29-4a-spot4a-2a	61.612	3.109	3.017	5.906	0.039	18.254	0.461	0	0.02	0.104	92.522
29-4a-spot4a-2b	63.984	3.177	3.329	5.93	0.014	18.325	0.652	0.016	0.065	0.027	95.519
29-4a-spot4a-2c	63.46	2.943	3.224	5.317	0.005	18.681	0.435	0.004	0.011	0.084	94.164
29-4a-spot4a-3a	64.376	1.642	4.407	7.517	0.009	18.988	0.089	0	0.005	0.043	97.076
29-4a-spot4a-3b	65.099	2.255	4.011	6.688	0.006	18.888	0.182	0.001	0.048	0	97.178
29-4a-spot4b-1a	52.167	14.699	0.732	3.07	0.01	17.35	7.631	0.198	0.858	0.366	97.081
29-4a-spot4b-1b	50.678	17.355	0.751	2.201	0.039	10.17	12.571	0.195	1.288	0.593	95.841
29-4a-spot4b-2a	58.523	7.641	1.946	5.111	0.014	20.44	2.193	0.081	0	0.039	95.988
29-4a-spot4b-2b	63.333	4.952	3.886	3.513	0.05	13.213	4.355	0.368	0.018	0.225	93.913
29-4a-spot4b-2c	60.549	5.615	2.735	4.322	0.016	16.653	1.904	0.049	0.007	0.105	91.955

Sample 29-4b	SiO2	CaO	K2O	Na2O	P2O5	Al2O3	FeO	TiO2	MgO	MnO	Total
29-4bspot2a-1a	64.619	3.167	4.378	5.819	0.02	18.862	2.309	0.048	0.576	0.178	99.976
29-4bspot2a-1b	63.548	3.683	4.188	6.006	0.034	19.657	2.599	0.055	0.525	0.259	100.554
29-4bspot2a-1c	63.591	4.181	3.587	6.356	0.049	19.85	2.313	0.073	0.597	0.086	100.683
29-4bspot2a-2a	65.578	2.188	5.086	5.696	0.059	18.073	2.009	0.491	0.543	0.209	99.932
29-4bspot2a-2b	63.763	3.492	4.024	6.192	0.066	19.499	1.809	0.284	0.335	0.096	99.56
29-4bspot2a-2c	63.237	3.817	3.339	6.483	0.063	19.945	1.579	0.245	0.393	0.104	99.205
29-4bspot2a-2d	62.431	4.105	3.39	6.34	0.076	20.693	1.393	0.231	0.39	0.146	99.195
29-4bspot3a-1a	63.516	7.003	3.94	3.82	0.019	14.63	3.733	0.194	1.969	0.412	99.236
29-4bspot3a-1b	68.565	2.902	5.485	3.688	0.023	14.848	3.284	0.333	0.284	0.134	99.546
29-4bspot3a-1c	66.108	3.818	4.645	4.23	0.019	16.364	2.606	0.342	0.253	0.096	98.481
29-4bspot3a-2a	68.347	3.624	4.639	3.524	0.024	15.238	2.719	0.209	0.245	0.31	98.879
29-4bspot3a-2b	55.152	11.238	1.17	3.583	0.009	26.057	2.036	0.047	0.067	0	99.359
29-4bspot3a-2c	69.97	2.401	5.446	2.934	0.034	13.211	3.099	0.245	0.215	0.227	97.782
29-4bspot5a-1a	57.756	8.839	1.04	5.647	0.003	25.036	1.101	0.035	0.04	0	99.497
29-4bspot5a-1b	58.531	7.844	1.487	5.483	0.007	21.912	1.481	0	0.164	0.081	96.99
29-4bspot5a-1c	61.651	5.755	1.506	7.409	0.004	22.805	0.838	0.017	0.059	0.085	100.129
29-4bspot5a-2a	61.114	6.544	1.58	6.309	0.001	22.726	1.391	0.024	0.136	0.113	99.938
29-4bspot5a-2b	62.404	6.573	2.304	5.31	0.01	22.156	1.607	0.06	0.252	0.049	100.725
29-4bspot5a-3a	69.459	1.48	4.961	3.138	0.028	14.381	2.993	0.328	0.585	0.15	97.503
29-4bspot5a-3b	54.938	10.183	0.982	4.716	0.006	25.997	1.628	0.067	0.172	0.106	98.795

Supplementary Table: Trace Elements (ppm) for Lasered Spots										
SAMPLE	**Si29**	**Ca42**	**Ti 49**	**Fe 57**	**Rb85**	**Sr88**	**Y89**	**Zr90**	**Nb93**	**Ba137**
25182d-3-1	284764.09	17372.2	1396.75	12192.44	252.59	222.66	5.92	1.94	2.69	924.97
25182d-4-1	293743.5	19845.62	2252.27	25896.25	288.91	131.98	26.75	11.54	6.96	700.14
25182d-4-2	299955.81	11580.08	1775.95	17081.29	315.27	170.22	19.33	4.4	5.81	754.82
25182d-4-3	308888.56	10093.19	1684.66	25016.59	347.64	151.2	22.98	5.24	6.65	625.9
25182d-4-4	142008.08	18213.68	91742.27	87741.88	108.62	99.24	27.54	9.15	190.69	395.21
25182d-5-1	270378.66	24464.07	1067.18	13100.04	194.81	270.27	6.78	38.3	3.38	1743.23
25182d-5-2	251580.56	57105.09	636.6	32798.41	122.85	495.15	21.69	14.49	0.951	431.41
25182d-5-3	142008.09	18590.06	4856.08	5338.51	51.61	42.67	3.72	15.07	11.42	171.94
25182d-5-4	3628826.75	397373.75	5558.63	304847.34	2431.59	2037.65	70.25	265.66	15.89	10515.6
d1-1-1	300563.5	19821.61	nd	nd	282.4	194.81	8.85	7.68	5.49	868.92
d1-1-2	295281.44	14712.48	nd	nd	264.46	178.27	11.37	3.85	4.44	641.89
d1-1-3	305939.06	30484.16	nd	nd	217.39	231.11	5.73	13.37	1.82	486.58
d1-2-1	276957.81	20665.38	nd	nd	254.39	221.91	8.13	3.89	4.18	752.31
d1-2-2	294159.59	24624.47	nd	nd	234.43	270.4	7.9	11.64	5.68	1117.27
d1-2-3	289017.75	25315.27	nd	nd	227.19	292.39	6.13	3.68	3.32	953.88
25182f-3a-1	310847.19	31653.48	nd	nd	241.85	220.25	6.57	2.56	4.34	445.9
25182f-3a-2	286166.38	60590.04	nd	nd	138.68	379.55	1.51	3.31	2.16	266.91
25182f-3a-3	306546.75	5298.59	nd	nd	404.25	133.38	3.9	0.414	2.7	686.5
25182f-3b-1	308603.44	18031.81	nd	nd	197.15	189.15	4.62	22.07	3.48	1455.41
25182f-3b-2	310987.41	8279.38	nd	nd	337.37	148.22	18.21	0.511	3.74	783.42
25182f-3b-3	308837.19	51456.87	nd	nd	219.38	369.96	5.37	1.35	6.85	705.63
25182f-4-1	315428.13	23282.35	nd	nd	237.17	211.43	14.88	23.31	6.64	745.37
f4-1-2	313698.53	8435.34	nd	nd	236.12	80.54	2.2	10.31	1.8	497.82
f4-1-3	319401.31	22091.7	nd	nd	190.82	240.96	11.72	1.9	7.68	486.76
f4-2-1	317110.84	34697.68	nd	nd	151.51	111.69	8.96	27.41	5.06	376.84
f4-2-2	324449.69	29519.99	nd	nd	143.13	245.15	7.47	15.16	3.38	294.57
f4-3-1	327394.47	46021.97	nd	nd	95.24	105.97	5.4	32.47	1.69	345.42
f4-3-2	306359.72	44769.07	nd	nd	120.38	174.58	15.15	29.83	30.23	510.73
f4-3-3	313698.5	49888.27	nd	nd	76.4	131.57	2.61	30.64	0.88	223.88

25182h-1-1a	282356.78	32581.17	472.28	6875.81	116.15	457.79	2.91	3.75	1.274	821.72
25182h-1-1b	318751.63	24050.87	1075.23	11392.28	186.53	274.35	4.97	11.55	3.43	908.73
25182h-1-2	269448.41	31455.7	1447.04	15768.85	166.36	308.38	6.45	15.07	4.12	645.66
25182h-1-3	290200.38	40000.26	14.93	457.79	10.75	308.92	nd	nd	nd	197.75
25182h-1-4	305915.72	11600.06	147.34	4689.52	248.34	365.2	1.11	0.469	0.708	2184.9
h5-2a-1a	291308.19	31766.18	nd	nd	4.77	209.37	0.301	<0.037	<0.0158	46.9
h5-2a-1b	275041.28	41783.95	nd	nd	21.47	633.73	0.279	<0.058	0.046	403.8
h5-2a-2	263028.09	10497.34	nd	nd	217.61	126.66	1.727	8.91	2.284	839.35
h5-2a-3	284203.09	35693.29	nd	nd	7.51	301.47	1.118	<0.054	<0.035	116.71
h5-2b-1	259756.05	38913.02	nd	nd	26.56	473.25	0.432	0.322	0.215	273.92
h5-2b-2	267795.97	29380.27	nd	nd	52.15	344.47	0.951	2.47	0.61	378.27
h5-2b-3	309818.78	7168.25	nd	nd	319.82	243.04	1.453	0.602	0.888	1962.67
h5-6a-1	274059.66	50533.75	nd	nd	35.16	549.02	1.188	0.152	0.509	427.99
h5-6a-2	312202.72	9753.37	nd	nd	282.06	347.09	0.254	0.054	0.064	1946.04
h5-6b-1	277098.03	41799.16	nd	nd	16.94	751.54	0.207	<0.069	<0.040	779.14
h5-6b-2	312903.88	3503.57	nd	nd	337.33	273.8	0.156	<0.072	<0.052	2016.01
h12-2a-1	314488.56	13131.99	2053.61	16181.85	317.89	199.53	12.08	17.4	10.37	1335.32
h12-2a-1b	319228.38	26567.54	3398.57	29501.21	163.08	172.79	10.27	136.65	10.68	1534.91
h12-2a-2a	289730.63	34189.41	31.93	778.3	16.74	282.09	0.502	<0.150	<0.105	152.9
J1-6a-1a	297015.63	21487.15	114.67	1449.71	70	258.37	1.11	0.591	0.388	289.94
J1-6a-1b	299413.59	23610.82	54.95	1693.65	86.08	424.49	0.51	0.74	0.314	818.46
J1-6a-2a	297515.78	29722.56	64.3	3135.5	69.94	508.5	0.57	0.8	0.254	919.82
J1-6a-2b	301157.13	26526.14	163.8	5286.19	63.61	322.74	0.74	4.05	0.534	468.41
J1-6a-3	292051.41	26858.13	386.92	3672.5	189.61	171.04	2.37	14.86	1.12	544.88
J1-6a-4		329472.06	315641.22	2280711.25	7791.21	2645.7	190.18	249.67	561.39	22529.6
J1-6b-1a	280276.66	22604.22	333.78	4657.68	102.57	223.66	1.633	3.74	2.293	364.55
J1-6b-1b	293701.5	13275.01	737.13	13723.79	191.12	99.78	4.45	12.46	3.65	500.27
J1-6b-2a	295426.34	11522.73	476.02	76833.75	111.28	107.6	2.235	14.16	2.082	271.55
J1-6b-2b	298661.03	1010.53	392.07	16688.27	52.9	26.66	1.21	3.98	0.503	132.31
J1-6b-3	313698.56	19142.09	554.95	9160.66	186.96	105.9	3.37	17.67	3.04	557.59
J1-6b-4	306640.22	830.55	29.83	429.9	448.78	177.02	<0.160	<0.127	<0.073	1623.9
J1-6b-5	nd	1568711.88	315641.19	3935863.25	5772.33	12840.69	143.31	425.53	866.98	30759.1

29-4a-1a-1a	296321.5	12664.11	97.93	1309.05	90.46	283.64	5.39	195.76	0.289	267.47
29-4a-1a-1b	300666.34	20041.15	198.21	6298.97	86.41	333.58	34.33	8219.39	0.668	314.02
29-4a-4a-1a	303742.13	16334.33	16.02	3900.94	89.16	302.26	1.87	30.9	nd	150.01
29-4a-4a-1b	300110.09	4929.2	19.23	1258.63	42.94	100.85	0.48	11.79	nd	43.89
29-4a-4a-2	296637.03	16422.57	139.62	4340.73	83.66	303.67	nd	9.89	0.65	234.13
29-4a-4a-3	302608.56	21612.29	95.19	4164.89	88.7	324.6	22.46	7.91	0.505	171.17
29-4a-4a-4	4170913.5	397373.75	6269.8	118314.71	1285.92	4163.2	2741.28	240421.52	21.5	1967.34
29-4a-4b-2a	273559.53	41049.05	1255.05	25049.24	116.02	417.12	14.85	53.07	6.05	596.96
29-4a-4b-2b	296043.38	91097.13	1991.3	35911.75	79.64	904.43	28.14	121.79	5.55	491.17

29-4b-1-1	nd	4169172	315641.13	2481061.5	68300.7	59254.13	1914.36	28633.12	896.96	357419
29-4b-2a-1	297148.88	28506.65	694.13	32331.47	147.43	353.18	9.19	38.21	2.71	642.77
29-4b-2a-2a	300061.47	61023.26	849.9	28138.93	103.49	678.86	7.99	22.18	1.65	1012.25
29-4b-2a-2b	291827.06	22900.91	730.04	15213.34	164.23	322.64	10.03	17.92	2.35	817.32
29-4b-2a-4a	142008.08	11050.5	4355.86	4666.65	102.38	114.34	11.02	12.55	13.84	738.26
29-4b-2a-4b	142008.08	5753.39	1597.48	3826.87	104.51	145.54	3.37	7.03	5.16	1100.31
29-4b-3a-1	308699.31	17957.9	877.43	74341.13	77.58	192.08	6.68	61.63	3.41	515.72
29-4b-3a-2	323274.09	48762.96	671.62	20558.22	120.26	564.78	2.98	49.95	1.76	344.37
29-4b-5a-1	271785.59	8976.62	401.22	101216.83	39.62	119.41	2.14	93.29	1.053	105.4
29-4b-5a-2	288685.88	27720.54	433.75	19478.8	90.08	355.9	3.02	22.21	1.152	234.09
29-4b-5a-3	142008.06	26469.68	32381.51	21187.54	65.61	75.22	190.73	50.87	93.21	194.33
29-4b-5a-4	5340321	397373.78	9560.54	448281.25	1851.9	4718.03	642.95	6337.29	38.72	7410.73

	La139	Ce140	Nd146	Sm152	Eu153	Gd158	Dy164	Er166	Yb174	Hf178
25182d-3-1	8.8	14.07	4.63	1.17	0.82	0.723	0.824	0.518	0.53	0.085
25182d-4-1	352.57	580.87	158.75	18.53	1.54	9.8	5.78	2.11	1.97	0.44
25182d-4-2	416.3	639	166.9	17.9	0.97	8.16	4.2	1.71	1.44	0.267
25182d-4-3	311.7	501.66	142.12	16.26	1.05	8.72	4.87	1.96	1.81	0.255
25182d-4-4	4.39	12.7	10.56	3.42	0.624	4.04	4.56	2.58	2.54	1.78
25182d-5-1	9.15	16.71	6.24	1.02	0.55	1.128	1.241	0.694	0.787	1.381
25182d-5-2	26.38	38.32	14.25	2.9	1.177	2.5	2.83	2.119	2.37	0.664
25182d-5-3	3.53	6.88	2.86	0.54	nd	0.585	0.612	0.392	0.513	0.483
25182d-5-4	90.61	159.48	61.85	13.42	4.8	9.33	11.46	6.23	5.95	5.89
d1-1-1	8.12	16.04	6.36	1.53	0.57	1.31	1.38	0.87	0.87	0.347
d1-1-2	71.42	141.29	44.29	6.4	0.53	4.41	2.44	1.071	0.919	0.195
d1-1-3	9.44	16.95	5.87	1.06	0.511	0.877	0.855	0.524	0.581	0.38
d1-2-1	13.08	24.03	9.19	1.72	0.509	1.26	1.238	0.764	0.814	0.209
d1-2-2	10.62	22.28	7.52	1.47	0.658	1.37	1.31	0.751	0.78	0.448
d1-2-3	8.53	15.56	5.87	1.06	0.753	0.969	0.991	0.565	0.651	0.168
25182f-3a-1	10.1	18.01	6.39	1.29	0.492	1.02	1.11	0.621	0.67	0.113
25182f-3a-2	2.05	4.19	1.47	0.245	0.267	0.278	0.204	0.107	0.144	0.149
25182f-3a-3	2.49	4.54	2.16	0.54	0.61	0.6	0.565	0.375	0.408	0.054
25182f-3b-1	5.63	14.96	4.74	0.75	0.5	0.67	0.79	0.469	0.514	0.69
25182f-3b-2	5	10.77	6.17	1.62	0.6	1.86	2.43	1.63	1.83	0.048
25182f-3b-3	10.44	18.47	6.16	0.98	0.71	0.87	0.85	0.444	0.482	0.039
25182f-4-1	11.87	24.23	9.66	1.98	0.75	2.13	2.29	1.53	1.69	0.61
f4-1-2	3.1	5.02	1.72	0.37	0.372	0.283	0.315	0.233	0.28	0.209
f4-1-3	7.62	15.66	7.12	1.7	0.77	1.82	1.98	1.13	1.42	0.126
f4-2-1	4.55	8.5	3.9	0.88	0.465	1.06	1.3	0.88	1	0.73
f4-2-2	6.2	14.39	4.02	0.8	0.62	0.9	1.06	0.73	0.85	0.475
f4-3-1	5.43	10.57	4.32	0.8	0.246	0.716	0.733	0.535	0.611	0.91
f4-3-2	14.07	23.4	10.25	2.11	0.85	2.21	2.43	1.46	1.54	0.9
f4-3-3	4.14	8.14	3.4	0.52	0.194	0.453	0.386	0.248	0.297	0.78

25182h-1-1a	8.26	12.81	3.79	0.58	0.84	0.494	0.573	0.283	0.306	0.153
25182h-1-1b	9.61	16.36	5.47	1.25	0.94	1.07	0.84	0.527	0.514	0.405
25182h-1-2	7.82	14.49	5.71	1.1	0.26	1.056	1.106	0.666	0.756	0.492
25182h-1-3	11.84	12.76	2.54	nd	0.84	0.2	0.048	nd	nd	nd
25182h-1-4	3.1	4.49	1.47	nd	0.59	0.175	0.223	0.08	0.11	nd
h5-2a-1a	4.59	6.97	1.403	0.174	0.541	0.086	0.0394	0.0152	<0.0061	0.0062
h5-2a-1b	10.18	12.5	2.34	0.219	1.185	0.134	0.056	0.0305	0.0192	<0.0135
h5-2a-2	5.19	9.89	2.72	0.55	0.27	0.364	0.295	0.161	0.165	0.26
h5-2a-3	56.41	96.12	23.97	2.68	0.897	1.261	0.348	0.077	0.0291	<0.0103
h5-2b-1	6.47	8.21	1.575	0.164	0.707	0.111	0.0647	0.0345	0.0369	0.0154
h5-2b-2	8.26	11.07	2.32	0.313	0.666	0.203	0.156	0.087	0.096	0.091
h5-2b-3	3.17	4.78	1.322	0.294	0.495	0.232	0.244	0.148	0.161	0.0424
h5-6a-1	7.83	10.45	2.3	0.346	0.743	0.243	0.226	0.098	0.114	0.0122
h5-6a-2	0.928	1.27	0.298	<0.080	0.581	0.034	0.046	0.0185	0.0127	<0.0108
h5-6b-1	10.41	12.18	1.98	0.145	1.266	0.091	0.054	<0.0152	<0.0179	0.0109
h5-6b-2	1.278	0.936	0.118	<0.108	0.641	<0.035	<0.0198	<0.0151	0.0123	<0.0205
h12-2a-1	16.61	28.44	9.84	1.92	0.548	1.92	1.98	1.151	1.203	0.629
h12-2a-1b	14.97	29.28	10.69	1.96	0.451	1.93	1.81	0.963	1.151	2.4
h12-2a-2a	6.14	8.62	1.85	0.19	0.691	0.117	0.065	<0.028	<0.042	<0.040
J1-6a-1a	3.69	5.37	1.44	0.39	0.549	0.152	0.141	0.074	0.071	<0.029
J1-6a-1b	4.35	6.21	1.51	0.228	0.586	<0.081	0.126	0.049	<0.043	<0.038
J1-6a-2a	4.56	6.49	1.4	0.85	0.809	0.099	0.132	0.051	0.06	<0.049
J1-6a-2b	5.29	8.5	2.01	0.282	0.624	0.153	0.173	0.112	0.12	0.093
J1-6a-3	7.8	12.82	3.88	0.75	<0.32	0.45	0.462	0.211	0.312	0.367
J1-6a-4	623.62	943.31	219.54	33.68	13.26	22.8	26.75	16.39	23.69	9.94
J1-6b-1a	11.23	13.76	3.26	0.476	0.603	0.295	0.299	0.177	0.183	0.093
J1-6b-1b	10.79	16.98	4.75	0.66	0.163	0.548	0.559	0.328	0.302	0.515
J1-6b-2a	9.01	26.43	5.4	0.524	0.284	0.417	0.466	0.25	0.97	0.76
J1-6b-2b	3.49	6.69	2.28	0.41	<0.27	0.309	0.4	0.135	0.219	0.16
J1-6b-3	8.95	14.93	4.81	0.83	0.239	0.577	0.667	0.311	0.325	0.702
J1-6b-4	0.765	0.553	0.099	<0.148	0.481	<0.055	<0.0252	<0.0253	<0.0206	<0.029
J1-6b-5	411.09	620.17	205.64	31.22	33.19	22.29	21.87	15.19	16.05	11.3

29-4a-1a-1a	0.908	2.23	1.25	0.65	nd	0.586	0.859	0.528	0.711	5.68
29-4a-1a-1b	2.366	4.7	1.4	0.426	0.521	0.991	3.18	5.16	11.41	195.57
29-4a-4a-1a	0.873	1.8	1.18	nd	nd	0.28	0.349	0.283	0.395	1.32
29-4a-4a-1b	1.087	1.811	0.696	nd	nd	nd	0.116	nd	0.08	0.468
29-4a-4a-2	3.12	4.88	1.6	nd	nd	0.27	0.246	0.136	0.14	0.205
29-4a-4a-3	2.81	8.63	7.19	2.64	0.298	3.24	3.98	2.11	2.04	0.174
29-4a-4a-4	174.75	380.88	172.22	55.59	8.84	90.74	247.93	381.38	828.48	8841.71
29-4a-4b-2a	28.04	94.8	20.31	3.23	0.67	2.7	2.63	1.572	1.69	2.05
29-4a-4b-2b	42.45	79.05	31.08	5.86	1.187	5.12	4.99	2.98	3.09	5.62

29-4b-1-1	2393.71	4099.35	1806.12	321.18	268.73	336.06	305.68	193.57	250.1	815.12
29-4b-2a-1	20.86	37.37	13.78	2.15	0.95	1.99	1.51	0.892	1.004	1.059
29-4b-2a-2a	11.75	17.71	6.6	1.19	1.16	1.157	1.214	0.83	0.702	0.879
29-4b-2a-2b	9.33	16.52	6.96	1.4	0.86	1.46	1.8	1.022	1.035	0.623
29-4b-2a-4a	2.129	4.55	3.01	0.5	0.694	0.882	1.075	0.906	1.25	0.524
29-4b-2a-4b	1.436	2.66	1.11	nd	0.407	0.293	0.423	0.349	0.354	0.252
29-4b-3a-1	11.87	25.84	9.14	1.44	0.321	1.262	1.233	0.729	0.886	1.521
29-4b-3a-2	4.7	7.31	2.49	0.51	0.39	0.419	0.403	0.375	0.422	1.48
29-4b-5a-1	7.64	16.35	5.33	0.343	0.15	0.433	0.412	0.237	0.327	2.47
29-4b-5a-2	6.25	10.36	3.63	nd	0.29	0.391	0.496	0.325	0.439	0.94
29-4b-5a-3	23.43	56.77	43.8	15.6	4.01	19.61	29.53	20.07	20.92	2.95
29-4b-5a-4	136.53	362.7	228.93	71.48	10.29	95.25	102.82	63.78	75.58	286.74

	Hf180	Pb206	Pb207	Pb208	Th232	U238
25182d-3-1	0.095	26.98	24.37	25.26	1.104	0.715
25182d-4-1	0.56	34.17	31.57	32.28	49.88	1.37
25182d-4-2	0.207	32.9	30.71	31.69	75.68	1.176
25182d-4-3	0.291	38.55	34.53	36.83	62.27	1.72
25182d-4-4	1.804	22.67	21.28	22.02	0.4	0.712
25182d-5-1	5.13	352.21	354.47	330.87	3.5	1.23
25182d-5-2	0.617	26.14	24.54	24.88	4.25	4.76
25182d-5-3	0.481	7.74	7.41	7.18	1.12	0.63
25182d-5-4	7.53	391.6	362.38	363.05	23	6.68
d1-1-1	0.371	42.28	39.23	39.98	4.32	1.34
d1-1-2	0.191	61.93	57.19	59.35	71.22	2.43
d1-1-3	0.399	46.09	43.42	44.24	1.709	0.645
d1-2-1	0.188	32.49	30.72	31.61	4.17	1.142
d1-2-2	0.404	34.58	31.9	33.55	3.86	0.998
d1-2-3	0.155	34.48	32.9	33.81	3.05	1.203
25182f-3a-1	0.121	27.08	24.43	24.91	1.87	0.415
25182f-3a-2	0.168	35.18	32.02	31.78	0.23	0.223
25182f-3a-3	0.054	35.76	32.86	33.41	0.83	0.328
25182f-3b-1	2.32	168.81	148.82	165.39	1.7	0.89
25182f-3b-2	0.034	34.54	31.89	32.62	0.71	0.447
25182f-3b-3	0.056	28.04	25.49	25.89	0.444	0.347
25182f-4-1	0.58	31.79	28.37	29.9	6.32	1.59
f4-1-2	0.263	25.3	23.16	23.19	0.56	0.391
f4-1-3	0.149	33.18	30.58	31.24	1.17	0.605
f4-2-1	0.77	30.13	28.3	28.51	1	0.528
f4-2-2	0.481	29.65	27.2	28.19	1.01	0.43
f4-3-1	0.9	12.9	11.47	11.99	1.37	0.476
f4-3-2	0.9	24.29	22.01	22.29	1.75	1.8
f4-3-3	0.82	10.41	9.4	9.74	0.76	0.278

25182h-1-1a	0.13	26.08	24.39	24.64	1.688	0.282
25182h-1-1b	0.315	26.59	33.69	25.34	4.15	0.755
25182h-1-2	0.472	22.78	20.44	20.92	4.98	0.804
25182h-1-3	nd	29.49	27.87	28.54	0.0042	nd
25182h-1-4	0.061	38.75	37.02	37.64	0.607	0.142
h5-2a-1a	0.0019	23.02	21.12	22.02	0.00036	<0.0037
h5-2a-1b	<0.0098	26.99	25.15	26.09	0.0532	0.0239
h5-2a-2	0.272	38.79	35.3	36.57	1.723	0.578
h5-2a-3	<0.0122	32.92	30.1	31.46	50.88	0.407
h5-2b-1	0.0151	17.31	16.24	16.49	0.1446	0.0478
h5-2b-2	0.097	30.47	27.9	29.3	0.785	0.167
h5-2b-3	0.0478	50.13	46.5	47.8	0.554	0.253
h5-6a-1	<0.0099	32.29	29.67	31.03	0.459	0.1194
h5-6a-2	<0.0091	50.57	46.49	48.34	0.0275	0.0293
h5-6b-1	<0.0105	29.88	27.24	27.98	0.0027	<0.0047
h5-6b-2	<0.0206	58.52	54.72	57.01	0.0076	0.0058
h12-2a-1	0.668	47.54	43.98	44.64	7.58	1.776
h12-2a-1b	6.48	387.33	336.12	364.74	8.85	13.64
h12-2a-2a	<0.0256	32.45	28.89	30.61	0.0251	0.0114
J1-6a-1a	<0.033	26	24.98	25.6	0.498	0.086
J1-6a-1b	<0.031	27.67	25.94	26.76	0.296	0.071
J1-6a-2a	<0.031	27.6	25.74	26.7	0.206	0.076
J1-6a-2b	0.095	28.92	26.96	27.67	0.793	0.285
J1-6a-3	0.467	29.51	28.02	28.78	1.84	0.458
J1-6a-4	8.34	1222.91	1111.85	1161.92	70.15	35.4
J1-6b-1a	0.112	29.03	26.74	27.89	0.758	0.26
J1-6b-1b	0.745	31.91	28.86	34.26	1.602	0.802
J1-6b-2a	0.829	22.06	20.96	21.35	1.385	0.831
J1-6b-2b	0.215	6.07	5.44	5.78	0.918	1.168
J1-6b-3	0.519	28.88	28.03	29.42	2.205	0.7
J1-6b-4	<0.0203	54.61	51	52.7	<0.0038	<0.0070
J1-6b-5	10.75	1221.52	1128.49	1172.77	94.73	32.69

29-4a-1a-1a	5.35	12.64	11.63	11.73	14.08	0.822
29-4a-1a-1b	192.66	12.09	11	11.48	11.92	12.89
29-4a-4a-1a	1.01	34.95	32.51	32.37	1.94	0.718
29-4a-4a-1b	0.428	9.39	8.3	9.08	0.508	0.224
29-4a-4a-2	0.385	25.01	24.1	23.44	1.275	0.347
29-4a-4a-3	0.602	22.5	20.6	20.99	0.737	0.313
29-4a-4a-4	8734.33	425.45	382	398.91	5603.97	3051.95
29-4a-4b-2a	1.92	130.21	142.69	127.91	17.96	5.19
29-4a-4b-2b	5.64	42.37	37.92	39.31	18.32	6.77

29-4b-1-1	812.63	7162.07	6564.93	6865.14	1514.44	527.52
29-4b-2a-1	1.183	26.92	24.91	25.21	9.46	4.75
29-4b-2a-2a	0.914	23.19	22.32	21.73	1.829	1.041
29-4b-2a-2b	0.551	28.57	26.56	27.02	2.105	1.276
29-4b-2a-4a	0.487	14.4	13.25	13.63	0.693	1.942
29-4b-2a-4b	0.273	17.38	16.3	16.52	0.424	0.641
29-4b-3a-1	2.47	75.54	64.72	65.07	5.04	4.71
29-4b-3a-2	1.64	23.97	22.93	23.1	1.726	2.32
29-4b-5a-1	2.249	13	11.68	11.8	4.76	2.383
29-4b-5a-2	0.916	20.88	19.29	20.02	2.283	1.315
29-4b-5a-3	2.86	13.65	12.71	12.68	3.28	19.45
29-4b-5a-4	281.43	377.22	357.62	357.59	86.08	86.84

BHVO Standard: Trace Elements (ppm) for Lasered Standard Spots										
SAMPLE	**Si29**	**Ca42**	**Ti49**	**Fe57**	**Rb85**	**Sr88**	**Y89**	**Zr90**	**Nb93**	**Ba137**
BHVO-2usgs1	232784.8	77842	14819.84	82886	8.96	354	21.69	150	14.32	115
BHVO-2usgs2	232784.8	77490	15164.72	83313	9.20	365	22.43	155	14.73	117
BHVO-2usgs3	232784.78	77933	15404.75	84353	9.21	366	22.08	155	14.98	119
BHVO-2usgs4	232784.8	78819	15746.07	85764	9.27	373	22.60	157	15.21	122
MEAN	**IS**	**78021**	**15284**	**84079**	**9.16**	**365**	**22.20**	**154**	**14.81**	**118**
stdev		565	390.62	1281.24	0.14	7.61	0.40	2.84	0.38	2.72
%RSD		**1**	**3**	**2**	**1**	**2**	**2**	**2**	**3**	**2**
BHVO-2usgs5	232784.75	78916	14437	92209	9.18	352	21.84	148	14.21	118
BHVO-2usgs6	232784.78	77061	14586	91649	9.07	359	22.41	152	14.36	113
BHVO-2usgs7	232784.78	75742	14687	91604	9.27	356	22.16	151	14.40	113
BHVO-2usgs8	232784.78	75400	14364	90562	9.16	354	21.77	149	14.07	113
MEAN	**IS**	**76780**	**14518**	**91506**	**9.17**	**355**	**22.05**	**150**	**14.26**	**114**
stdev		1594	145.45	687.11	0.08	3.01	0.30	1.60	0.15	2.41
%RSD		**2**	**1**	**1**	**1**	**1**	**1**	**1**	**1**	**2**
BHVO-2usgs9	232784.81	74907	13682	89821	8.77	332	20.94	142	13.59	111
BHVO-2usgs10	232784.81	76508	14504	92734	9.30	353	21.63	149	14.30	116
BHVO-2usgs11	232784.81	77076	14542	91431	9.26	353	21.60	148	14.32	114
BHVO-2usgs12	232784.81	75752	14467	90653	9.18	348	21.56	148	14.20	113
MEAN	**IS**	**76061**	**14299**	**91160**	**9.13**	**347**	**21.43**	**147**	**14.10**	**113**
stdev		941	412.18	1238.66	0.24	9.88	0.33	3.27	0.35	1.82
%RSD		**1**	**3**	**1**	**3**	**3**	**2**	**2**	**2**	**2**

SAMPLE	La139	Ce140	Nd146	Sm152	Eu153	Gd158	DY164	Er166	Yb174	Hf178
BHVO-2usgs1	14.33	33.59	22.40	5.76	1.94	5.44	4.76	2.09	1.85	3.93
BHVO-2usgs2	14.71	34.37	23.13	5.84	1.95	5.53	4.50	2.23	1.91	4.04
BHVO-2usgs3	14.81	34.71	22.85	5.88	2.09	5.54	4.78	2.21	1.94	4.08
BHVO-2usgs4	15.02	35.24	23.54	5.73	2.00	5.59	4.69	2.38	1.87	4.13
MEAN	**14.72**	**34.48**	**22.98**	**5.80**	**2.00**	**5.53**	**4.68**	**2.23**	**1.89**	**4.05**
stdev	0.29	0.69	0.48	0.07	0.07	0.06	0.13	0.12	0.04	0.09
%RSD	**2**	**2**	**2**	**1**	**3**	**1**	**3**	**5**	**2**	**2**
BHVO-2usgs5	14.45	33.66	22.69	5.75	1.98	5.61	4.72	2.20	1.95	4.13
BHVO-2usgs6	14.53	34.05	23.26	5.63	1.99	5.45	4.66	2.18	2.01	4.15
BHVO-2usgs7	14.64	33.95	22.55	5.68	1.96	5.62	4.66	2.22	1.89	4.06
BHVO-2usgs8	14.42	33.55	22.42	5.57	1.90	5.35	4.54	2.17	1.86	4.07
MEAN	**14.51**	**33.80**	**22.73**	**5.66**	**1.96**	**5.51**	**4.65**	**2.19**	**1.93**	**4.10**
stdev	0.10	0.24	0.37	0.08	0.04	0.13	0.08	0.02	0.07	0.04
%RSD	**1**	**1**	**2**	**1**	**2**	**2**	**2**	**1**	**4**	**1**
BHVO-2usgs9	13.78	32.14	21.55	5.50	1.84	5.28	4.43	2.15	1.90	3.82
BHVO-2usgs10	14.51	33.66	22.49	5.55	1.90	5.31	4.65	2.16	1.84	3.87
BHVO-2usgs11	14.44	33.10	22.76	5.58	1.92	5.32	4.68	2.13	1.87	3.96
BHVO-2usgs12	14.20	33.37	22.25	5.74	1.89	5.31	4.59	2.16	1.82	3.85
MEAN	**14.23**	**33.07**	**22.26**	**5.59**	**1.89**	**5.31**	**4.59**	**2.15**	**1.86**	**3.88**
stdev	0.33	0.66	0.52	0.10	0.03	0.02	0.11	0.01	0.04	0.06
%RSD	**2**	**2**	**2**	**2**	**2**	**0**	**2**	**1**	**2**	**2**

SAMPLE	Hf180	Pb206	Pb207	Pb208	Th232	U238
BHVO-2usgs1	3.89	1.77	1.60	1.54	1.11	0.36
BHVO-2usgs2	4.01	1.74	1.59	1.79	1.15	0.37
BHVO-2usgs3	4.04	1.76	1.59	1.65	1.13	0.39
BHVO-2usgs4	4.01	1.76	1.62	1.70	1.13	0.39
MEAN	**3.99**	**1.76**	**1.60**	**1.67**	**1.13**	**0.38**
stdev	0.07	0.01	0.02	0.10	0.02	0.02
%RSD	**2**	**1**	**1**	**6**	**2**	**4**
BHVO-2usgs5	4.15	1.49	1.49	1.43	1.14	0.41
BHVO-2usgs6	4.13	1.65	1.45	1.64	1.13	0.42
BHVO-2usgs7	3.87	1.62	1.54	1.55	1.08	0.39
BHVO-2usgs8	3.87	1.66	1.52	1.54	1.09	0.37
MEAN	**4.01**	**1.61**	**1.50**	**1.54**	**1.11**	**0.40**
stdev	0.16	0.08	0.04	0.09	0.03	0.02
%RSD	**4**	**5**	**3**	**6**	**3**	**5**
BHVO-2usgs9	3.93	1.52	1.49	1.52	1.10	0.40
BHVO-2usgs10	3.90	1.60	1.45	1.52	1.15	0.41
BHVO-2usgs11	3.88	1.74	1.57	1.52	1.11	0.40
BHVO-2usgs12	3.80	1.54	1.52	1.46	1.08	0.40
MEAN	**3.88**	**1.60**	**1.51**	**1.51**	**1.11**	**0.40**
stdev	0.06	0.10	0.05	0.03	0.03	0.00
%RSD	**1**	**6**	**3**	**2**	**3**	**1**